PFC/RR 88-17

FAILURE MODES AND EFFECTS ANALYSIS

OF FUSION MAGNET SYSTEMS

by

Martin Zimmermann,

Mujid S. Kazimi, Nathan O. Siu, and Richard J. Thome

Plasma Fusion Center

and the

Department of Nuclear Engineering

Massachusetts Institute of Technology

Cambridge, Massachusetts 02139

FAILURE MODES AND EFFECTS ANALYSIS
OF FUSION MAGNET SYSTEMS

ABSTRACT

A failure modes and consequence analysis of fusion magnet system is an important contributor towards enhancing the design by improving the reliability and reducing the risk associated with the operation of magnet systems. In the first part of this study, a failure mode analysis of a superconducting magnet system is performed. Building on the functional breakdown and the fault tree analysis of the Toroidal Field (TF) coils of the Next European Torus (NET), several subsystem levels are added and an overview of potential sources of failures in a magnet system is provided. The failure analysis is extended to the Poloidal Field (PF) magnet system. Furthermore, an extensive analysis of interactions within the fusion device caused by the operation of the PF magnets is presented in the form of an Interaction Matrix. A number of these interactions may have significant consequences for the TF magnet system particularly interactions triggered by electrical failures in the PF magnet system.

In the second part of this study, two basic categories of electrical failures in the PF magnet system are examined: short circuits between the terminals of external PF coils, and faults with a constant voltage applied at external PF coil terminals. An electromagnetic model of the Compact Ignition Tokamak (CIT) is used to examine the mechanical load conditions for the PF and the TF coils resulting from these fault scenarios. It is found that shorts do not pose large threats to the PF coils. Also, the type of plasma disruption has little impact on the net forces on the PF and the TF coils. But the out-of-plane loads at the inner corners of the TF coils can increase substantially for a wide range of scenarios, and the magnitude of these loads depends highly on the terminal constraints on the internal PF coils.

Acknowledgements

Table of Contents

FAILURE MODES AND EFFECTS ANALYSIS
OF FUSION MAGNET SYSTEMS

List of Figures

List of Tables

FAILURE MODES AND EFFECTS ANALYSIS OF FUSION MAGNET SYSTEMS

<div align="right">

Chapter 1

INTRODUCTION

</div>

1.1   Fusion Magnet Systems

Fusion is currently one of the largest worldwide research efforts which aim at developing new energy sources for the future. Mainly four groups of countries are supporting fusion research at the present time, namely Japan, the Soviet Union, Western Europe and the United States. The amount of money being spent on research in fusion technology and engineering is large and has recently been between 300 to 600 million dollars per year in each of these groups of countries.

There are two basic approaches to controlled fusion energy that are being pursued at the present time: inertial confinement fusion and magnetic confinement fusion. In general, in order to make a fusion reaction work and produce a self maintained reaction for a certain period of time, it is required to confine the fusion fuel for a sufficiently long period of time at high particle density and temperature. Inertial confinement fusion approaches these necessary conditions by compression of solid fusion fuel for a sufficiently long time. For instance, one method employs lasers with high power density which are focused on a fuel pellet. When the pellet is heated up fast enough, i.e. high particle density and temperature are achieved simultaneously, fusion reactions can be initiated and self maintained until the reactive forces in the pellet overcome the inertial forces and the pellet is torn apart.

The magnetic confinement concept uses magnetic fields to confine a plasma, which is an ionized gas of fusion fuel, in a reaction vessel. The plasma is obtained by heating the fusion fuel by induced currents, electromagnetic waves or injection of fast neutral particles, for instance. In order to achieve high plasma

densities, it is required to confine the plasma by strong magnetic fields. Again, confinement time and plasma temperature must be high enough to allow for fusion reactions and a positive net output of energy.

This study addresses some aspects of the magnetic confinement fusion approach. Within this approach, there are again several different concepts. The problem is clearly to achieve high temperature (leading to high particle velocities) and long confinement times at the same time.

Magnetic confinement is based on the physical principle that electrically charged particles tend to follow magnetic field lines. These field lines act like a guiding center, around which the charged particles may gyrate. Therefore, there are several different ideas for fusion reactors with magnetic confinement, such as mirror machines or tokamak devices. In mirror machines, the plasma is confined in a magnetic bottle, where particles are reflected back into the bottle by strong magnetic fields at its ends. However, for reasons of large losses of particles and energy, and confinement stability considerations, systems with closed magnetic field lines such as tokamaks are favored at the present time. In a tokamak, ring shaped closed magnetic field lines are produced by toroidal coils. Assuming a constant magnetic field B_t along a toroidal line of radius R, the total electrical current NI_t within an area of radius R is given by

$$\int_0^{2\pi} B_t R d\theta = \mu_0 NI_t \tag{1.1}$$

where θ is the toroidal angle. Performing the integration in Eq. 1.1 then yields

$$B_t = \frac{\mu_0 NI_t}{2\pi R} . \tag{1.2}$$

Neglecting field ripple effects, this toroidal field B_t could then be produced by a number of N TF coils, each carrying a current of magnitude I_t, as illustrated in Fig. 1–1. Eq. 1.2 also shows, that when the magnetic field is purely toroidal, it scales inversely to the radius R, since

$$B_t(R)R = B_t(r)r = constant . \tag{1.3}$$

This effect leads to a field gradient that, together with centrifugal effects which are caused by particles following a toroidal magnetic field line, will cause a drift of these particles in a direction perpendicular to the (usually horizontal) plane of the guiding center. However, particles of different charge will drift in opposite directions, causing an electrical field in the vertical direction to develop. This electrical field will cause another particle drift, and both drifts combine to drive the plasma towards a larger radius (i.e., the outside wall of the vacuum vessel).

In order to counteract these drifts, helical guiding magnetic field lines are used so that the particles will move as often towards the midplane as away from it on average. Such helical magnetic field lines can be obtained by adding a magnetic field B_p of circular type around the toroidal magnetic field lines, i.e., in the minor (poloidal) cross section of the torus with major (toroidal) radius R.

In the tokamak concept, this magnetic field B_p is produced by a ring current I_p which is carried by the plasma itself. This plasma current I_p is induced by a unidirectional change of magnetic flux, where the plasma acts like the second winding of a transformer coil, and the primary winding is made up of solenoidal ring coils concentric to the torus, as illustrated in Fig. 1–1.

Since such a unidirectional flux change can only be maintained for a finite time, these coils need to be operated in a pulsed mode. Also, due to the cylindrical symmetry of the field lines, the magnetic field B_p will be stronger on the inside than on the outside of the torus. An additional magnetic field in the vertical direction is therefore needed to correct those differences and allow for radial equilibrium, and it can be generated by solenoidal ring coils as well.

There is an additional important effect of the plasma current I_p. Since the plasma has an electrical resistivity, the plasma current will contribute to the heating of the plasma, an effect which is generally referred to as ohmic heating of the plasma.

Thus, the magnet system of a tokamak needs to consist of coils able to perform three basic tasks:

B_t: toroidal magnetic field
B_p: poloidal magnetic field
I_p: plasma current

I_t: toroidal coil current
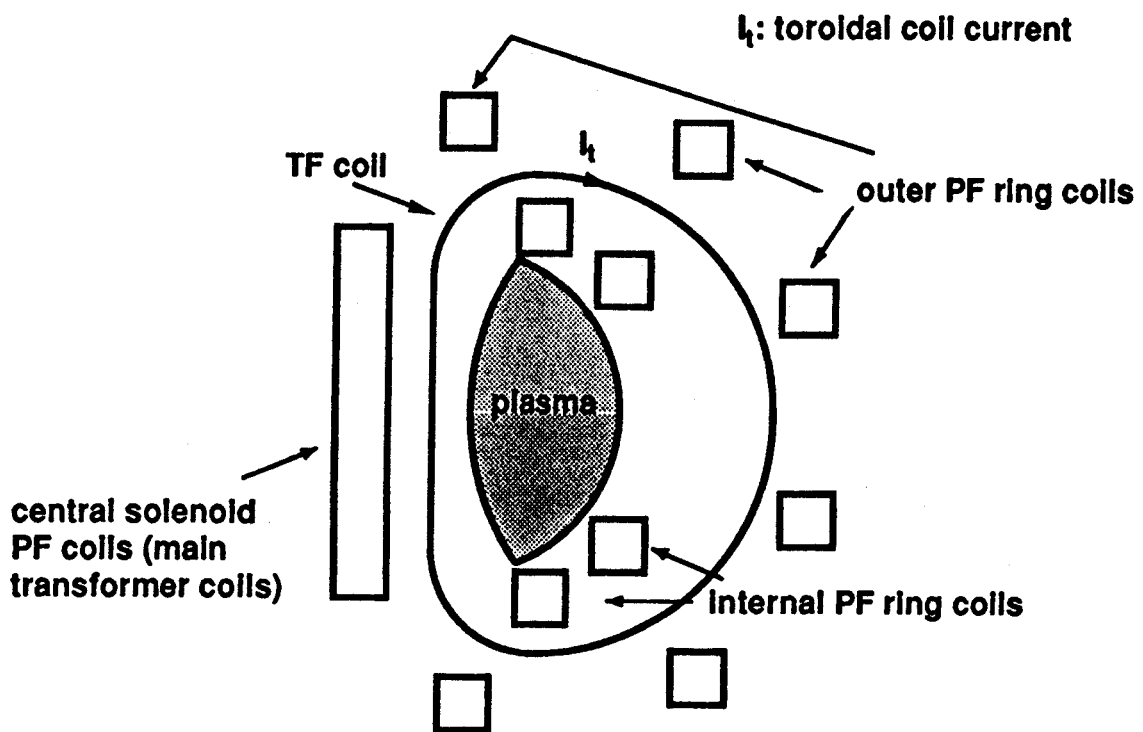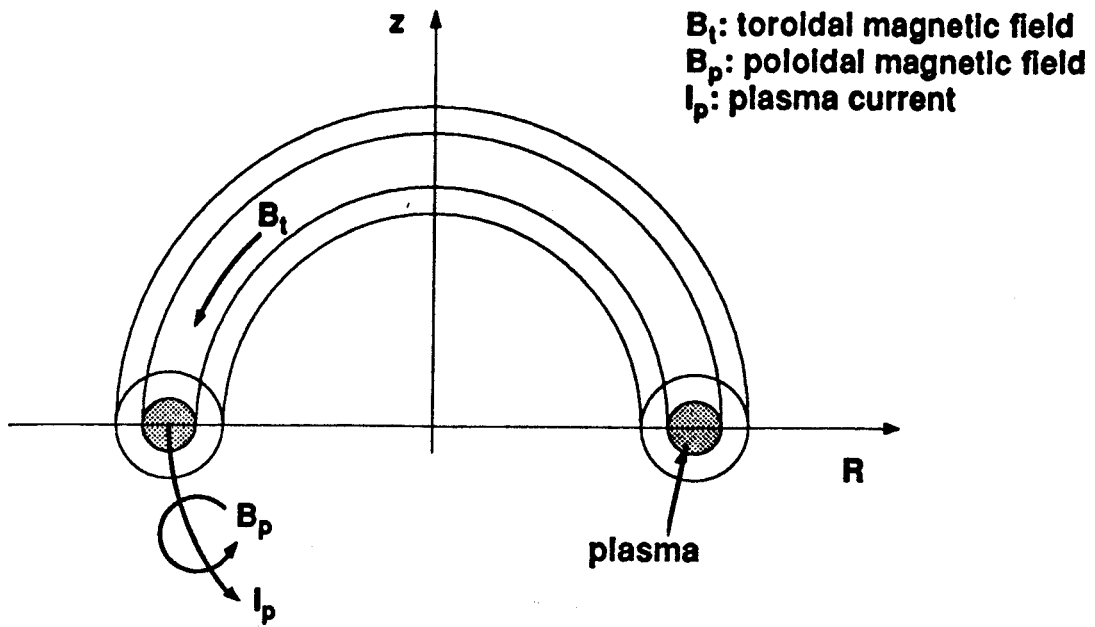
Fig. 1-1. Scheme of a Tokamak Coil System

1. To produce the toroidal magnetic field;

2. To induce the plasma current by providing enough unidirectional flux change; and

3. To produce the magnetic fields required for stabilization and shaping of the plasma.

The fulfillment of these tasks will require magnet systems of very large scale, which produce enormous magnetic fields and store large amounts of energy. Such magnet systems can be regarded as being essentially fusion specific devices for which no technical analogs existed in the past.

1.2 Reliability Aspects in Fusion R&D

At the present time, a number of major experimental tokamak machines are operating or being designed. In the United States, the Tokamak Fusion Test Reactor (TFTR) is operating in Princeton, New Jersey, and a compact machine, the Compact Ignition Tokamak (CIT) is planned for the same site in the early 1990's. In Western Europe, the current experimental machine, the Joint European Torus (JET) in Culham, Great Britain, is likely to be succeeded by the Next European Torus (NET), which might start operation around the year 2000 and is of significantly larger size than CIT. The new machines are expected to achieve conditions better than energy breakeven when fueled with a mixture of Deuterium and Tritium (D-T). The currently operating machines have been operating with Deuterium fuel and may be upgraded for use of D-T fuel in the future.

For fusion in order to fulfill its goals and become an economical and publicly acceptable major source of energy in the future, the reliable and safe operation of future fusion devices must be proven once the technical feasibility of fusion has been demonstrated. At the present time, the designs of fusion systems involve large uncertainties about their reliability. However, early design decisions, i.e., decisions made in the current R&D phase, will have a large impact on the performance and costs of the final design.

Therefore, reliability and safety considerations need to be incorporated into the design of fusion machines or reactor subsystems during all phases of the design. Design decisions should be based on an overall design concept and be reviewed continuously as more detailed information becomes available. An appropriate design concept should allow to project the consequences of present design developments on the safety and costs of future devices, thereby improving the design and the allocation of design efforts. This is important since it allows for communicating the desirable reliability and safety goals, and examining the impact of various design options on the projected cost of electricity. Such approaches to the cost assessment of fusion reactors have already been developed [Sheffield 1986].

In addition, there have been a number of studies on the safety and reliability of magnet systems, some of which will be discussed in the following.

In an early study of superconducting magnet systems [Hsieh 1978], engineering safety features of magnet systems were examined. A preliminary assessment of accident initiators and potential failure consequences for a generic superconducting magnet system was made, including structural, thermal–hydraulic and electrical safety concerns. Also, an approach to fusion magnet safety was outlined, and it was concluded that a number of elaborate engineered safety features would be required to limit the risk of a loss of mission of a fusion reactor due to magnet failure.

The International Tokamak Reactor Study (INTOR) (see, for example [INTOR 1986]) included a comparison of alternative approaches to the design of TF magnets. This comparison was based on a weighted matrix of such aspects as the maturity of technology, their reactor compatibility, their reliability and costs [INTOR 1982], but the weighting factors were based on engineering judgment rather than quantitative failure analysis. Furthermore, a number of studies on selected aspects of magnet safety have been conducted as part of INTOR, like a study on the consequences of severe magnet failures which could lead to damage of surrounding structures [Arendt 1981]. For example, the potential effect of a complete rupture of a coil winding with subsequent missile generation was evaluated.

In recent years, several experimental facilities have been used to study magnet failures and safety features, and availability records of such devices were increasingly kept. One such device has been TESPE (Toroidales Energie Speicher Experiment) [Jüngst 1987], where a set of toroidial coils was used to study for example magnet discharge behavior and arcing failures. Also, the Large Coil Task (LCT) [Ulbricht 1987] provided vast insights into the manufacturing, operation and failure handling of toroidal field coils of large scale for the first time.

While these studies investigated mainly the safety features of magnets, the availability of magnet systems was included in a study by Musicki [Musicki 1983]. A Monte Carlo method was employed to calculate the approximate availability of a fusion mirror machine. The cost of electricity was computed as a function of the availability, and its sensitivity to several design changes was examined. Safety considerations were not included in this study. It was concluded that adding a redundant unit will be preferable to increasing the availability of a single unit for major subsystems of the magnet systems. The entire magnet system was identified as one of the potential major unavailability driving reactor subsystems, i.e., its contribution to the overall unavailability of the reactor can be large compared to that of other reactor subsystems. This was found to be due to the high importance of the magnet system for the operation of the entire plant and since the redundancy options for coils are very limited.

In a following study [Watanabe 1986], this fusion reactor availability analysis was extended to model systems with normal, degraded, and failed states. However, both studies indicated the lack of reliability data as the major effect leading to large uncertainties in the availability analysis. It was concluded that the error in modeling the system can only be reduced by doing careful analysis of reactor design studies.

In another study [Piet 1986], an overview was given of how to incorporate safety and economical considerations into design decision making. This approach, risk–based design, suggested probabilistic risk assessment (PRA) as the basis for decision making in order to enhance fusion safety and plant availability, and

yields a generic method to compare design options. Also, system interactions can be highlighted, since a PRA requires an examination of the entire system, possibly leading to the search for less complex solutions, which are in turn likely to yield more reliable designs.

This framework was later extended and applied to the design of the Compact Ignition Tokamak [Cadwallader 1987]. The objective was to identify all failures that could possibly lead to a loss of mission of CIT. A Failure Modes and Effects Analysis (FMEA) for loss of mission was performed and yielded significant insight into the failure pathways which can contribute most to a possible loss of mission. The magnet system was identified as one of the fusion device subsystems whose failure could lead to a loss of mission for CIT. Since CIT will use D–T (Deuterium–Tritium) fuel, safety considerations will become increasingly important, and risk–based design will become more useful and required to fulfill safety regulations.

In the European fusion research program, a reliability and availability assessment program is being conducted for NET [Bünde 1987a]. Several constraints on the availability of the NET reactor regarding successful experimental and diagnostic operations have been imposed in order to achieve the goals of NET. The reliability and availability assessment is based on a Failure Modes, Effects and Criticality Analysis. The goal is to improve the design of the system by updating the reliability and availability assessment in an iterative procedure as more information becomes available. Reliability actions are proposed during each iteration based on the sensitivity of the availability of critical components or subsystems to design changes. Critical components or subsystems are those systems, which can be regarded as unavailability drivers of the fusion plant.

1.3 Objectives of this Study

The objective of this study is to contribute to improving the reliability of fusion magnet systems and reducing the risk associated with the operation of magnet systems. Areas of uncertainties about modes of failures and fault consequences are identified. Failures of the electrical system of the PF magnets are examined as an example of those areas.

Previous sections have shown, that magnet systems are of major importance for the technical feasibility of fusion and the operation of fusion devices. In addition, issues like development, manufacturing and operation costs, maintenance, i.e., the repair and replacement of magnets, and the safe deposition of the stored magnetic energy in case of faults need to be incorporated in the design. Magnet systems are potential unavailability drivers and magnet failures may lead to a loss of mission of the entire fusion device. The redundancy options for the coils are furthermore severely limited. Nevertheless, despite of the high importance of magnet systems, the database of magnet failures and fault consequences is still weak and further analysis is needed.

This study is therefore partitioned into two parts, a failure analysis of fusion magnet systems, and an analysis of the consequences of an exemplary group of failures which are electrical failures in the PF magnet system.

The failure analysis is presented in Chapter 2 and helps to identify areas which might require further design modifications. Based on the functional breakdown and the preliminary fault tree analysis of the NET TF coils [Bünde 1987a], several failure levels including physical failure modes are added using a variety of sources from the literature (the main source being the INTOR study, see for example [INTOR 1986]). This failure analysis is then extended to the PF magnet system, and the major differences of potential failure modes of the TF and PF magnet systems are discussed. Furthermore, for the first time an extensive analysis of interactions within the PF magnet system and with other reactor subsystems, which are caused by the operation of the PF magnets, is performed.

The failure mode and interaction analysis from Chapter 2 shows that the major differences in the failure modes of the TF and the PF magnet systems arise from the pulsed operation of the PF magnets. This operation mode will require a complex electrical and control system for the PF magnets. This implies a large potential for interactions triggered by electrical failures in the PF magnet system.

Therefore, the objective of the second part of this study is to examine the potential consequences for the TF and the PF coils resulting form electrical failures in the PF magnet system. This analysis is presented in Chapter 3. Based on an examination of reported electrical failures and on the potential properties of future electrical systems of PF magnets, fault scenarios are selected. These fault scenarios are then simulated using a simplified electromagnetic model of CIT.

Finally, Chapter 4 includes a summary of the results, conclusions that are obtained in this study, and recommendations for areas of future work.

The appendices include the notation that is used for the fault tree analysis, the operation and load scenario for the external PF coils of CIT, the potential disruption scenarios for CIT used for the fault consequence analysis, and the simulation models that are used in Chapter 3.

Chapter 2
FAILURE ANALYSIS OF MAGNET SYSTEMS

An analysis of the failure modes of the entire magnet system is needed as a first step to identify design areas which might require further modifications. It can also be helpful to identify potentially important contributors to system failures. Therefore, the main intention of the failure analysis in this Chapter is to obtain an improved understanding of the functional interactions within this complex system rather than to give a detailed description of failure modes which can occur for specific magnet designs. However, in order to include lower levels of physical failures which, e.g., can show the impact of interactions between magnet subsystems, a more specific design needs to be considered. The main reference design for the failure mode analysis in this study is that of the TF magnet system for the Next European Torus (NET). The NET reliability and availability assurance program has already established a concept for a failure modes, effects and criticality analysis of the NET toroidal field magnet system. This includes a functional breakdown of the magnet system and preliminary fault and event trees (see, for example [Bünde 1987], [Bünde 1987a], and [Bünde 1988]).

The analysis in this Chapter builds on the concepts and the currently available results of this NET program. Furthermore, the notation of the Plant Component Identification Scheme (PCIS) of NET [Bünde 1988a] is used throughout this Chapter wherever applicable. Such an identification scheme is found to be very helpful in organizing the system breakdown and the failure analysis.

In this study, a failure mode analysis for a superconducting TF magnet system is presented. Some modifications of the system boundaries are made and the NET fault trees are extended to include several levels of failure modes defined in terms of physical failures rather than component unavailability. It thereby provides an overview of potential sources of failures in fusion magnet systems. The failure mode analysis in this Chapter is furthermore extended to the PF magnet system while the NET analysis examines the TF magnet system.

Boundaries for the analysis of the PF magnet system are suggested and the main differences in the failure modes of the PF and the TF magnet systems are identified. Furthermore, for the first time an extensive analysis of the interactions with the TF magnets and other reactor subsystems, which are caused by the PF magnet system, is performed. For this interaction analysis the concept of a Fault Interaction Matrix suggested in earlier studies [Piet 1986] is extended to an Interaction Matrix showing interactions occurring under normal operating and fault conditions.

Clearly, since the database for fusion magnet systems is being developed at the present time, and existing magnet systems and magnet designs show considerable differences, the failure analysis presented in this Chapter can only be representative for the design of a "generic" magnet system which is believed to have similar properties to future magnet systems. In this regard, this analysis cannot be considered as being final or complete for a specific magnet design.

2.1 Functional Breakdown of the Magnet System

A functional breakdown yields the basis for further failure analysis of the magnet system. For a system with a variety of tasks like the magnet system, a design will be desirable where the different tasks can be achieved independently, that is the design is desired to be functionally decoupled. This will not always be achievable or may be impossible. Hence, the design of a magnet system leads to a number of interactions within the system. Those interactions will be discussed in Chapter 2.3 in more detail since they are not explicitly represented in the failure mode analysis in Chapter 2.2.

The magnet system of a tokamak reactor consists of TF and PF coils. The TF coils have to provide the toroidal magnetic field. Those coils will have to carry very large currents, on the order of 10 MA per coil, and are likely to remain energized for long periods of time in order to keep the energization costs low. Also, in order to avoid large energy losses in these coils, the TF coils of future magnet systems are expected to be superconducting.

PF coils are needed to induce the plasma current and to produce the magnetic fields which control and stabilize the plasma shape and its position. Therefore, these coils need to be operated in a pulsed mode, where the length of a single pulse will probably lie between a few seconds to a few minutes. Since the problem of energy losses is therefore less severe than for TF coils, resistive or superconducting PF coils may be imagined for future reactors, but superconducting coils will be highly preferable.

Following these considerations, the entire magnet system can be broken down into the TF and the PF magnet systems† (*AB* respectively *AC* in the PCIS notation‡). Each of these magnet systems can then be broken down further into four major types of subsystems. These are the coil system, coil cooling system, power supply system and the protection and control system, as illustrated for the TF magnet system in Fig. 2–1.

Each magnet system needs several coils to perform its tasks and three types of coil systems can be distinguished:

1. TF coil systems (*ABA*), of which an entire TF magnet system will have approximately 10 to 20 and which are alike and feature superconducting coils;

2. An external PF coil system (*ACA*), which consists of coils of the same type, and performs the task of inducing the plasma current and providing the basic shape of the plasma in an integrated way, i.e., there are no coils assigned to a single function only. Therefore, a further breakdown of this system into single coils is not performed. These external PF coils are likely to be all normal– or all superconducting; and

3. An internal PF coil system (*ACB*), which is likely to feature resistive coils since they are operated under severe environmental conditions.

---

† Throughout this report, magnet system refers to the entire TF or PF magnet system, while the term coil system refers only to the coil winding and its directly connected equipment. Thus, a magnet system may consist of several coil systems.

‡ The PCIS notation from NET [Bunde 1988] is introduced in this section and mostly used in future sections without mentioning the name of the system or component. PCIS notations are always in *italics*.
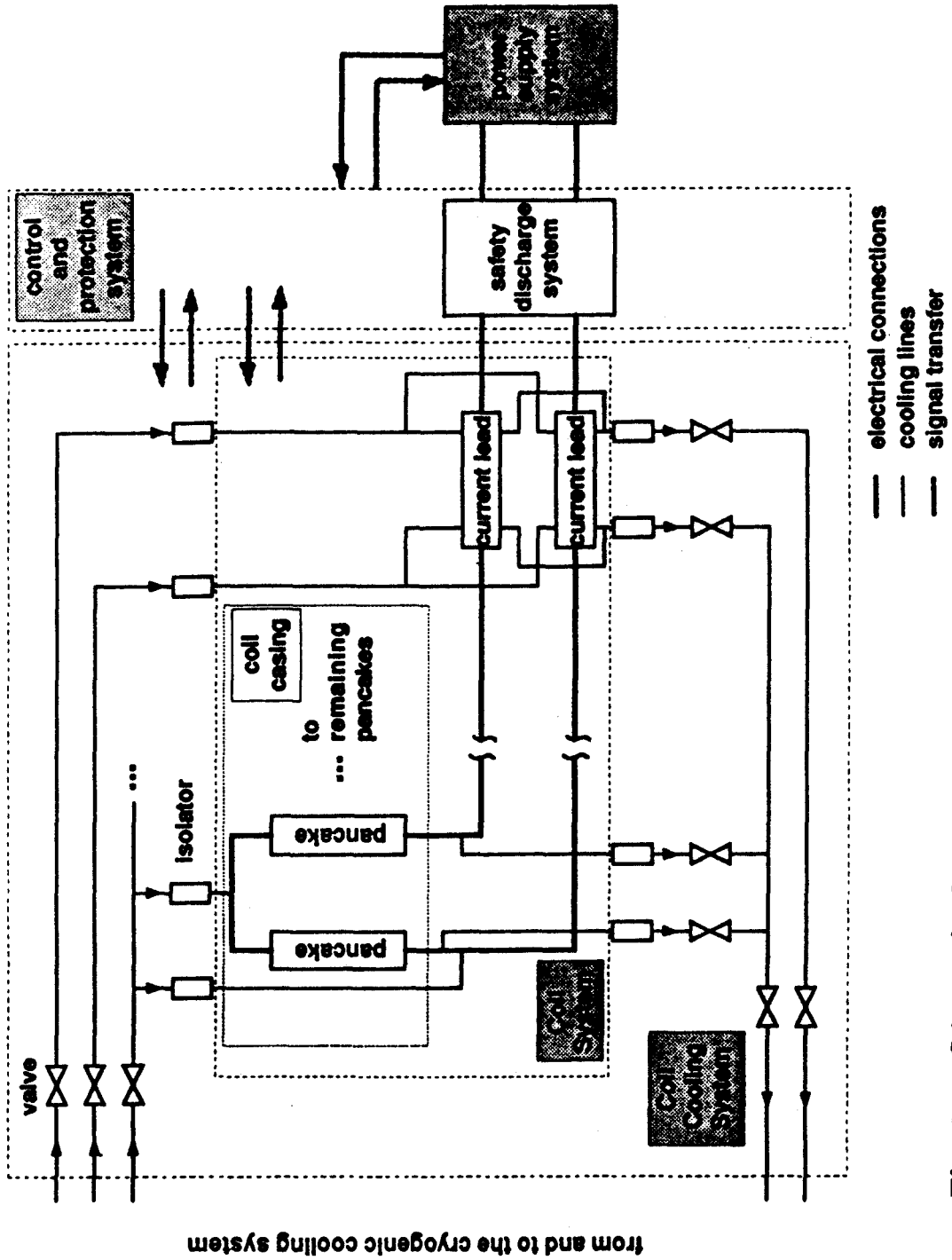
Fig. 2-1 Scheme of a Generic Magnet System
(Based on the Design of the NET TF Magnet System [Bünde 1987])

Each coil contributes to the control of the plasma position and shape, but more than one coil will be required to fulfill a single control function for the plasma. This again suggests that the system of internal coils be considered as a whole and not by breaking it down into single coils.

Each coil within a coil system is treated equally, i.e., as having the same functional breakdown, and the breakdown of a single coil system is shown in Fig. 2–1 for a TF coil. Each coil is expected to consist of several pancakes (*GM*), which are connected in series to form the coil winding. The winding obtains its electrical power from two current leads (*GD*). The pancakes and the electrical connections between them will be cooled, and cooling pipe connections for coolant inlet (*GK*) and outlet (*GA*) are required. Depending on the manufacturing and assembly of the pancakes (e.g., whether a single pancake or a double pancake design is used), those coolant pipe connections may be designed quite differently. For most superconducting magnets, in particular for TF coils, the winding will be embedded in a coil casing (*GL1*) which partially supports the operational loads on the conductor and protects the pancake arrangement against external impacts. A casing for auxiliary devices (*GL2*) may also be required for parts of the cooling system and the instrumentation of the coils [Bünde 1987].

The TF coil cases will be supported by the central support structure (which is not connected to the central stack of PF coils), a gravitational support structure, and an intercoil support structure, which mainly supports the out-of-plane loads† on the TF coils. The entire support structure will be referred to as *BQ*. The PF coil supports are different for coils in the central stack and the outer coils. Central PF coils will be supported by a central support column structure, while the outer coils may be supported by the TF coil case or by a separate intercoil structure. The internal coils are integrated in the TF coil structure.

Electrical instrumentation of the coils (*GY1*) and the current leads (*GY2*) is also included in the coil system. Coolant flow rates, coolant temperature and pressure will be measured at several locations in the cooling system of the

---

† Out-of-plane loads are loads acting in a direction perpendicular to the plane of the coil current.

winding and the leads. Furthermore, each pancake will incorporate instrumentation for voltage and current measurements, ground fault monitoring, and strain gauges for strain and displacement measurements [Dinsmore 1986].

The coolant for each coil system will be provided by a coil cooling system (system *ABK* for a TF coil system and system *ACK* for the entire PF coil system). It can be expected that these cooling systems have to provide cryogenic coolant, such as liquid helium (LHe), liquid nitrogen (LN$_2$) or both. The coolant is provided by a cryogenic coolant system for the entire plant. A coil cooling system consists of the main coolant supply lines for the winding and the leads. The coolant flow rate will be regulated by valves at the inlet and outlet of each main coolant pipe as illustrated in Fig. 2-1. The flow rate in the pancakes will probably not need to be adjusted during operation, but can be adjusted once at the beginning of operation under use of orifices or manifolds as proposed for NET. Since the coil case and the main coolant pipe may have different electrical potential, electrical isolators will be needed between them [Bünde 1987], as shown in Fig. 2-1.

The electrical power for the coils is provided by the power supply system. For the TF coils, alternate coils will be connected in series to reduce the potential for unbalanced (asymmetric) forces on the TF coils under fault conditions. Therefore, and because of the steady state-like operation mode of the TF coils, two power supply units, one for each set of alternate coils, are sufficient. The TF coil power supply system (*ABL*) may be set up as illustrated in Fig. 2-2 [INTOR 1985]. Cooled busbars (*GW*) will be needed to connect power supplies and current leads. Furthermore, a separate protection circuit may be required for each TF coil (in particular when superconducting coils are used), in order to ensure the safe discharge of energized coils in the case of a failure. Such a protection circuit consists of a dump resistor (*GU*) with appropriate cooling and a safety discharge switch (*GS*), and is considered to be part of the protection and control system (*ABY*). The PF coil power supply system (*ACL*) is significantly more complex than the TF coil power supply system since each PF coil follows a different current scenario. This system will be described in more detail in Chapter 3.1.
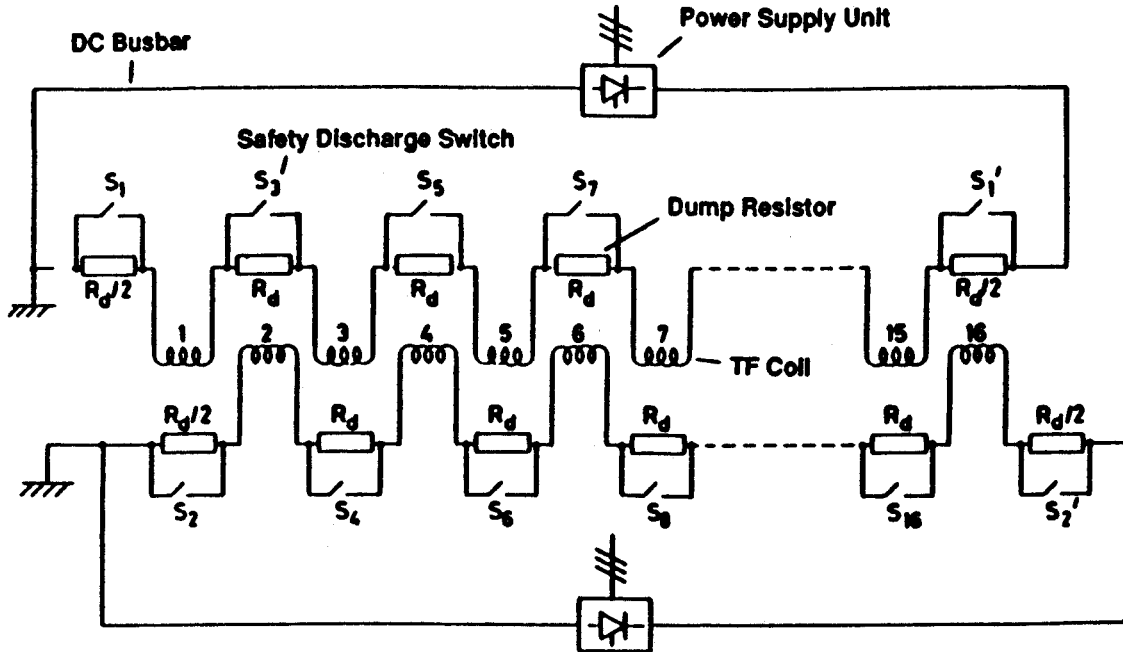
Fig. 2-2. Scheme of a TF Magnet Power Supply [INTOR 1985a]

The last subsystem of the TF or PF magnet system is the protection and control system (*ABY* and *ACY*, respectively). It includes all instrumentation and protective devices not included in the coil system, the coil cooling system or the power supply system, and provides the communication between each of these subsystems for the TF and the PF system. The protection and control systems obtain commands and control signals from higher level control systems, the magnet system, and related reactor subsystems (like the fueling system), and decide upon magnet shutdown when disturbances or failures are indicated. For a superconducting magnet system, this protection and control system will therefore include quench detection modules and a fast external discharge system [Dinsmore 1986]. The PF control and protection system will be significantly more complex, and is described in more detail in Section 3.1.

The choice of the subsystems and the breakdown of the magnet system is important for the clarity of the failure analysis and a good choice may simplify the tracking of failure modes and interactions in the system significantly. For the presented functional breakdown, the boundaries of the coil cooling system and the protection and control system are most difficult to draw. The coil cooling system will have strong connections to other parts of the cooling system. As an example, coolant flow rates, temperature, pressure and the level of impurities in the coolant depend on the coil cooling system and on the overall cryogenic cooling system. However, including the overall cryogenic cooling system in the coil cooling system would destroy the modular structure of the fault trees (one fault tree per coil system), and lead to a system much more difficult to examine. Also, the cryogenic cooling system, although mainly supplying the magnet system, can be regarded as an external supply whose design has little implications for the design of the magnet system.

This is very similar to the external TF coils power supply system which provides power for the two power supply units of the TF coils. However, it is clearly different from the external PF coils power supply system (as will be shown in Chapter 3.1) since its design is deeply connected to the design of the other parts of the PF magnet system.

The boundaries of the protection and control systems should be determined so that instrumentation and control devices are excluded whose functioning is connected to a very high degree to the operation or the environmental conditions in another subsystem. This is, for instance, the case for the instrumentation of the coils (*GY1* or *GY2*), but not for the safety discharge system of the coils (*GU* and *GS*). However, the actions of control or protection devices may still contribute highly to the interactions between systems across the system boundaries as will be seen in Chapter 2.3.

2.2   Failure Mode Analysis of Magnet Systems

In this section, a failure modes analysis of a magnet system is presented as it emerges from the functional breakdown of the magnet system which is described in Chapter 2.1. The analytical method which is used in this study to derive the failure modes is fault tree analysis. Fault tree analysis is now a widely accepted tool for failure mode analysis, but the completeness may be difficult to achieve for complex systems. There have been new approaches to the generation of fault trees, like the Logic Flowgraph Methodology (LFM) [Guarro 1985], where the failure modes of the system are derived from a physical model, and which lead to an improved construction process for fault trees. However, since LFM requires quantification of the progression of system disturbances, and the current database on the operation of magnet systems does not provide such information, simpler methods are currently more rewarding. Fault tree analysis is used in this study like in other programs (see, for example [Bünde 1987a]).

In a fault tree analysis, the fault trees are developed by starting from a postulated "top event" of the system failure mode and progressing downward to lower levels of failures. Lower level failure modes are obtained by answering questions like "which process(es) or failure(s) can cause the top event to occur". By progressing downward, newly derived failure modes become themselves top events of the given level in the fault tree. The procedure stops when further breakdown of the failure modes would not yield any further contribution to achieving the goal of the analysis, or cannot be performed due to lack of knowledge about the failure mechanism(s). Failure modes of the first category will be called basic failure modes. The entire fault tree finally shows the various failure sequence paths whose occurrence yields the top event and gives the logical connections between the failure modes which lead to the top event. The set of tools which is used to present these connections is described in Appendix A.

For the magnet system, the top event is "failure to provide the magnetic field required for plasma operation". This means, that any event which makes the operation of the plasma impossible or unsafe and thereby requires a deviation

from the desired operation schedule during a certain period of time is defined as a failure event. The period between failure initiation and failure clearance is called downtime and can range from a few minutes or hours to years, depending on the severity of the fault consequences. As an example, detected quenches may not necessarily cause damage, and may be associated with short downtimes, while structural coil failures may lead to downtimes on the order of several months.

The top event can be caused by a failure of the TF *or* the PF magnet system to provide the magnetic fields required for plasma operation, and thereby by a failure in any of the magnet subsystems. For this part of the fault tree, which is shown in Fig. 2-3, the failure modes can be described in general as "unavailability of a system" and [Bünde 1987] has used this notation to derive a similar fault tree. The important result from structuring the system and the resulting fault tree in this way, is that the highest levels of the fault trees contain only *OR*-gates, which can simplify the reliability assessment (i.e., the quantification of top event failure probabilities) significantly.

In the following sections, the fault tree structures for the four major subsystems of the magnet system are presented. The TF magnet system is taken as an example, and the differences from the PF magnet system are discussed in the last section.

2.2.1   The Coil System

The functional breakdown of the coil system translates directly into the fault tree structure shown in Fig. 2-4 for a single superconducting coil system. The total number of TF coil systems can be approximately 10 to 20 (it is 16 for NET and 20 for CIT). In this section, the fault trees and the major failure modes for each of the failures in the lowest level in Fig. 2-4 are discussed.

2.2.1.1   Internal Failure in a Single Pancake

The fault tree for a single superconducting pancake, which consists of several turns, has internal support (a conduit), and is designed to be cryostable, is
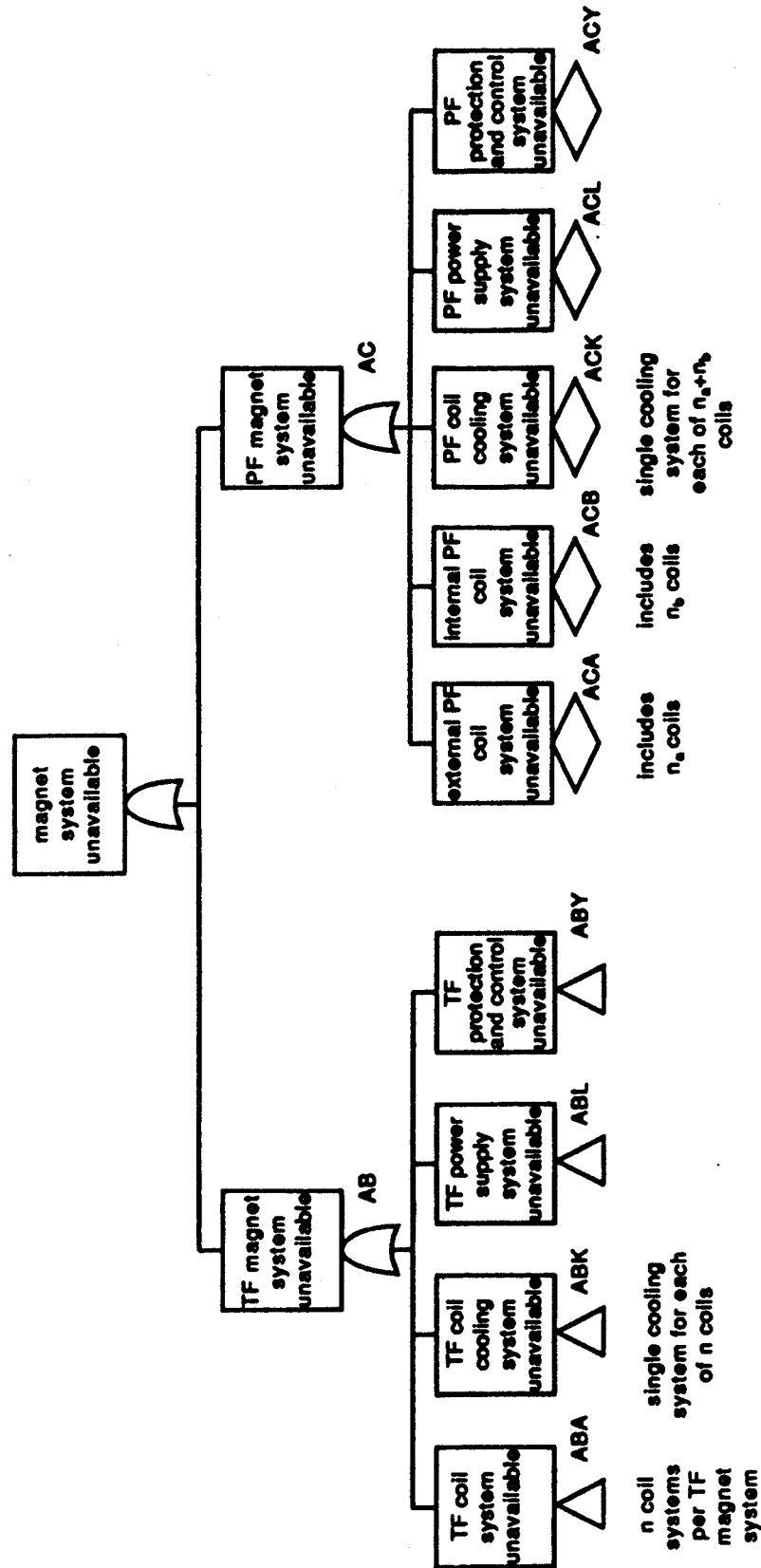
Fig. 2-3 System Fault Tree for the Magnet System (Based on Concept from [Bünde 1987])
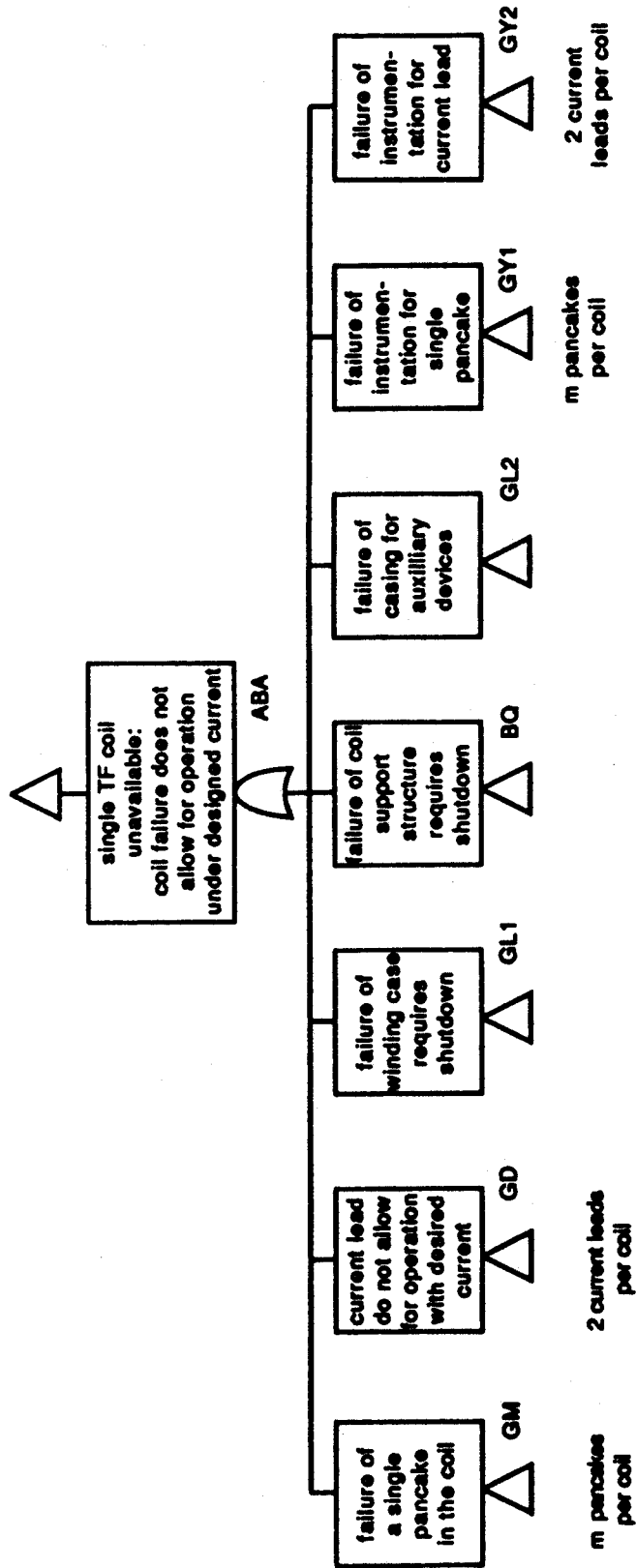
Fig. 2-4 System Fault Tree for a Single TF Coil System (*ABA*); (Modified Fault Tree, Based on Fault Tree from [Bünde 1987])

shown in Fig. 2–5. Cryogenic stabilization means, that the conductor can recover after it has lost its superconductivity for a short time, at least for most possible disturbances. Currently used materials for superconducting magnets of large scale are *NbTi*, and in fewer applications *Nb₃Sn*.

These superconductors must be operated within a three–dimensional parameter space of conductor temperature, magnetic field and current density (see, for example [Raeder 1981]). The boundary curves of this allowable parameter space yield the so called critical values for temperature, field strength and current density which may not be exceeded without losing the superconducting properties of the conductor. Since the maximum allowable temperature is in the range of a few *Kelvin* the conductors must be cooled by a cryogenic coolant such as LHe (usually at 4.2*K*). However, when a conductor loses its superconducting properties locally, its resistance increases rapidly and the resistive spot becomes an internal heat source. This heating could lead to propagation of the resistive zone along the conductor, which is called a quench. This can be avoided in most cases when the conductor is cryogenically stable. Then, a stabilizer which is usually made of copper or aluminum, but at least a material whose resistivity is lower than that of the superconducting material when it is resistive, is needed to carry the coil current for the time the superconductor needs to cool down and recover, so that the superconductor can carry the current again.

In general, a pancake fails when it loses its superconducting properties permanently, develops a short, arcs within itself or to surrounding structures, or when its internal structure fails. Fig. 2–5 illustrates that this can happen when the electrical insulation of the pancake to ground or between turns fails. The insulation to ground will be very design specific and has to withstand high voltages during fast external discharges of the coil. The insulation between turns can fail for several reasons. Mechanical penetrations of the insulation, permanently or under special load conditions (e.g., during emergency discharges) can lead to local shorts and arcing in the coil, e.g., when an insufficiently supported sensor lead is pressed against the insulation, a failure that has already been reported in a magnet failure survey [Thome 1986].
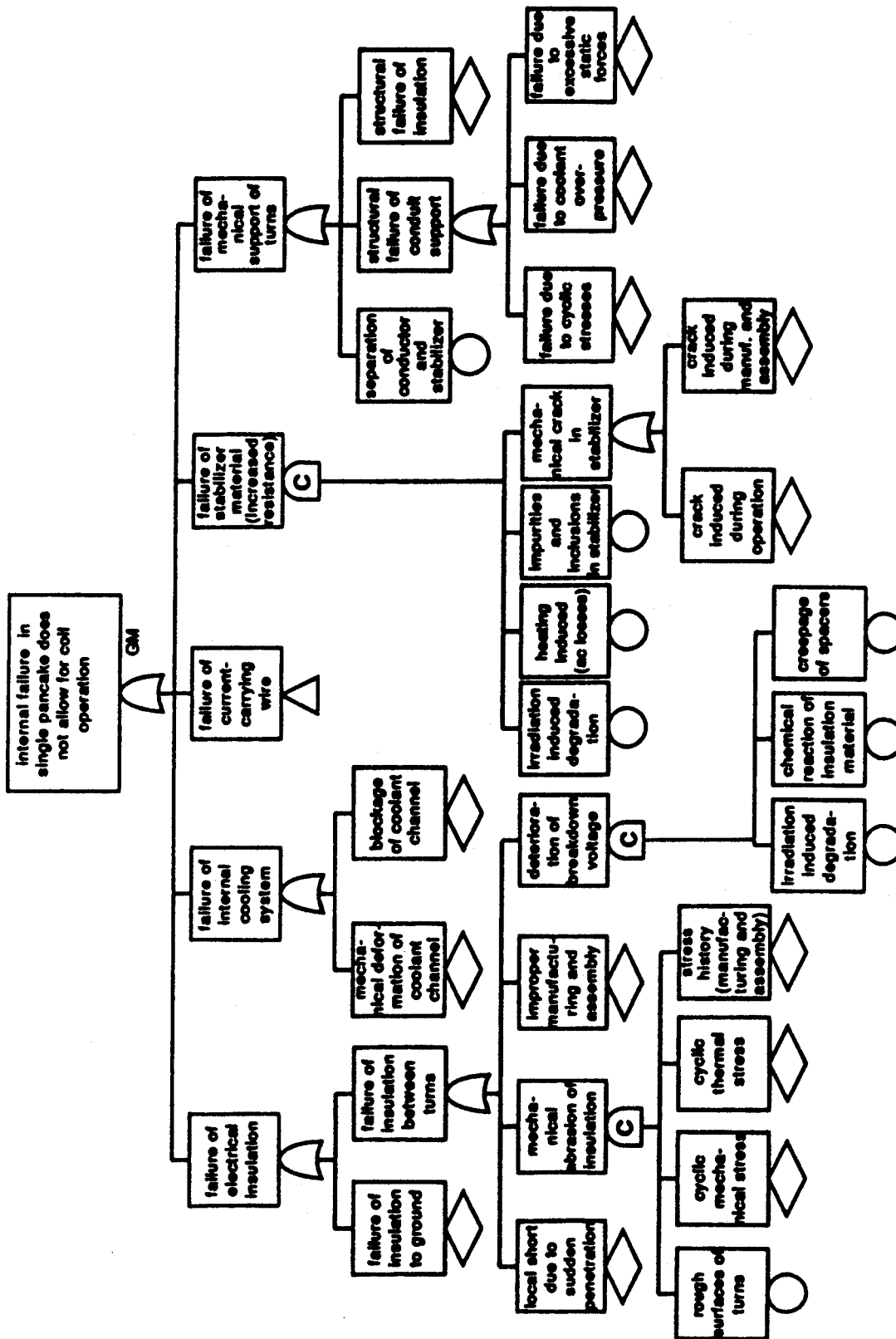
Fig. 2-5 Fault Tree for a Single Pancake (*GM*)

The insulation can also fail due to fatigue from repeated mechanical loading. Cyclical shear stresses in the insulation may lead to cracking, and a severe degradation of the insulating properties. If the insulation bears part of the mechanical load on the conductor, then its structural failure can lead to a loss of the mechanical integrity of the coil. This may be of particular importance for superconducting magnets, where the insulation may bear a larger portion of the total load since the superconducting wire may not be able to support a similarly large portion of the load than the wire in resistive magnets.

The cyclic mechanical and thermal stresses, together with the consequences of previous stresses, e.g., a deterioration of the insulation due to excessive stresses during previous quenches or disruptions, can abrade the insulation steadily, finally leading to wear–out failures. The cyclic mechanical loads on the TF coil insulation results from the interaction of the TF coil currents with the cyclic magnetic field of the PF coils. This causes loads on the conductor, part of which may be transferred to the insulation. In this regard, mainly the shear stresses resulting from the out–of–plane loads on the TF coils are important. But, abrasion can also occur due to differential movements between insulation and turns in circumferential direction, caused by different mechanical or thermal stresses, e.g., due to different elasticity moduli or thermal expansion coefficients.

Abrasion is supported when rough surfaces of the turns are present, which is determined by manufacturing, assembly or design tolerances on surface quality. Differential movements can also be reduced when the turns are tightly packed [Hsieh 1978]. This failure behavior is an example of a situation where multiple continuous effects or continuous combinations of them may lead to the failure of the entire part. Such a relationship is referred to by a CAND–gate notation [Siu 1988], which will be retained for the remainder of this study. Improper assembly and manufacturing of pancakes may also lead to insulation failure. This has been reported in a failure survey [Thome 1986], where in one case the insulation in a coil was even locally missing. Also, flaws or metal inclusions, etc., may occur but should be detectable during the burn–in phase of the magnets. The importance of the assembly and manufacturing process emphasizes the need for an extensive testing and quality control program of the magnets before they are implemented and operated in the final plant, so that early failures can be detected and repaired more easily.

The breakdown voltage of the insulation can be deteriorated continuously by multiple continuous effects. Depending on the choice of insulation materials, it can be very sensitive to irradiation, e.g., due to radiolytic decomposition of organic insulations or glues [Hsieh 1978], or undergo chemical reactions with surrounding material, e.g., organic glues. The breakdown voltage can also be lowered by a reduction of the distance between surfaces of different electrical potential, e.g. when coolant channel spacers experience creep. Also, if cooling channels were used within insulation between turns (which is not assumed here) a warmup of the coolant may reduce its breakdown voltage, in particular for helium coolant.

The pancake can also fail when its internal cooling channels fail. The cooling channels can be deformed by sudden mechanical loads on the conductor (e.g. disruption loads) or overpressurization. Overpressure could for example occur during quenches and fast external discharges when the entire coolant heats up and causes a fast pressure rise when the pressure is not relieved by rupture disks or similar devices [INTOR 1985a].

Furthermore, a blockage of cooling channels can arrive from the accumulation of impurities like abraded material or from the external cooling system. Also, ice can be built up at bottlenecks of the cooling system, e.g., impurity water or N_2 in liquid nitrogen cooled systems, or also O_2 or N_2 impurities in a system cooled with liquid helium.

A very important failure mode of the pancake is the failure of the current carrying superconducting wire itself, for which a fault tree is shown in Fig. 2–6. Either a structural failure of the wire or a degradation of its current carrying capability can lead to the top event, but the importance of single failure events for causing the top event strongly depends on the chosen superconducting material, which is *NbTi* or *Nb₃Sn* for current magnet systems.

A degradation of the current carrying capability, i.e., an increase in the resistivity of the conductor or a reduced parameter operation space for the temperature, magnetic field, and current density can be induced by three different continuous effects. In general, *Nb₃Sn* is capable of withstanding a

higher magnetic field and carrying a larger current density than *NbTi* at the same temperature. However, the critical current density for Nb_3Sn degrades rapidly above a certain neutron fluence limit as the result of radiation induced disorder while *NbTi* is essentially insensitive to irradiation [Gross 1984, Salpietro 1987]. Also, the current carrying capability of Nb_3Sn is very sensitive to strains. In this regard, the manufacturing and assembly process is of importance, but strains during operation can also damage the conductor.

Furthermore, heating of the superconductor can contribute to failure initiation. Potential heat sources for the conductor are alternating current (AC) losses during operation, heating due to movement of the current carrying wire in a magnetic field, and nuclear heating. AC losses are caused by changing magnetic fields and are particularly high during disruptions. Two types of AC losses can be distinguished: hysteresis and eddy current losses. Hysteresis losses, are about proportional to the diameter of the superconducting wire and and of the stabilizer, and lead to internal and external heating of the current–carrying wire. Eddy current losses can be significantly reduced by adding barriers of high resistance (e.g., *CuNi*) to the stabilizer [Raeder 1981].

Heating of the conductor can also be caused by frictional heating because of differential movements between insulation and conductor [INTOR 1985a] (due to different thermal expansion coefficients and magnetic loads), and can arrive from movements in the winding case, e.g., due to unstable fixing or lack of tension in the packing under magnetic loads [INTOR 1982a]. Also, nuclear heating, i.e., heat derived from prompt gamma capture in the conductor and adjacent structures can contribute to conductor damage.

The current carrying wire can also experience structural failure, which can be caused by the combined effect of strain and irradiation damage. In particular Nb_3Sn is an inherently brittle material, and the total strain resulting from manufacturing, assembly and operation must be kept below 0.2% [INTOR 1985a]. This means, that the strain history is of high importance for Nb_3Sn magnets, and the conductor must be well constrained during operation.
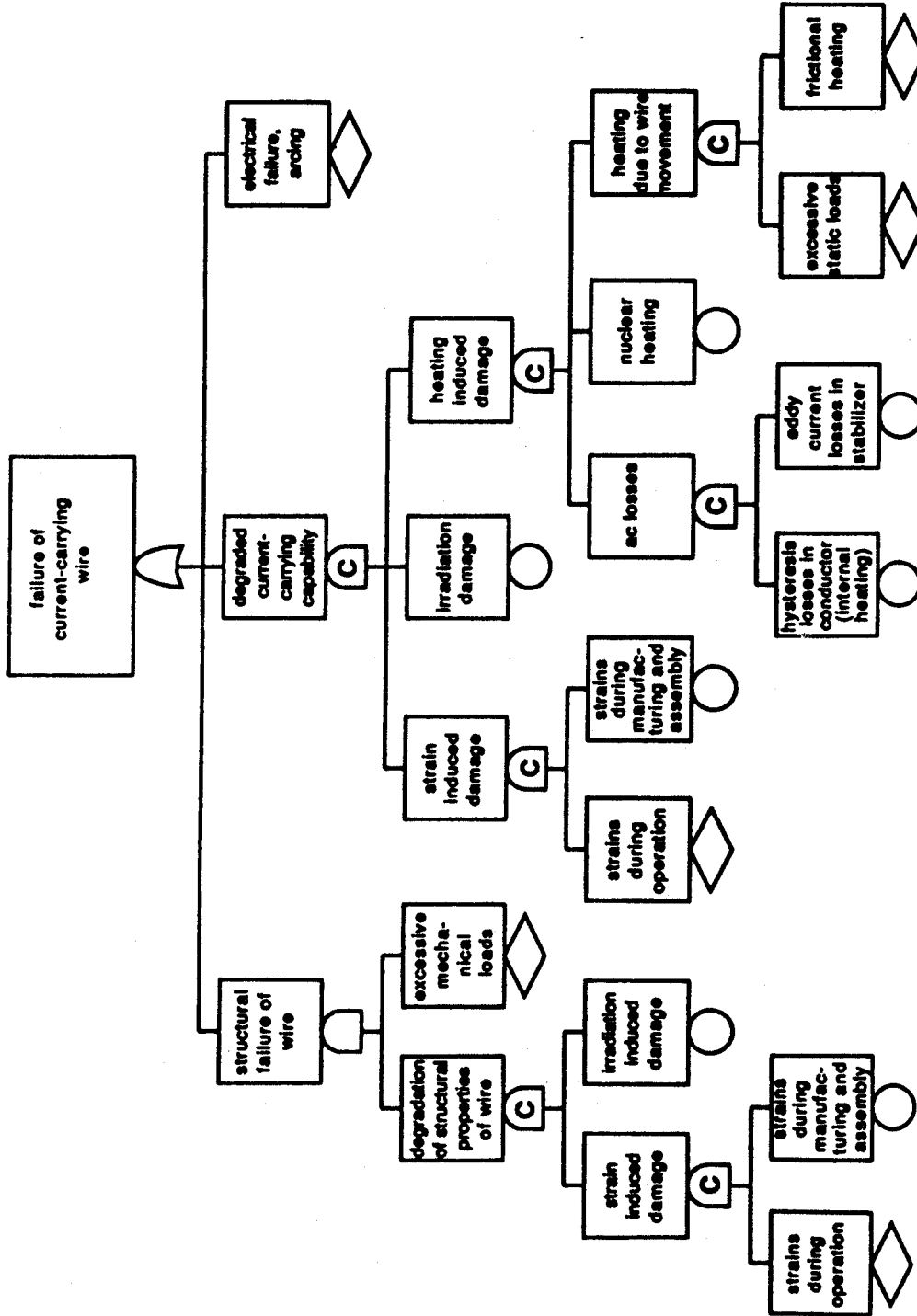
Fig. 2-6 Fault Tree for Failure of the Current-Carrying Wire of a Superconducting Coil

The effect of irradiation on the structural properties of *NbTi* and *Nb₃Sn* needs more study. Cracks developing in the conductor material could lead to structural failure. Cracks reduce the effective current carrying cross section of the conductor, leading to higher local current densities, increased local mechanical loads, and possibly quenches.

Like the wire, the stabilizer can fail to perform its task when its resistivity increases during operation, that means more heat is produced in case of a quench since the process of current transfer from the wire becoming normalconducting to the stabilizer would be delayed and the current carrying stabilizer would produce more heat as well. In most applications, aluminum or copper are used as stabilizer material, and the biggest problem may be the irradiation induced damage [Raeder 1981]. However, cracks in the stabilizer resulting from cyclic or excessive operational loads, or from errors during manufacturing or assembly, can lead to an increased resistance since the effective current carrying cross section is reduced. The crack propagation may then even be accelerated by the increased current density, heating and mechanical loading of the remaining effective cross section.

Impurities or inclusions in the stabilizer material may lead to a higher resistance of the stabilizer than rated at the beginning of operation. Another, although nonpermanent and less significant contribution to an increased stabilizer resistance can be AC losses, which may lead to an increased operating temperature of the stabilizer and thereby higher resistivity. Finally, the pancake fails if it looses its mechanical support. This can be caused by separation of the conducting material from the stabilizer due to deterioration of the bonding strength [INTOR 1982a], or structural failure of the insulation if it is used as additional conductor support [INTOR 1985a].

A variety of conductor designs include a conduit support structure [INTOR 1982], so that a structural failure of the conduit would lead to the failure of the pancake. The conduit structure can fail due to fatigue caused by cyclic mechanical loading, or by sudden excessive electromagnetic forces, e.g., during a quench or disruption. Furthermore, the conduit has to withstand large internal

coolant pressures (depending on the specific design) that may occur during fast external discharges of the coil [INTOR 1982a].

2.2.1.2 Failure of the Current Leads

The design of current leads for fusion magnets strongly depends on the conductor and cryostat design. In general, the leads need to cross the cryostat boundary and will require flexible support to allow the movements of conductor and leads under operation. This may be accomplished by bellows [Ulbricht 1987].

The leads will connect normal and superconducting wires, and a complicated cooling system (often with two coolants, LN_2 and LHe), is required. Therefore, the current leads are considered to be a very sensitive element in the design of magnet systems [Bünde 1987]. Failure of the current leads may be caused by failure of the insulation, a structural failure of the lead support and/or encapsulation structure, a structural failure of the lead itself, or when the leads are insufficiently cooled [Bünde 1987]. A fault tree for the current lead is shown in Fig. 2-7.

Such failures of the current leads are of high concern, since local discharges or arcs could develop, which could effectively shortcircuit the entire coil and involve the deposition of most of the coil energy in a highly concentrated manner at the leads (see, e.g., [Arendt 1981]), since no external safety discharge can be initiated.

A particular problem of leads cooled with helium may be the temperature sensitivity of the breakdown voltage of helium [Arendt 1981]. In order to prevent discharges through the coolant, the helium temperature needs to be well controlled, in particular during fast external discharges of the coil which may lead to heating of the coolant and high voltages at the leads.
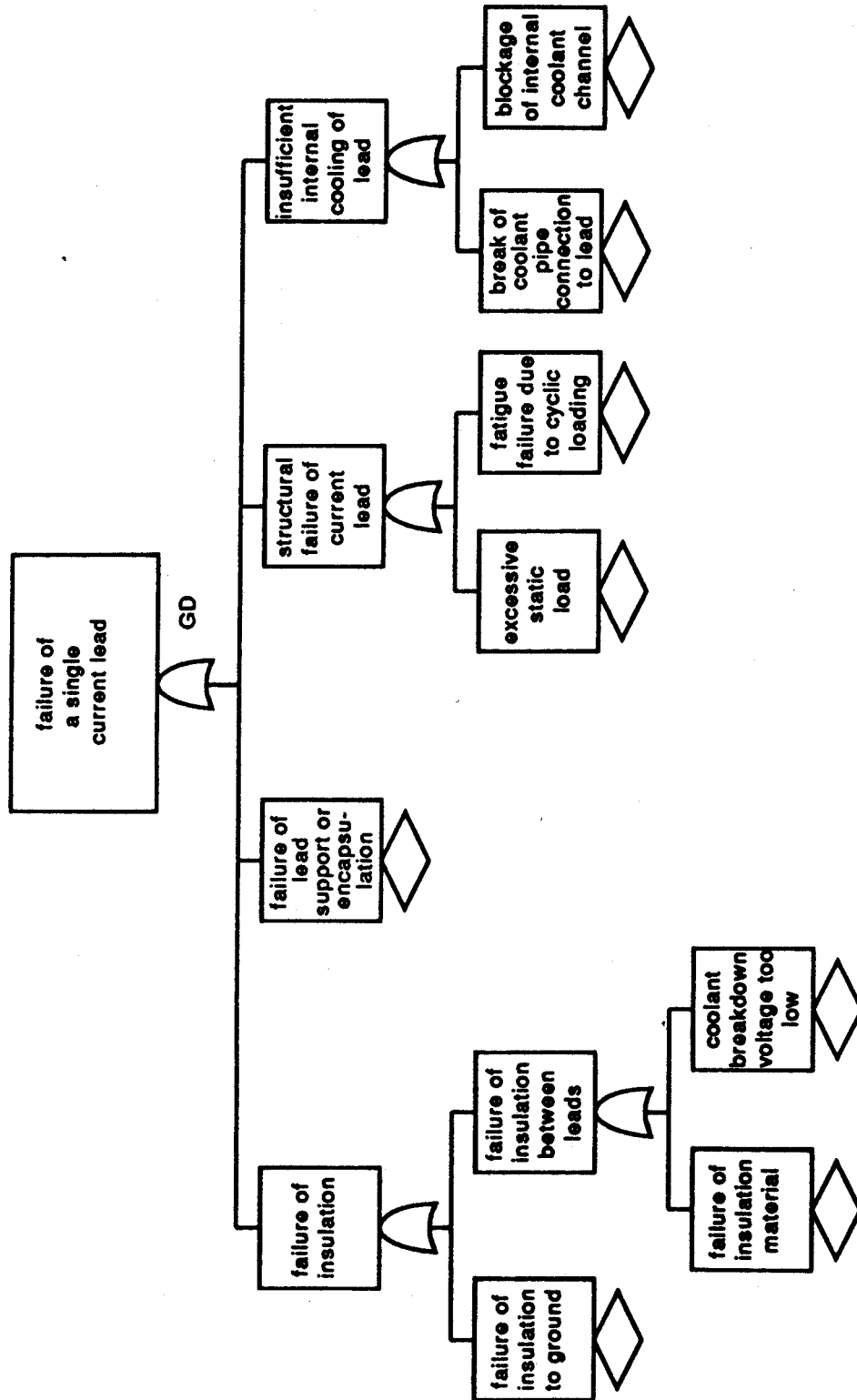
Fig. 2-7 Fault Tree for Failure of a Single Current Lead (*GD*)

2.2.1.3 Failure of Coil Casing

The casing of the coils supports the operational loads on the conductor and transfers them to the coil support structure, thereby constraining conductor movement. The coil case experiences static (e.g., the centering force on the TF coils) and cyclic loads (e.g., the out–of–plane loads on the TF coils), which may lead to a break of the casing due to fatigue or excessive static stresses (e.g., during quenches or disruptions). Also, the case will have to be cooled since the eddy current losses in the case may be high. This causes a potential for pipe failures like leaks or pipe breaks [Bünde 1987]. The energy losses can be reduced by adding barriers of high electrical resistance to the case, although this may reduce the mechanical strength of the casing.

2.2.1.4 Failure of the Coil Support Structure

The TF coil support structure fails if the central support structure, the intercoil support structure or the gravitational support structure fails.

The failure modes of the central support structure depend on whether the bucking or the wedging concept is chosen. With the bucking concept, the loads from the TF coils are transferred to the support structure for the stack of central PF coils. The centering (inward) force, and the torque on the TF coils are well supported in this design, but the differential rotational movements between both support structures are undesirable. Therefore, although JET has used a bucking design, the wedging concept is proposed for machines like NET, and is under discussion for the International Tokamak Experimental Reactor (ITER), mainly driven by reliability concerns about the bucking design.

With the wedging concept, there is no direct contact between the central support structures of the TF and the PF coils, and thus friction between these structures is avoided and the PF coil support is free to expand radially. Instead, the forces and moments are transferred between adjacent coil cases by friction. Since the out–of–plane loads on the TF coils are cyclic, there is a potential for fatigue failure of the support structure. Also, repeated relative motions may lead to wear at wedging surfaces. Furthermore, asymmetric loads,

e.g., caused by nonsimultaneous discharges of the TF coils, may lead to local displacements of the wedges, and the gap between the TF and the PF support structure may be lost. In addition, the strength of the material may degrade due to irradiation, depending on the shielding between the support structure and the plasma.

The intercoil structure is also subject to cyclic loads and high static loads in the event of asymmetric loads on the TF coils, which can lead to structural failure. Structural constraints in radial directions, can lead to thermal stresses on the intercoil structure.

Flexibility in radial direction is also important for the gravitational support structure in order to allow for thermal expansion of the coil and to reduce the thermal stresses. Furthermore, cyclic rotational movements of the coils need to be reacted, and the static weight of the coils is to be supported. The vertical loads on the coil structure during disruptions can be significant and can reduce the available margin for operational loads permanently. Therefore, the gravitational support structure may fail due to fatigue (taking into account the stress history) or overloads.

2.2.1.5 Failure of Electrical Connections (Joints)

There are three failure modes for electrical connections with coolant inlet or outlet [Bünde 1987]: the coolant piping (mainly welds) could leak or break, the electrical connection could break down due to insulation or material failure, and mechanical loads, e.g., arriving from constraints on the movement of the joints, can cause a break of the joint.

2.2.1.6 Failure of Casing for Auxiliary Devices

A casing for auxiliary devices like joints or instrumentation may be needed to insulate them from areas of different electrical potential and protect these devices against external impacts. Such a casing has been proposed for the NET design. The failure modes are the break of the casing itself [Bünde 1987] or a breakdown of the electrical insulation of the casing.

2.2.1.7 Failure of the Protection and Control Equipment

The protection and control equipment of the coil system has to detect and transfer signals to higher level control and protection systems (like e.g., *ABY*). The mechanisms which can lead to the failure of this signal detection and distribution process are very similar for all kinds of measurements when the signals are processed and forwarded electrically. Fig. 2–8 shows a fault tree for such systems. The top event of this fault tree is the failure of the system to provide the correct signal as input to another control system, i.e., the wrong indication of an existing condition or no indication of an out–of–bound condition. The processed signal can either be a continuously sensed signal or a signal describing whether a limit condition is reached. The top event can then occur when the sensing equipment itself fails or the signal is deteriorated during the following signal processing stage.

A failure of the sensor hardware, which will depend on the type of measurement, will cause an instrumentation equipment failure. Hardware failure will also strongly depend on the environmental conditions at the sensor location, and thereby on sensor placement and the robustness of the sensor and measurement principle. Calibration errors will be important, and can be caused by a shift of calibration points during operation or by errors in the initial calibration (mainly human errors). This may be of particular importance for the setting of limit values [Schnauder 1987], and can lead to consistent systematic errors. Also, in case of active sensors requiring external energy, the placement of sensor leads will be important for failures involving sensor power outages. Therefore, the placement of the sensors and leads, and their assembly may have a strong impact on the reliability of the sensor instrumentation.

Signal processing failures can also occur due to hardware failures or when the signal is deteriorated by external sources. Hardware failures include failures of signal transmitting cables and signal amplifiers. The signal can be deteriorated during processing when signals deciding upon the same issue are coupled by the instrumentation system, leading to dependent signal processing. Furthermore, electrical noise from the environment, e.g., resulting from magnetic fields, flux jumps or coil motions may lead to the misinterpretation of signals.
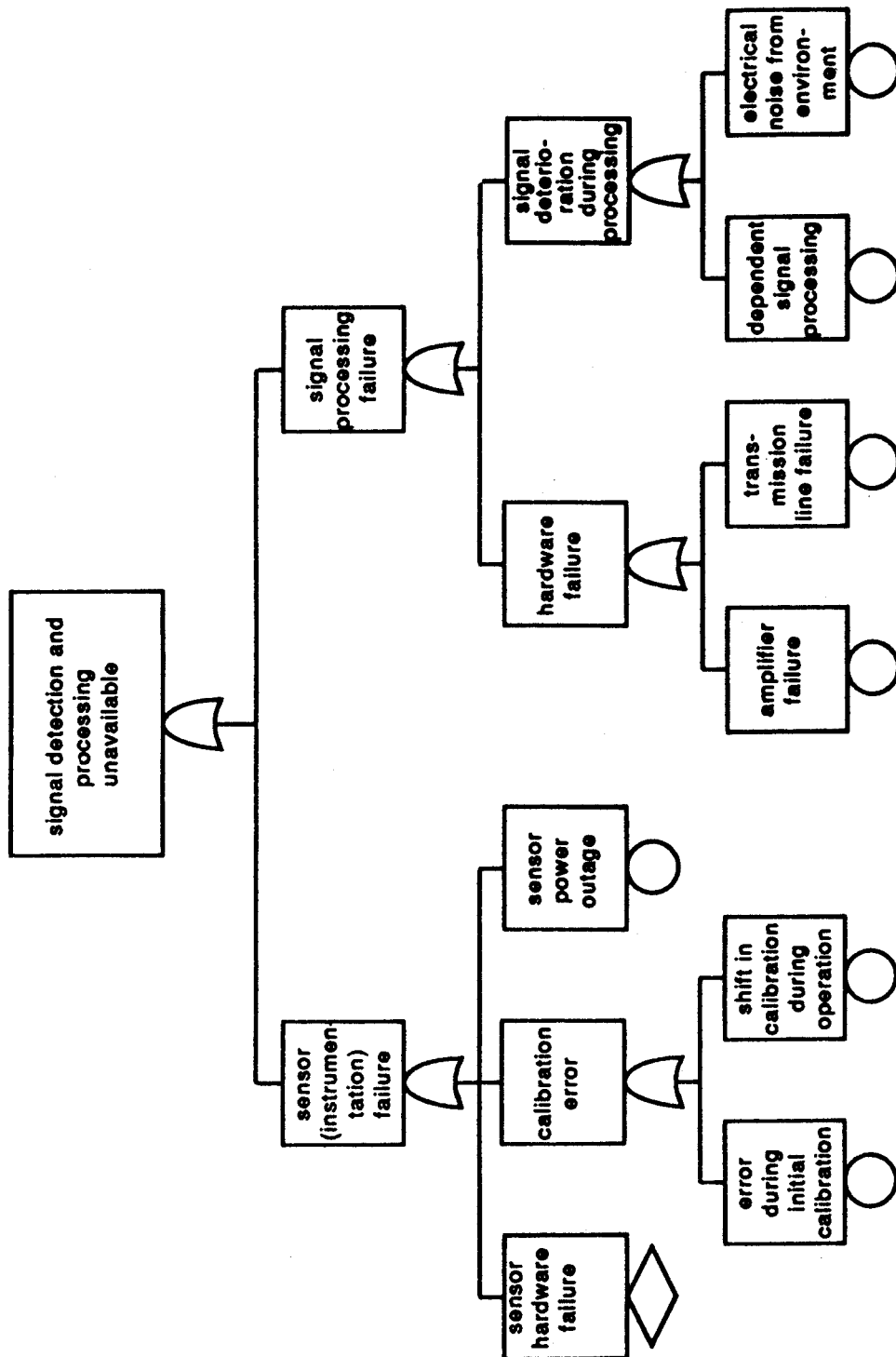
Fig. 2-8 Fault Tree for the Unavailability of Signal Detection and Processing

As an example, it may be difficult to distinguish between a coil quench or a short circuit from a noisy signal. Again, the hostile environmental conditions for the sensors need to be taken into account when sensor equipment is selected.

Clearly, the failure rates for the measurement and processing of a single variable also depend on the monitoring, repair and maintenance procedures. Voting logics (like 2–out–of 3 voting logics proposed for most of the NET instrumentation [Bünde 1987]) may be used to rely less on single measurements and to enhance the overall reliability. Also, the principles of physical and functional diversity need to be applied to increase the availability and reliability of the system.

It could even be argued that enough redundant sensors should be placed in the system to make repairs due to signal processing failure a rare event, since switching from a failed to a back–up sensor would be sufficient to keep the operation going after a sensor fails. But, this would probably be unacceptable for commercial reactors, and functional diversity of sensors, i.e., sensors measuring the same variable but based on different physical measurement processes, and cross checking of signals is preferable. However, common mode failures may still be possible and reduce the reliability of such a system.

2.2.2 The Coil Cooling System

The coil cooling system (ABK) is unavailable when it cannot provide sufficient cooling for the coil winding or the current leads. The cooling systems for the coil winding and the current leads are not connected within the boundaries of the coil cooling system, except by the overall plant cryogenic cooling system if the same coolant is used, and therefore failure of any of these systems can lead to the top event independently. Furthermore, the current leads cooling system fails when its LHe or LN_2 supply system is unavailable.

Failure of any of the cooling systems with a single coolant can then occur due to a failure of the main coolant supply line, the supply lines to a single pancake arrangement or a current lead, or due to failure of its regulation and control system. This observation allows for a modular structure of the fault tree

for the coils cooling system as it is illustrated in Fig. 2–9. However, while the fault tree structure for a coolant supply line or a regulation and control system is the same for each cooling system, the failure rates for the basic failure modes will depend on the specific device used, e.g., there will be differences in the failure rates of devices supplying LHe or LN_2, and due to the location of the device, i.e., depending on its environment. Therefore, the reliability output for the top event of each subtree can be different, but the logical combinations of events leading to the top event will be the same.

Fig. 2–10 shows one of these subtrees, the fault tree with the top event "unavailability of a single coolant supply line". This top event can occur when the cooled device is insufficiently supplied with coolant, there is a loss of support or casing for the coolant distribution or regulation network, or the electrical insulation of the coolant supply line breaks down. Insufficient coolant supply can be caused by a loss of coolant flow or a loss of coolant. However, it needs to be decided which disturbances in the coolant supply are tolerated, e.g., whether a "small" leak needs to be repaired immediately or can be tolerated until the next routine shutdown.

Leaks leading to loss of coolant may occur in regulating devices like valves and manifolds or in the piping, where welded connections may particularly contribute to leakages and the quality of manufacturing and assembly becomes important. The coolant flow can be lost when the cooling pipes are deformed, e.g., due to sudden excessive loads or when coolant spacers fail structurally, e.g., due to fatigue combined with creepage. Furthermore, the coolant lines can be blocked when coolant impurities accumulate or ice builds up, e.g., water, O_2 or N_2. This is most likely at bottlenecks like regulating devices or coolant inlets and outlets.

Structural failure of the support or casing of the coolant distribution network can arrive form cyclic thermal and mechanical loads or from sudden excessive stresses, e.g., unbalanced electromagnetic forces in the case of a discharge of a single coil. The electrical insulation of the coolant pipes to the surrounding structure (which may have a different electrical potential) will also

FT1: failure of a cooling system with a single coolant (LHe or LN$_2$)
FT2: single coolant supply line unavailable (e.g. main supply line or supply line to a single lead)
FT3: failure of the coolant distribution system (fault tree given in Fig. 2-10)
FT4: failure of the control and regulation system (fault tree given in Fig. 2-11)
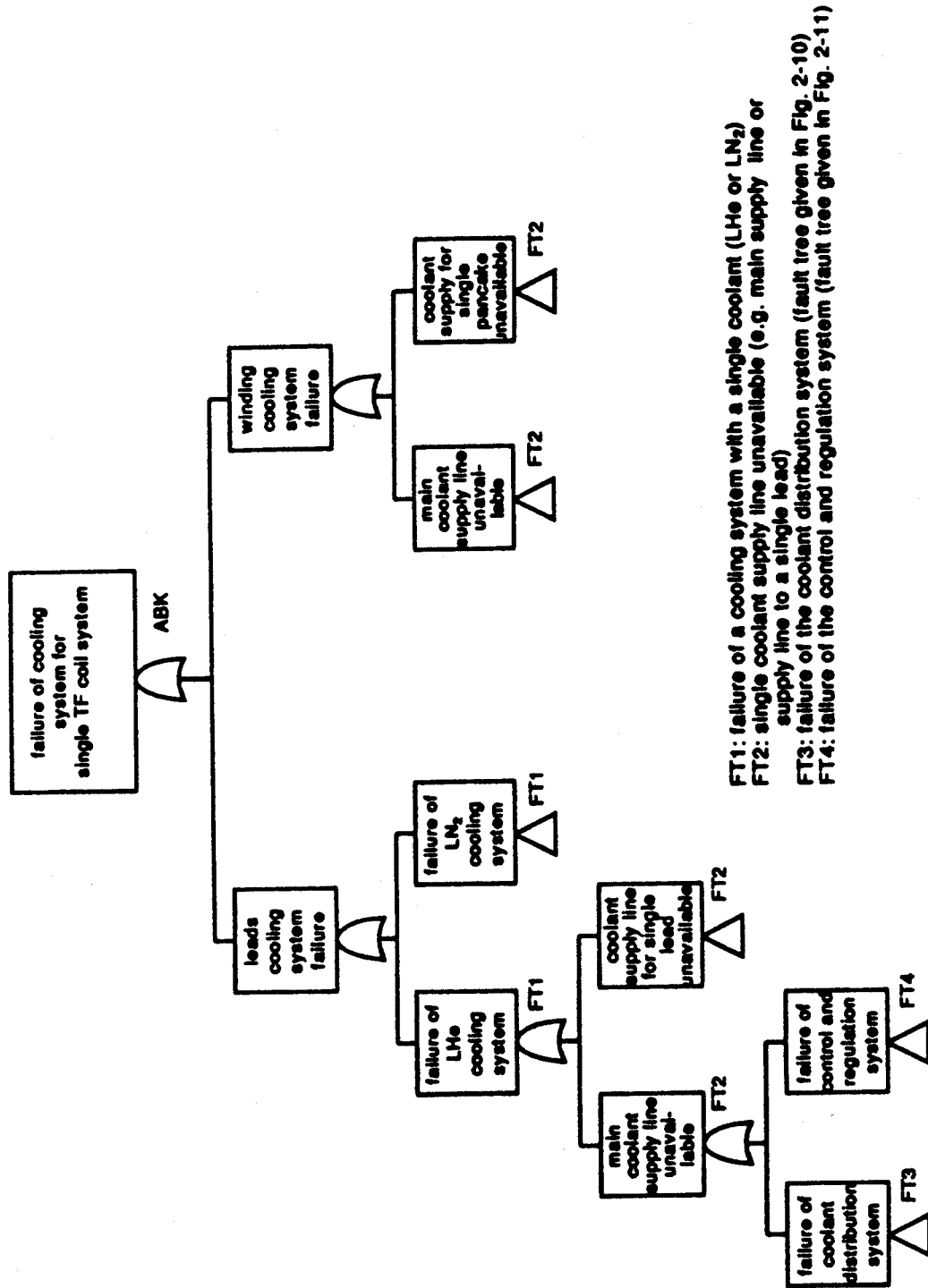
Fig. 2-9   Generic Fault Tree for the Coil Cooling System of a Single TF Coil (*ABK*)
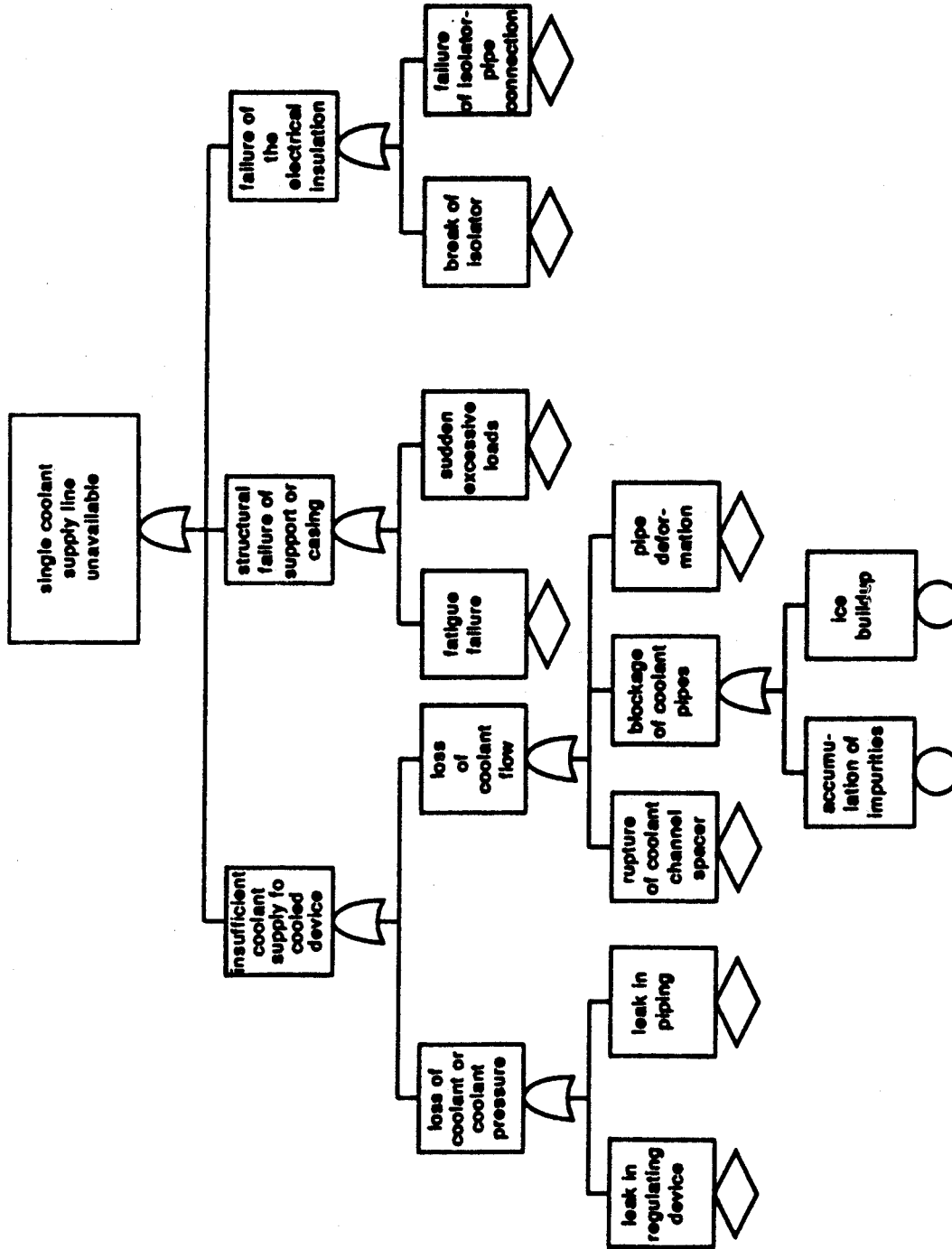
Fig. 2-10 Fault Tree for the Unavailability of a Single Coolant Line

be necessary. The NET design uses isolators at the coolant in- and outlets of each supply line to a single pancake arrangement or a single lead [Bünde 1987], as illustrated in Fig. 2-1. A break of the isolator or structural failure of the connection between isolator and coolant supply line may lead to a failure of the insulation.

A fault tree for the failure of the control and regulation system of a coolant supply line is shown in Fig. 2-11. A failure of the regulating device(s) or the monitoring instrumentation can lead to the top event. The regulating devices may be passive or active, like only one-time adjusted manifolds or valves, and there can be several such devices in a single coolant supply line. Passive and active devices may fail due to miscalibration or wrong initial adjustment, which can be caused by human error. Also, such devices can experience shifts in the calibration during operation. For active devices with moving parts, erroneous movements can lead to failure. Such movements can be caused by mechanical problems, e.g., wear or increased friction in moving joints during operation, leading to conditions where no or only limited movement is possible anymore. Also, signal processing failures, e.g., the misinterpretation of command signals, may cause erroneous movements.

The cooling system instrumentation can fail when any of the pressure, temperature, or mass flow rate measurements at the coolant in- or outlet are unavailable. However, the principle of physical diversity of measurements may be used here, and the *OR*-gate in the fault tree may be replaced by a 2-out-of-3 decision logic, i.e., only two of the three measurements are required for the controller [Bünde 1987]. Each of the sensors could also be designed redundantly. The fault tree for a single measurement failure is provided in Fig. 2-8.
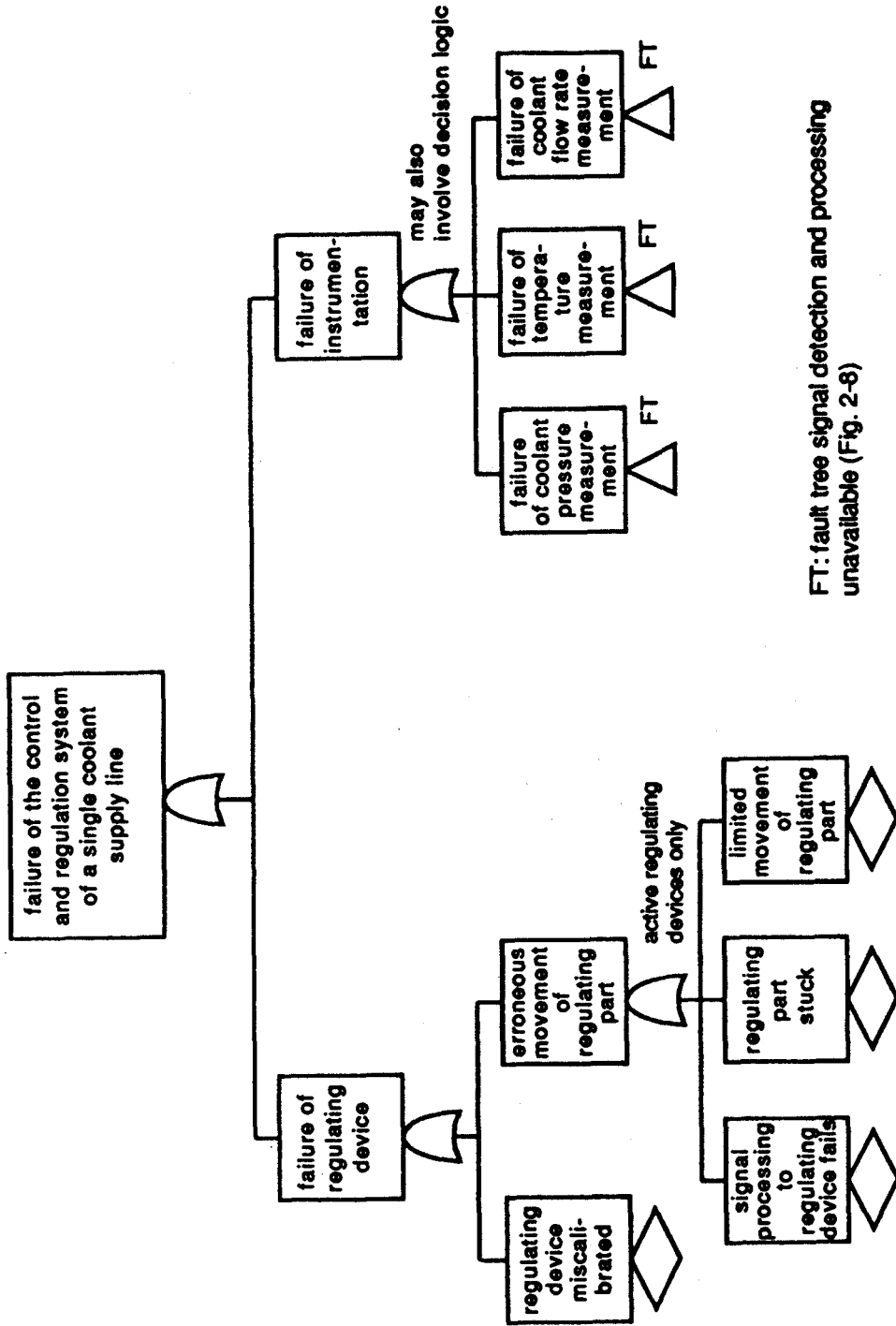
Fig. 2-11 Fault Tree for the Control and Regulation System of a Single Coolant Supply Line

2.2.3 The Power Supply and Control System

The power supply system of the TF coils, which is illustrated in Fig. 2–2, will become unavailable when a power supply unit or the busbar network fails. The DC power bus can fail when it is insufficiently cooled, a structural failure like a wire break occurs, or the insulation fails. The failure modes of a power supply unit are not broken down further, since they will depend strongly on the internal electrical layout of the power supply unit, i.e., its thyristors, diodes, resistors, etc.

The TF protection and control system, for which a fault tree is shown in Fig. 2–12, has to control the TF coil current during ramp–up, periods of constant current, and current ramp–down. Therefore, only a single variable needs to be controlled, which furthermore changes very slowly, and the breakpoints for coil energization and deenergization arrive from a higher level controller. Then, the TF coil control system fails when a current control module becomes unavailable or the communication between the control module and the power supply is unavailable.

There are also three systems which are safety related and belong to the protection system. In order to avoid excessive unbalanced forces during coil quenches, a quench detection module uses information provided by the pancake instrumentation about the current imbalances in the coil to decide upon the initiation of mitigating action. This action is likely to be a fast external discharge of all coils, or at least of those coils that are connected in series [Dinsmore 1986]. However, the fast external discharge system can be unavailable due to equipment failure or failure of a protection module.

The equipment consists of the safety discharge switch and a dump resistor. Its failure modes are hardware failure of the switch dump resistors or of the signal processing to the switch (fault tree given by Fig. 2–8). Assuming that the switch has to open on demand (in case of a fast external discharge command), it can either be stuck open or closed or it may function but vibrate and cause arcing at its contacts. The dump resistor can fail due to insufficient cooling and overheating during a fast external discharge, or when a mechanical
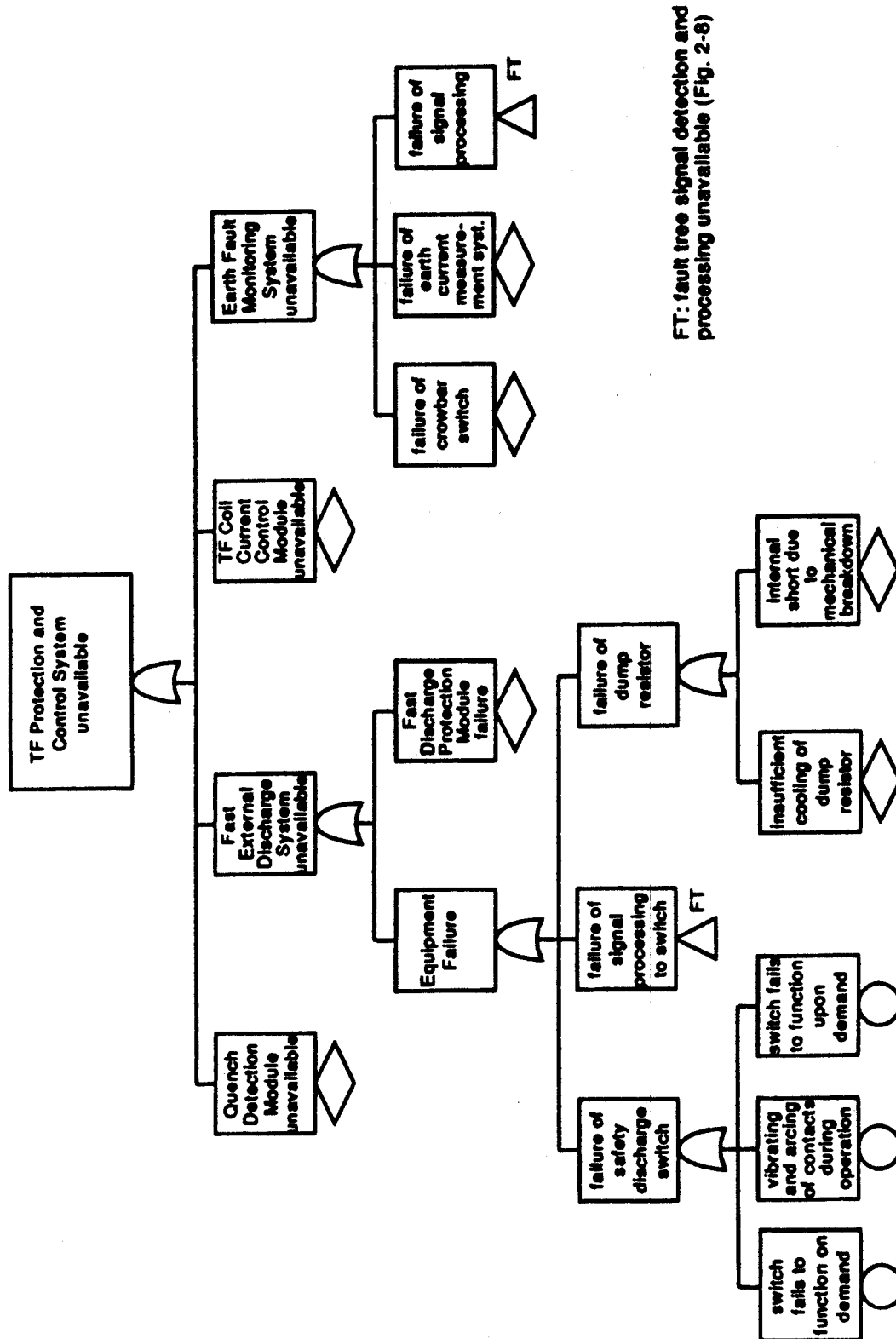
Fig. 2-12 Fault Tree for the Protection and Control System of a Superconducting TF Coil

failure leads to an internal short, reducing the resistance of the resistor (since then the discharge will take longer).

A fast discharge protection module [Dinsmore 1986] then checks the coil conditions during the discharge and decides upon continuation of the discharge. It may therefore be useful to install an adjustable resistor instead of a constant resistor, so that the protection module can adjust the resistor to the coil voltage and can achieve the best possible current decay or energy removal time. Since a rheostat may not be practical because of the high discharge currents, such an adjustable resistor may be made up of a collection of resistors and switches.

The ground fault monitoring system has to sense currents in the neutral conductor and command the closure of a crowbar switch, by which the coil is effectively bypassed. Thus, any failure of the crowbar switch or of the current measurement and signal processing system can lead to outage of the earth fault monitoring system.

2.2.4 Discussion

2.2.4.1 TF Magnet Failure Analysis

It has been the objective of the failure mode analysis in the previous sections to give an overview of failure modes of a magnet system in order to allow to identify areas of particular interest to the designer. It is found, that the fault trees contain mostly *OR*–gates at higher level of failures. At lower levels, several failures (or states of performance degradation) are caused by continuous combinations of multiple variables. Often, such failures involve cyclic mechanical loadings of equipment under severe environmental conditions. Therefore, a lifetime or reliability analysis will be of high importance, and constant failure rates may not be sufficient to describe the failure behavior arriving from such effects like irradiation and fatigue.

The environmental conditions are also a major factor for a large number of failure modes of the instrumentation and signal processing. Also, the logic used to decide upon control actions on the basis of multiple measurements, the repair

logic and the maintenance schedule will determine the reliability of the instrumentation. Manufacturing and assembly tolerances and errors may also have large impact on the reliability of the magnets. This suggests, that extensive testing of the coils should be performed prior to their installation in the fusion device, in order to detect and repair burn–in failures caused by manufacturing and assembly errors with reduced efforts and costs. This is also of importance since the impact of human errors in the calibration or limit value setting for instrumentation and regulating devices can then be reduced.

The failure mode analysis also demonstrates the importance of adequate cooling of electrical equipment that can be heated during operation (e.g., by AC losses). Furthermore, these effects show the importance of an interactions analysis, since failures of electrical equipment may be related to those of the cooling system, or more importantly, mechanical loads on TF coil structures can stem from the operation of the PF coils. The latter effect will be further analyzed in Chapter 2.3.

In summary, the qualitative failure analysis of previous sections provides an assessment of potential sources of failures in a magnet system. It can now be used as the basis for a quantitative, i.e., risk and reliability analysis, which evaluates the contributions of single failure modes to the reliability of the entire system.

2.2.4.2 Differences between the TF and the PF System

The previous failure mode analysis has primarily dealt with a superconducting TF magnet system. In the following paragraphs, the basic differences between the TF and PF systems are discussed, assuming that the PF coil system can feature superconducting and resistive coils.

PF coils may experience significant bending stresses during operation. Part of these stresses arrive from the interaction of the PF coil currents with the fringe field of the TF coils. More significant bending stresses may be introduced by the discrete vertical supports of the PF coils, and possibly lead connections when they lead to radial or vertical constraints on the PF coils. Also, the

pulsed operation of PF coils may generate higher heating losses in the coils than for the TF coils. In addition, some PF coils (in particular outer PF coils) have very long turns, leading to long coolant channels. Therefore, it might be necessary to divide the coils into separately cooled sections (particularly for superconducting coils) in order to keep the temperature rise between coolant inlet and outlet within the desired range. However, the larger number of coolant connections per pancake in such a design can contribute to a higher failure rate due to failure of coolant pipe connections.

Separately powered coil sections have also been proposed, mainly for internal PF coils [Salpietro 1988], for reasons of maintenance and repair access. However, additional leads are required for this arrangement. The IC coils are also particularly close to the area of fluence production, and require heat and radiation resistant materials. The IC coils will furthermore be heavily loaded under disruptions (mainly compressive stresses), and the eddy currents during disruption may exceed the rated coil currents. Therefore, redundant coils may be required to achieve high reliability of the IC coils.

Space limitations on the stack of central solenoid PF coils may furthermore require high current densities. Therefore, a degradation of the insulation or the current carrying capability of the conductor may become of particular concern for this group of PF coils.

For reasons of symmetry, external PF coils below and above the midplane are connected in series. The electrical connections between both coils add a potential for shorts to power or ground, failure of their cooling equipment, and mechanical failure of the electrical connections to the coils and of the encapsulation structure. Furthermore, the lead placement for the central solenoid PF coils is very tight since the leads are designed coaxially to reduce magnetic field errors. Clearly, this results in an increased danger of shorts between coil terminals due to displacement caused by mechanical loads or breakdown of the insolation between leads.

The support structure for the central solenoid stack has to avoid contact with the central support structure of the TF coils. But it may also be required

to avoid vertical loads of the central solenoid coils on each other, and to support repulsive loads on the upper and lower coils. Failure to provide this support could lead to significant consequences for conductor reliability. The support structure can fail due to its cyclic thermal and mechanical loading or under excessive loads caused by disruptions or quenches (or external events, like earthquakes). It is furthermore subject to irradiation. However, because of the shielding effect of the TF coil structure, the level of irradiation will be reduced for the PF coils compared to the TF coils.

The electrical and control system for the PF magnets is significantly different from that of TF magnets, and will be described in detail in Chapter 3.1. The self– and mutual inductances of the coils vary with their locations, and each coil need to be considered separately in the electrical analysis. In particular, the design of safety discharge resistors needs to be adapted to each coil's circuit.

A mixture of superconducting and resistive coils may be used for the external PF coil system ACA. For instance, the resistive coils could be located to shield the superconducting coils against field changes and irradiation. Furthermore, they may be operated during phases of the pulse of particularly high loads on external PF coils. Thereby, the loads on the superconducting coils may be reduced during these phases. Otherwise, this may require very different current scenarios for superconducting and resistive coils, and make electrically independent circuits for super– and normalconducting coils necessary [Salpietro 1988].

Normalconducting coils may be able to support in plane forces without conduit support, but laminate structures may have to be used [Thome 1988] and the laminate bond strength becomes of particular importance. Resistive coils will also be ohmically heated during a pulse (possibly even adiabatically [Thome 1988]), and the combined effect of cyclic thermal and mechanical loads under irradiation and ohmic heating needs to be considered. Also, the strength behavior of the conductor at low operating temperatures, e.g., the temperature of LN_2, may become a concern. Furthermore, the cooling process may become discontinuous, since most of the cooling is performed between pulses.

2.3 Interactions Analysis for the PF Magnet System

As has already been discussed in previous sections, the PF Magnet System has to initiate and induce the plasma current and to control the position and shape of the plasma. This requires a characteristic PF coil operation scenario, where each coil pair follows a different current scenario in a pulsed operation mode. It distinguishes the operation of the PF coils strongly from that of the TF coils. Therefore, interactions within the PF magnet system and with other reactor subsystems, which are caused by the PF magnet system can be divided into two groups. There are interactions occurring due to the operation of magnet systems in general, e.g., interactions via the cooling system, and interactions which are caused by the characteristic operation of the PF coils and are thus unique for the PF magnet system.

In general, there are six basic mechanisms by which the PF magnet system can interact with other systems:

1. Electromagnetic interaction, e.g., via eddy currents induced in the surrounding structures or electromagnetic (Lorentz) forces due to the interaction of magnetic fields with current carrying structures or wires;

2. Mechanical interaction, i.e., the application of direct mechanical stresses or forces, e.g., via a common support structure or broken parts during a failure;

3. Interaction by thermal coupling, i.e., direct or indirect heat transfer between magnets and surrounding equipment or other coils, e.g., via common cooling media and structures;

4. Electrical interaction, i.e., interactions via electrical connections, not by induced currents, e.g., resulting from undesired intermittent connections or electrical coupling via busbars;

5. Plasma interactions, i.e., interactions which lead to forces, currents, etc., resulting from the behavior of the plasma, e.g., plasma disruptions; and

6. Control interactions, which are caused by control instruments or operators, e.g., wrong indication of a failure situation, or human errors.

A useful tool for visualizing the large number of interactions that can be caused by the PF magnet system, is found to be an Interaction Matrix. Such an Interaction Matrix includes interactions occurring during normal operation and under fault conditions. It is a straightforward extension of the concept of a Fault Interaction Matrix which was suggested by Piet [Piet 1986] and later applied to a loss of mission analysis for CIT [Cadwallader 1987], but has also been used in other contexts (see, for example [Garrick 1984]).

An Interaction Matrix for the PF magnet system is shown in Table 2–1. It describes the impacts and types of interactions caused by the four main PF magnet subsystems in the left column on each of the reactor subsystems in the top row. Most matrix elements contain one or multiple potential interaction processes, which shows the large amount of coupling introduced into the reactor by the PF magnet system. Most of the coupling is due to the characteristic operation of the PF magnets, either directly e.g., by the effect of changing magnetic fields, or indirectly, e.g., by the large number of control actions and the strong impact and reliance on feedback information from the plasma. Some of the main effects resulting from this group of interactions are discussed in the following paragraph.

Within the PF magnet system, the coils may induce currents in each other which can cause additional heating of the coils and may even lead to quenches in superconducting coils under certain failure conditions. The changing magnetic PF fields also lead to cyclic forces on the PF coils, in vertical and radial direction. These magnetic fields produce out–of–plane forces on the TF coils by interaction with the TF coil currents. When the magnetic fields above and below the midplane are symmetric, the out–of–plane forces and the torque (about the torus axis) sum up to zero for a complete TF coil but still produce an overturning moment (about the midplane) on the TF coils.

Also, the changing currents in the PF coils interact with the fringe fields from the TF coils to produce cyclic bending moments on the PF coils. However, this effect is small because the TF coils generate a magnetic field that is essentially toroidal. Since some PF coils may be supported by the TF coil

Table 2-1. Interaction Matrix of the Poloidal Field Magnet System

	Poloidal Field Coil System (ACA and ACB)	Poloidal Field Coil Cooling System (ACK)	Poloidal Field Coil Power Supply System (ACL)	Poloidal Field Coil Protection and Control System (ACY)	Toroidal Field Magnet System (AB)	Vacuum Vessel and Shield System (AAD)	Divertor System (AAE)	Cryogenics Cooling System and Cryostat (AE/AK)
Poloidal Field Coil System (ACA and ACB)	EM: Induced currents; M: via support structure; T: via cooling channels and common cooling system	EM: Induced currents and changing field interactions; M: coil movements, support	EM: changing magnetic field (signal processing and conditioning); M: coil movements, support	EM: magnetic field (changing and steady) (signal processing and conditioning); M: penetration of internal sensors	EM: out-of-plane force, overturning moment, torque induced currents (ac losses); M: via common support structure	EM: induced currents (ac losses); M: sudden penetration (e.g. missile, broken coil)	EM: induced currents, EM forces; M: sudden penetration (e.g. missile, broken coil)	EM: induced currents, in cooling equipment (e.g. pipes), changing magnetic field; M: sudden penetration
Poloidal Field Coil Cooling System (ACK)	T: via common part of cooling system	╱	E: leakages (-> shorts)	E: leakages (-> shorts)	T: via connected cooling systems (e.g. main coolant pipes)	╱	╱	T: via coolant; M: coolant pressure
Poloidal Field Coil Power Supply System (ACL)	E: shorts, grounding, intermittent connections via grounding system; P: plasma disruption	E: coupling with auxiliary power supplies (pulsed currents via common transmission lines and external supply)	E: between power supplies (grounding, external system, busbars, coupling may be particularly important in case of mixed use of nc and sc coils)	E: Poloidal Field PfC system power supplies	P: plasma disruptions; E: coupling between TF and PF power supplies (external system, grounding, transmission lines)	P: plasma disruptions	P: plasma disruptions	P: plasma disruptions
Poloidal Field Coil Protection and Control System (ACY) (all signal processing and control equipment not included above)	P: plasma disruptions; C: control errors; M and E: sensors and sensor leads	P: plasma disruptions; C: control error (regulating equipment and sensors)	C: control errors (preprogrammed control, operator action, configuration, feedback control)	C: control errors; E: dependent signal processing	P: plasma disruptions; C: control errors in feedback system from TF to PF coils	P: plasma disruptions	P: plasma disruptions; C: control errors in case of sweeping magnetic field on divertor plate)	P: plasma disruptions

EM: electromagnetic interaction, e.g. induced currents or electromagnetic force
M: mechanical interaction, e.g. mechanical stresses or penetration
T: thermal coupling
P: coupled by the plasma, e.g. plasma disruptions
C: control errors, e.g. control system malfunctioning or operator errors
E: electrical interaction, e.g. coupling via busbars

	Central Plant Protection, Instrumentation and Control System (X, AY)	Plant Power Supply System (L, M, AL)	Plasma Heating System (RF and NBI) (AF, AG)	Plasma Fueling System (D-T fuel) (AM, AN)	First Wall (AAB) Blanket (AAC) Limiter System (AAF)	Intermediate Cooling Cycles (AO)	Plant Engineered Safety Features (B)	Civil Support Structures (R, AD)
Poloidal Field Coil System (ACA and ACB)	EM: changing magnetic field (signal processing and conditioning)	EM: changing magnetic field	EM: pulsed magnetic field (interference with valve and pump operation, and RF waves) M: sudden penetration (e.g. missile)	M: sudden penetration (e.g. missile, broken coil)	EM: induced currents, ac losses, magnetic field (convection), M: sudden penetration P: plasma disruptions	EM: changing magnetic fields (pump and valve operation), ac losses M: sudden penetration	EM: changing and steady magnetic fields (although outside main reactor building)	EM: pulsed electro-magnetic forces, induced currents
Poloidal Field Coil Cooling System (ACK)	E: leakages (-> shorts)	E: leakages (-> shorts)						
Poloidal Field Coil Power Supply System (ACL)	P: plasma disruptions	E: coupling via grid - PF power supply compensation network	P: plasma disruptions E: coupling between generators	P: plasma disruptions	P: plasma disruptions			
Poloidal Field Coil Protection and Control System (ACY) (all signal processing and control equipment not included above)	P: plasma disruptions E: dependent signal processing and conditioning	P: plasma disruptions E: dependent signal processing and conditioning	P: plasma disruptions C: control error (heating control uses PF PIC information)	P: plasma disruptions C: control error (fueling uses PF PIC information)	P: plasma disruptions		C: failure detection instrumentation	

EM: electromagnetic interaction, e.g. induced currents or electromagnetic force
M: mechanical interaction, e.g. mechanical stresses or penetration
T: thermal coupling
P: coupled by the plasma, e.g. plasma disruptions
C: control errors, e.g. control system malfunctioning or operator errors
E: electrical interaction, e.g. coupling via busbars

Table 2-1 (cont.). Interaction Matrix of the Poloidal Field Magnet System

supports (e.g., the intercoil support structure), loads on the PF coils can also be transferred to the TF coils. The operation of the PF coils requires a large number of control actions, which can be influenced by the pulsed magnetic fields from the PF coils. This may lead to higher failure rates for signal processing or other sensitive electrical or controlling devices, causing them consequently to omit control actions or commit undesired actions. Also, devices that are operated electrically, such as solenoid operated valves, may malfunction. Therefore, the impact of the magnetic field is somewhat similar to that of an external event like an earthquake and could thus be regarded as a common mode failure initiator for a large number of systems [Piet 1986].

The behavior of the plasma depends also heavily on the performance of the PF coil system. Failure to provide the desired current scenario in the PF coils may quickly lead to a plasma disruption, where the plasma current decays abruptly. This may cause heating and mechanical loads on surrounding structures and the PF and TF magnets. The power supply system for the PF coils requires high peak power but has to handle high power returns from the coils during a pulse as well. These power scenarios can lead to strong electrical coupling with the public grid or other power supplies (e.g., to the TF coils, or auxiliary supplies) in the fusion device, if no adequate compensation equipment is provided.

This interaction analysis of the PF magnet system demonstrates the potential for interactions with a large number of reactor subsystems under normal operation and fault conditions. This means, that those interactions need to be considered in the reliability analysis of magnet systems under two aspects:

1. Under conditions of normal operation of the PF coils, the interactions can contribute to basic failure modes of other reactor subsystems, as it was already shown for the TF magnet system in Chapter 2.2; and

2. Under fault conditions of the PF magnet systems, the interactions can lead to consequences in other reactor subsystems and need to be considered in the fault consequence analysis of the PF magnet system.

The first aspect contributes to the difficulties involved in quantitative failure analysis of the magnet system, since time dependent basic failure rates may need to be considered, and multiple effects like irradiation and cyclic stresses may act together to cause basic failure modes. This aspect will not be pursued further in this study.

The second aspect requires further analysis of fault scenarios and the quantification of fault consequences in order to decide upon the importance of those effects on the design of the magnet system. This aspect will be discussed in more detail in Chapter 3.

Chapter 3

CONSEQUENCE ANALYSIS OF ELECTRICAL FAILURES OF THE PF MAGNET SYSTEM

Differences between the TF and the PF magnet systems arise from the characteristic operation mode of the PF magnets and are mainly reflected in differences in the electrical and control systems of both magnet systems. For the PF magnets, these systems will be significantly more complex since more operating parameters need to be controlled in a tight time frame. Therefore, the electrical and control system of the PF magnets is selected for further study, and electrical failures of the PF magnet system will be examined in this Chapter. In the first part, the features of an electrical and control system for the PF magnets, as it might look in future devices, are examined. Then, a specific design, that of the CIT machine, is chosen as a basis for the selection of specific fault scenarios. The consequences of an exemplary class of failures on the PF magnet system itself and on other reactor subsystems, caused by interactions as discussed in Chapter 2.3, are investigated for several selected fault scenarios. Part of the results have been reported in [Zimmermann 1988].

3.1 The Electrical and Control System of the PF Magnets

The electrical and control system of the PF magnets needs to fulfill two basic tasks: (1) to provide the predesigned voltages and currents at the coil terminals; and (2) to allow for fast corrections of these voltages and currents depending on the state of the plasma. In order to accomplish these tasks, designs for devices like CIT or NET include PF coils external and internal to the TF coils. The external PF coils will be operated in a current control mode following a preprogrammed current scenario, and will adapt only slowly, on a timescale of a few seconds to changes of the state of the plasma. Considering the large inductances of the external PF coils and taking the shielding effect of the structures between these coils and the plasma into account, fast control of these

coils would require the capability for fast and large changes of coil voltages. This would require high voltage power supplies, which would have to deliver unrealistically large amounts of electrical power. Therefore, the fast control on a timescale of a few milliseconds is performed by the internal PF (IC) coils, since they are located very closely to the plasma and allow for fast changes of the magnetic field while requiring significantly less power than would be needed for fast control of the external PF coils. However, unlike the TF coil power supplies, most of the PF coil supplies still need to provide high current ramp rates and bidirectional currents and coil voltages due to the pulsed mode of operation.

For fusion devices like NET and CIT the public grid may therefore not be used as the only power source, and storage capabilities for mechanical energy like motor flywheel generators will be required. Both power sources may then feed their power into a possibly redundant busbar, which connects all PF power supply units. In order to correct the power factor and compensate for reactive power, capacitor banks will be connected to the busbar. Furthermore, load breaking equipment for fast connection of the busbar to ground, and standby power equipment (e.g., a diesel generator) may be installed.†

The PF coil power supplies are connected to the busbar by load breaking switches. Since each coil follows a different current scenario, each pair of external coils above and below the midplane and each of the IC coils is likely to be powered independently. Such an arrangement has been proposed for CIT [CIT 1988] and NET [Hicks 1986], and avoids a switching network between coils, while its economical disadvantages seem to be acceptable when compared to an integrated power supply scheme.‡

Each of the coil power supply units may consist of a network of unidirectional power supply modules. A switching network between these

---

† The information about the PF power supply system of NET was obtained from a personal communication with R. Bunde, The NET Team, Garching, West Germany, in April 1988. For CIT, this information was obtained from [CIT 1988].

‡ Personal Communications with J.H. Schultz, MIT Plasma Fusion Center, August 1988.

modules and the coil terminals will be required to obtain the desired output voltage at the current leads. Such a system is illustrated in Fig. 3–1.

Each power supply unit has its own local control and protection module, which conditions all signals needed for controlling the output voltage. It furthermore provides status information for the higher level control system. The power supply unit is protected against overcurrents and –voltages by a protection network, which is likely to be passive. A ground fault monitoring system senses currents in the neutral conductor. In case of a ground fault, a crowbar switch is closed by which the coil is effectively bypassed. The desired timing of the reaction scenario may depend on the current state of the PF coil power supplies in order to keep the loads on the external power supply small [Bertolini 1987].

The switching network between a power supply unit and the current leads makes the final modulation of the output voltage during the pulse. It contains an arrangement of reverse–make switches which are used for changing the direction of the output current. Furthermore, a circuit breaker unit will be installed. Such a unit essentially consists of a circuit breaker and a resistor in a parallel arrangement. Therefore, when the circuit breaker is closed, the effect of the resistor on the output voltage is very small. However, when the circuit breaker opens, the coil current will be redirected through the resistor, causing a sudden voltage drop at the coil terminals and leading to a high current ramp rate in the coil. Therefore, the circuit breaker may be used for two tasks: (1) to provide most of the fast voltage drop at the coil terminals which is required to create the loop voltage necessary for plasma initiation [Bertolini 1987, Salpietro 1988]. This also leads to reduced requirements for the power supply modules; and (2) the circuit breaker–resistor arrangement can be used to deposit energy during the pulse, which will reduce the amount of reactive power that is fed back into the busbar when the coils are deenergized. This may thereby compensate for part of the power changes during a pulse.

Therefore, the circuit–breaker network needs to be capable of breaking high currents, and additional protection equipment will be required to achieve reliable and safe operation. There are two basic paths to protect this equipment, that is
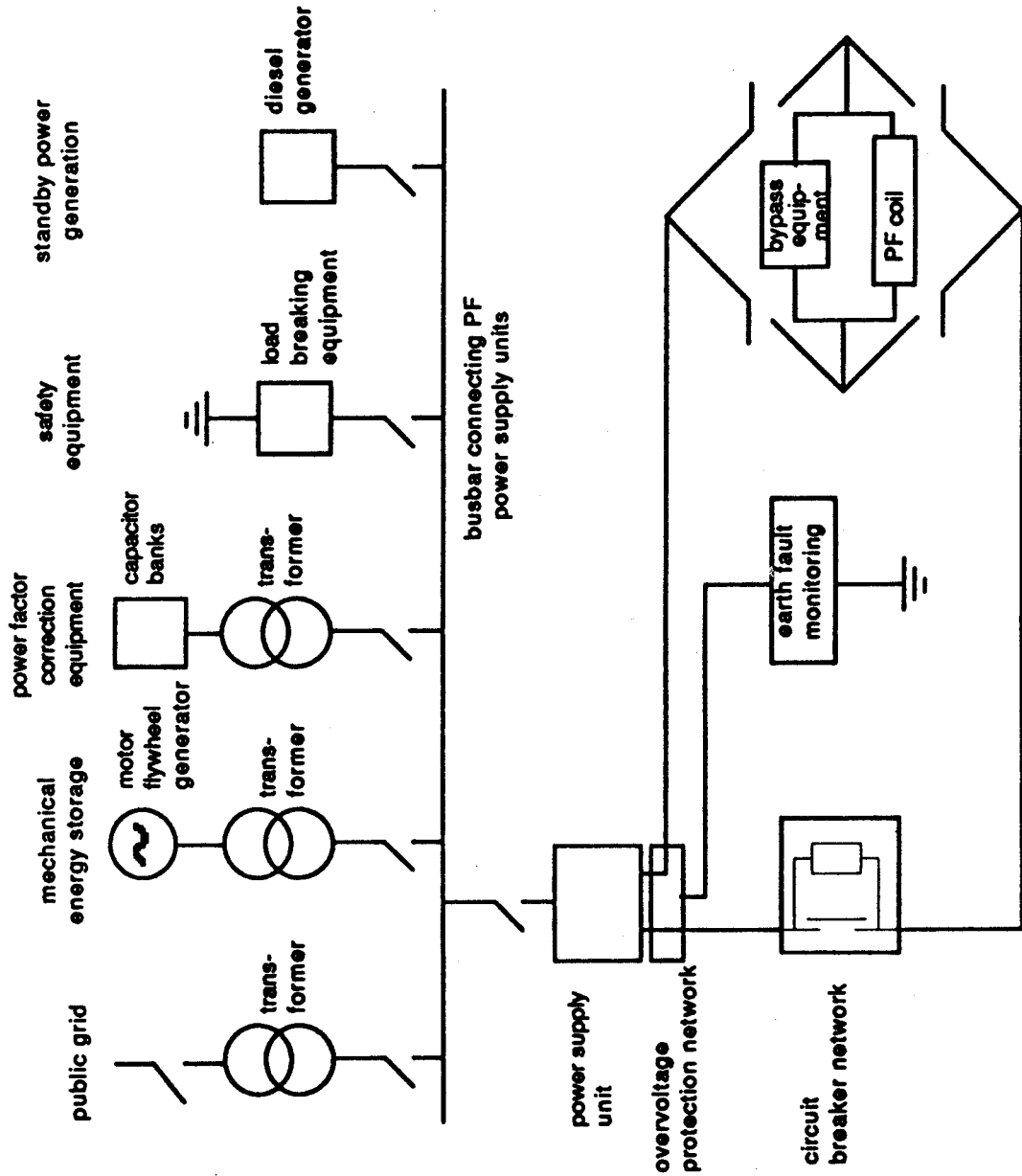
Fig. 3-1 Scheme of a PF Power Supply System

to open the circuit breaker only when it carries no current, or to close the circuit breaker again when it is vibrating and arcing. This can be achieved by providing an artificial zero of the current during switching, where an arrangement of a precharged capacitor and a saturable inductance can be used to compensate for the current through the circuit breaker. Furthermore, a combination of a damping resistor and a bypass switch may be used to dampen vibrations of the circuit breaker and extinguish arcs between its open contacts [Bertolini 1987].

The reliability of the described part of the PF power supply and control system already depends to a high degree on the reliability of the signal processing, control commands, and the fulfillment of time requirements in the system. However, this part of the system still does not take the state of the plasma into account and is essentially an open loop controller.

The feedback information from the plasma is needed for plasma control and protection and is used by two basic systems, the plasma protection and current control system (PPCC), and the coil and plasma safety protection system. This is illustrated in Fig. 3-2.

Information about the state of the plasma is provided by a plasma diagnostics system, which yields signals for the magnetic field, the magnetic flux, the plasma current, the current density, and monitors runaway electrons in the plasma. The variables that need to be controlled are the vertical and radial position of the plasma, the plasma shape, and the plasma current. This control is accomplished by separate control modules for each of the control variables, and the control signals are transformed into corrective coil output voltages and sent to the local power supply unit controllers. However, the reference profiles for the control variables representing the waveform information of the coil currents and the waveform breakpoints for the coil current scenarios, are provided for each control module from a high level control system. These waveforms may be set by operator action or actions of safety systems and may be unchanged during operation [Bertolini 1987, Dinsmore 1986]. They may also be varied in response to the state of the plasma on a slow timescale of a few seconds.
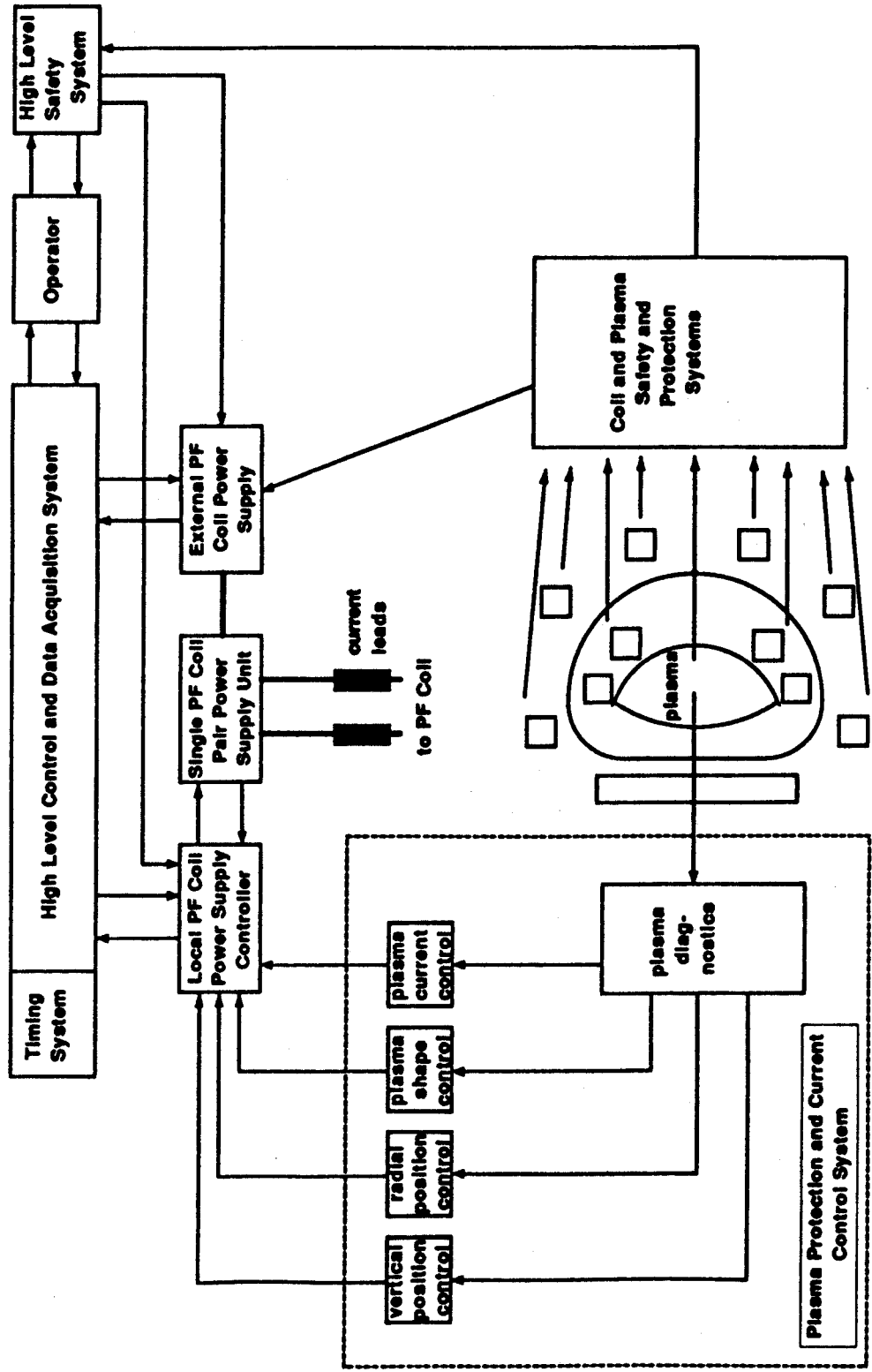
Fig. 3-2 Scheme of a Power Supply and Control System for PF Magnets

The coil and plasma safety protection system comprises the fast external discharge and quench detection system for the TF coils, but also a system for the detection of plasma fault conditions and for the soft termination of a pulse. The soft or orderly termination of a pulse is provided by a pulse termination network (PTN), when dangerous or undesirable plasma conditions arrive, such as consistently undesirable values of measured variables or plasma disruptions. Undesirable plasma conditions are monitored by modules for disruption detection and detection of faltering plasma breakdowns, and are transferred to the plasma fault protection system, which decides upon altering control modes in the PPCC or issuing a signal to the PTN module for a soft termination of the pulse [How 1986].

However, the plasma fault protection system will also communicate with the auxiliary plasma heating (e.g., RF heating or neutral beam injection) and the fueling system, which contribute to the control of plasma temperature and current density [How 1986].

Potential actions taken by the PTN comprise switching off the auxiliary heating power, removing the power from the PF power supply system, and controlling the plasma current to zero.   It is desired to perform the last two actions very smoothly within a few seconds, in order to protect the power generators and supplies, and to reduce the loads resulting from a decay of the plasma current.   However, such a procedure may also fail in some cases and lead to a plasma disruption [How 1986].

In summary, the PF power supply and control system is an internally highly coupled system which has to control multiple coupled variables on a fast time scale.   This implies a complexity that can be expected to lead to a large potential for fault initiation in this system.

3.2   Electrical Failures of the PF Magnet System

For the PF magnet system, it is required that the reference profiles for the coil currents can be followed, and disturbances can be quickly controlled in order to fulfill its tasks properly and safely. Therefore, any failures leading directly to undesirable or dangerous coil current profiles will be of high importance, and such electrical failures will be examined in this section.

Electrical failures can arise from failures in the coil winding or at the current leads, and virtually all faults initiated in the PF power supply and control system are electrical failures. Failures of the first type are discussed in Chapter 2.2 and arrive mainly from mechanical overloads and thermal loads, combined with the effects of irradiation. Failures of the latter type occur when the PF power supply system (ACL) or the PF protection and control system (ACY) fails. The fault trees for these systems are presented in Fig. 3-3 to 3-6. The PF power supply system will be unavailable when the external power supply or any of the internal single power supply units is unavailable as illustrated in Fig. 3-3. In this context, unavailability means that either no or only limited power can be provided, the desired safety of the power generation or conversion cannot be achieved, or the output voltage or current scenarios do not agree sufficiently with the desired output profiles.

The operation of each power supply unit requires much monitoring, and the availability of signal detection and processing equipment is very important, within the system as well as for its communication with the remaining power supply units, as shown in Fig. 3-4. Since the setup of the power supply modules within a power supply unit may have to be changed during a pulse, configuration errors arriving from a higher level control system or the operator can lead to electrical failures. Furthermore, some power supply equipment and the busbars will need to cooled, and in order to reduce the number of failure modes, passive air cooling will be preferable but not always possible, e.g., due to space constraints.

For actuators like trigger devices and switches, wear-out and fatigue failures are potential major failure modes, and the number of pulses together with the
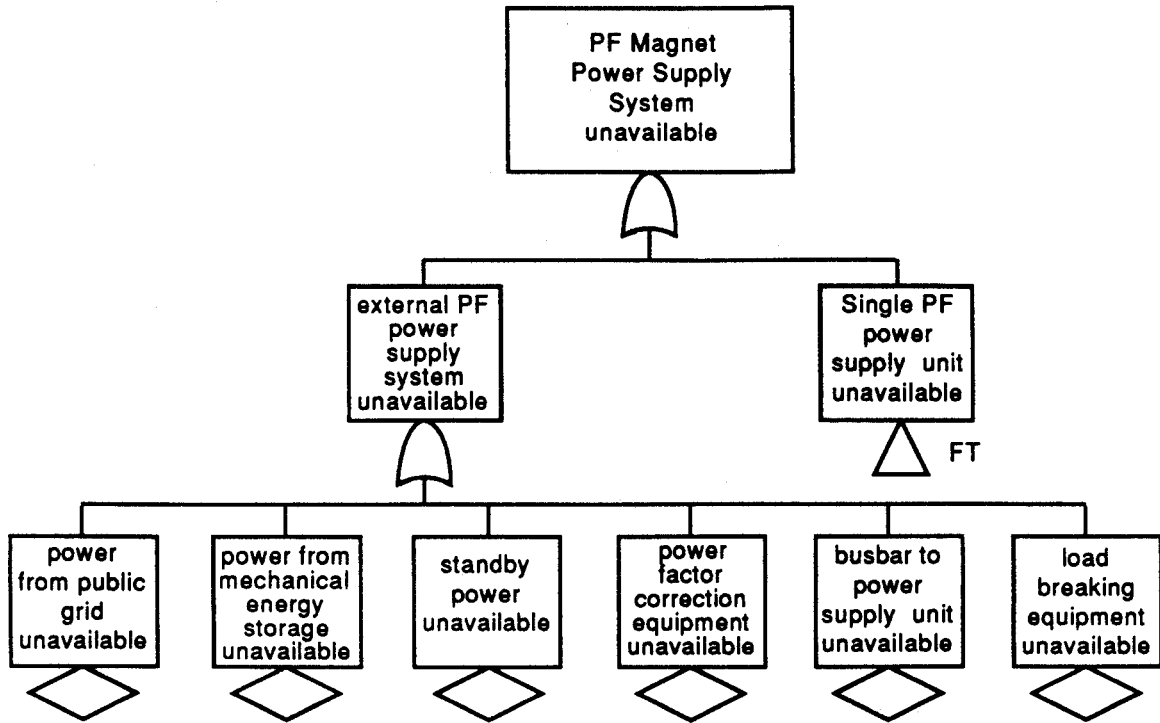
FT: Fault Tree Single Power Supply Unit Unavailable (Fig. 3-4)

Fig. 3-3. System Fault Tree for the PF Magnet Power Supply System

environmental conditions need to be taken into account for their design. Those actuators are mainly part of the switching and protection network, for which a fault tree is shown in Fig. 3–5. However, insufficient cooling of equipment and spurious operation of equipment, possibly caused by interactions with surrounding equipment, may also contribute to failures of the switching and protection network to a high degree.

The PF protection and control system fails when any of its subsystems becomes unavailable, as the fault tree in Fig. 3–6 illustrates. The reliability of its equipment will depend to a high degree on manufacturing, assembly and maintenance procedures. The system setup should therefore be as simple as possible to avoid failures of the protecting and control equipment failures that overshadow the failures of the equipment to be protected or controlled (e.g., this has already been observed at TFTR [Greenough 1987]).

Fig. 3-4. Fault Tree for Failure of a Single PF Power Supply Unit
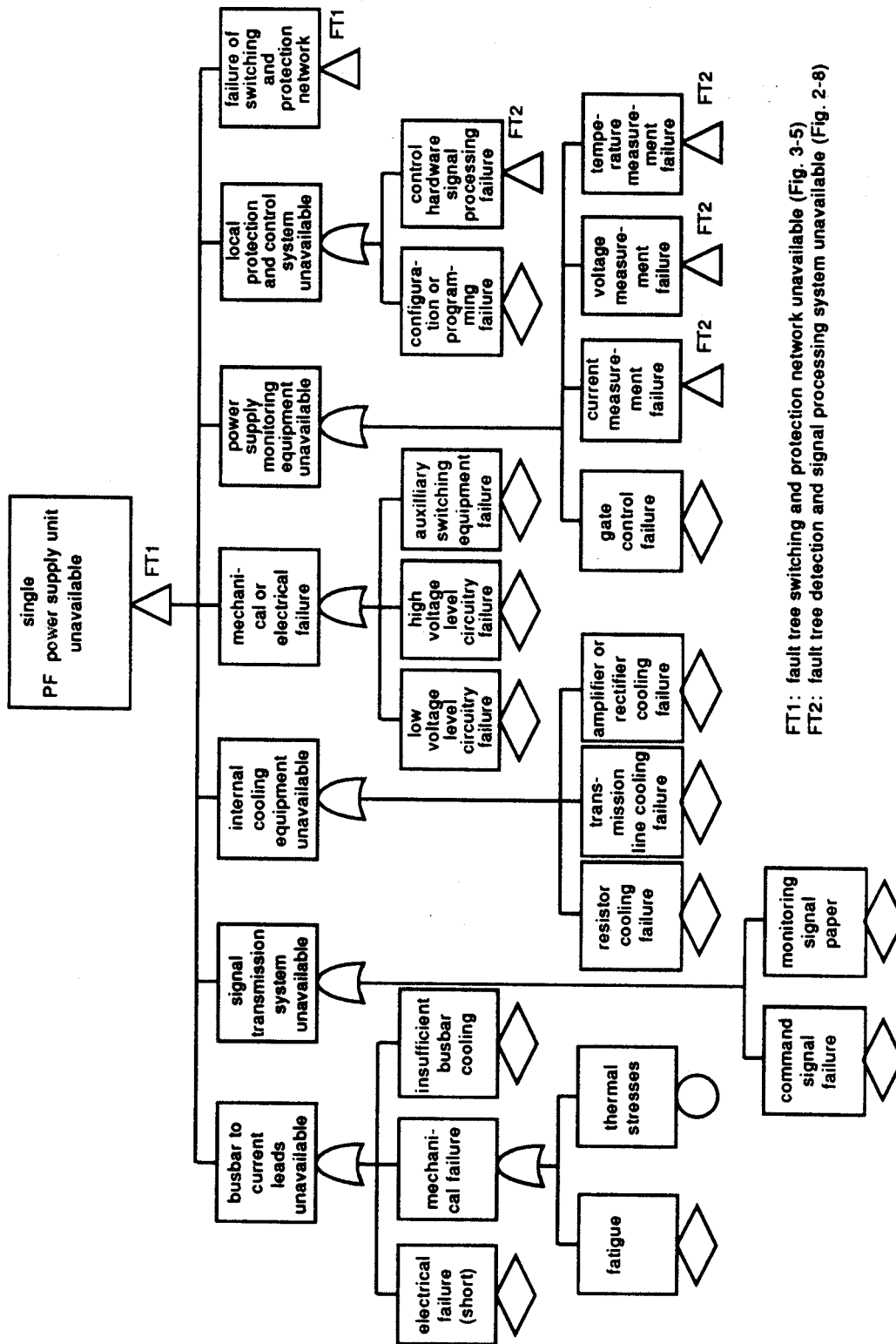
FT1: fault tree switching and protection network unavailable (Fig. 3-5)
FT2: fault tree detection and signal processing system unavailable (Fig. 2-8)
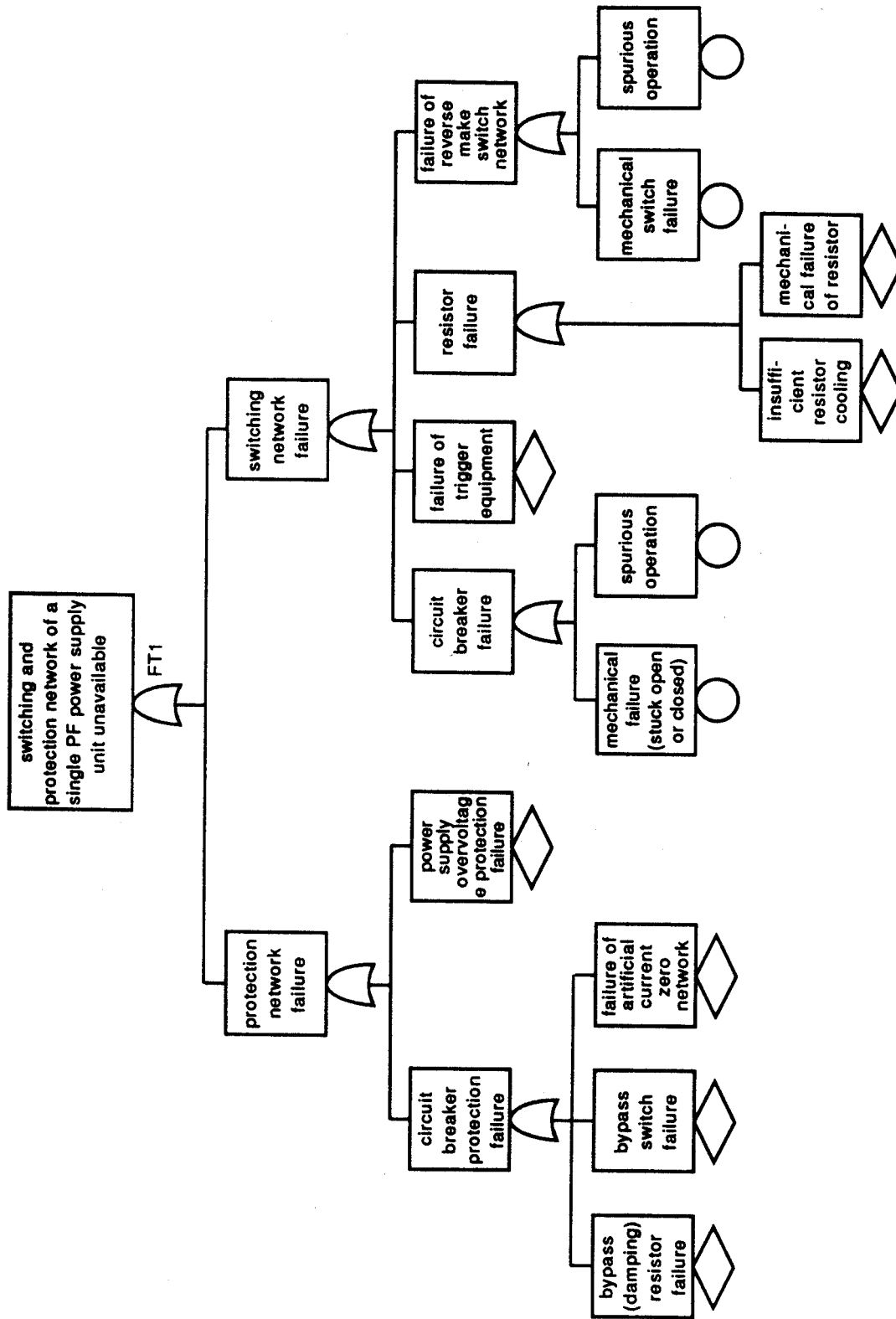
Fig. 3-5. Fault Tree for Unavailability of the Switching and Protection Network of a Single PF Power Supply Unit

In summary, the fault trees for the PF power supply and control system show a much larger number of potential failure modes than the comparable systems for the TF coils (see Chapter 2.2.3). Therefore, results for the failure analysis of the TF system cannot be directly transferred to the PF system. Instead, the PF power supply and control system needs to be analyzed separately.

3.2.1 Reported Electrical Failures of Magnet Systems

The database for failures in fusion magnet systems is not well developed at the present time. Although a number of large experimental fusion facilities have already been operating for several years, little failure data has been published so far. In this section, electrical failures of magnet systems reported in three recent studies are summarized. These are reports about TFTR [Greenough 1987], JET [Huart 1986], and a survey of failures [Thome 1986] in the U.S. This analysis yields some insight into the quantification of the contribution of single failure modes to system failures. However, the database is too small to be representative for the entire system. Table 3-1 contains a partial list of failures that were reported in the aforementioned studies, and some general aspects of this data will be emphasized in the following paragraphs.

The large number of control devices and actions in the system contribute to a high degree to electrical failures. This was particularly emphasized in the JET study [Huart 1986]. For the switching network, the flywheel generators, and the power supplies, control and command and alarm monitoring failures made the largest contribution. It was suggested that only careful selection of components, control of the manufacturing process, and extensive testing before start of operation could reduce these faults.

For TFTR and JET, the protection logic and fault detection system was identified as another strong contributor to failures. The number of protective devices should be minimized, since a sophisticated detection and protection system was found to experience frequent failures, often attributed to uncontrollable shifts in calibration of monitoring equipment during operation.

Fig. 3-6 Fault Tree for the Poloidal Field Protection and Control System
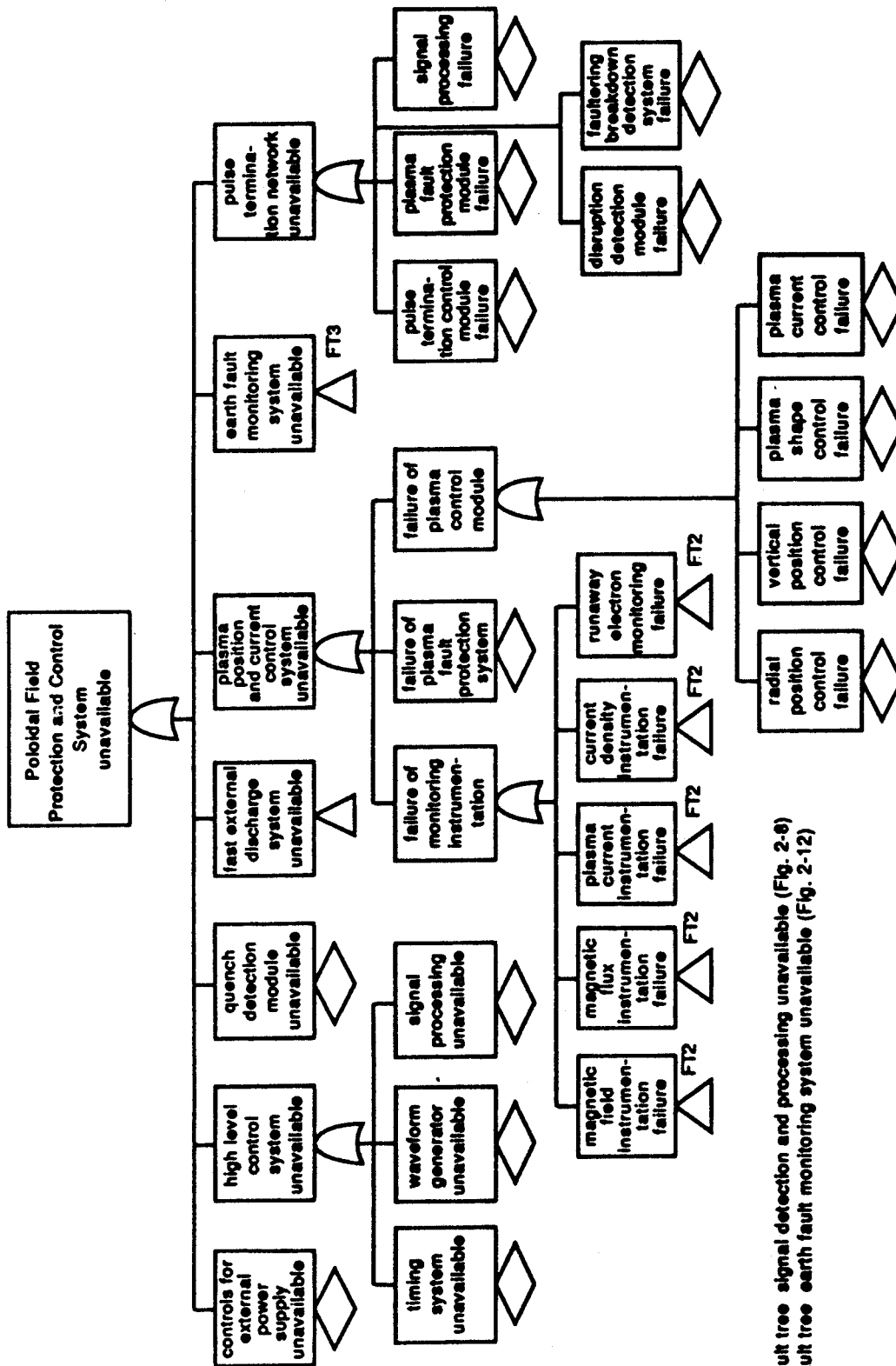
FT2: fault tree signal detection and processing unavailable (Fig. 2-8)
FT3: fault tree earth fault monitoring system unavailable (Fig. 2-12)

Ref.	Failure Event	Potential Cause of Failure
	Failure of Coil or Current Leads	
3	overcurrent in lead	na
3	internal short sensor lead-coil	mechanical overload, design of sensor lead
3	turn-to-turn short in coil	mechanical abrasion of insulation
3	lead short to ground	inadequate support
3	ground short of coil	inclusion in insulating material
3	overvoltage and turn-to-turn short	mechanical overload
3	overheating and arcing of coil	inadequate coil cooling
	Failure of Power Supply and Control System	
1	control board (for communication) failure	vibrations (?)
1	misoperation during shutdown scenario	disturbed signal processing due to electrical noise
1	spurious operation of fault detector	miscellaneous causes, design complexity
1	failure of reaction scenario for control power outage	poor implementation of reaction scenario
2	cooling system outage	sensitivity to foreign materials
2	control and command failure(s)	miscellaneous causes, complexity of control system
2	alarm monitoring failure	na
2	failure of protection logic	na
3	overcurrent at leads (and burnout)	miswired power supply
3	rectifier failure	electrical noise
	Failure of Switching and Protection System for Power Supplies	
1	mechanical failure of reverse make switch(es)	fatigue
1	failure of crowbar switch	environmental conditions
1	failure of air valve in cooling system for electrical equipment	complex electrical operation
1	mechanical failure of switches in circuit breaker arrangement	fatigue
2	loss of control over circuit breaker	na
2	fracture of reverse make switches	fatigue
2	spurious intervention of protection logic	na
2	outage of cooling system	sensistivity to dirt
2	failure of alarm monitoring	na
2	control and command failure(s)	na
3	excitement of coil in field opposing direction	na
3	short in magnet	insulation failure of dump resistor
3	overheating of dump resistor	inadequate cooling
3	overcurrent at coil	programming error in control logic
3	uncontrolled rise of power supply voltage	defective software algorithm

na: not available
References: 1: [Greenough 1987]; 2: [Huart 1986]; 3: [Thome 1986]

Table 3-1. List of Reported Electrical Failures of Magnet Systems

Furthermore, a number of early wear–out failures of switches and circuit breakers were reported, as well as switch failures caused by the effect of environmental conditions. Similarly, the operation of the cooling system was found to be sensitive to foreign materials in a number of cases.

Some of the failures reported by Thome, et. al., [Thome 1986] seemed to cause more severe consequences than those reported from operating experience at JET or TFTR. This suggests, that a large number of failures with little consequences and short downtimes may not have been reported. However, configuration errors in the power supply, and failures of the switching networks still appeared on the list of failures, together with a number of failures in the coil winding or at the current leads. Considerable damage to the magnet system was reported for several of these cases. This furthermore demonstrates that a fault consequence analysis of electrical failures of the PF magnet system must consider failures of the winding, the leads, and the power supply and control system.

In summary, there is a large potential for electrical failures in the PF magnet system, but the complexity of the system and the lack of reliability data currently does not allow for a determination of all failure modes that could possibly occur in such a system. Furthermore, such a list of failure modes if it existed would be very design specific. However, all such failures will cause consequences for the voltage and current profiles in the coils. Therefore, the analysis of current and voltage fault scenarios in the coils can be used as the first step to estimate the consequences, and evaluate the risks associated with such failures.

Those potential electrical failures can be grouped into two basic categories:

1. Electrical shorts of a coil pair or a single PF coil; and

2. Erroneous control switching, leading to undesired voltages at the coil terminals.

For a fault consequence analysis, specific fault scenarios need then to be chosen from these two failure categories, for a specific PF coil arrangement and current scenario.

3.3   Selection of Fault Scenarios

This section describes the process adopted for the selection of fault scenarios in the PF magnet system. This selection is made for a specific magnet design, the CIT machine, in order to prepare fault scenarios that are then simulated using a simplified electromagnetic model of CIT. CIT provides a good reference design, since its PF magnet arrangement and operation scenario is very similar to expected future experimental machines, like NET or ITER, and the results of these simulations are then related to those machines. The types of consequences of particular interest during the fault scenario selection process are the loads on the external PF and the TF coils, and the temperatures in the external PF coils.

3.3.1   The Reference Design: CIT 2.1m Machine

CIT is considered as a next major step in the US magnetic confinement fusion program to demonstrate the technical feasibility of fusion by achieving conditions better than breakeven, and operating in an ignited plasma regime. The CIT machine is rather compact with a major radius of 2.1m and a high field of 11T at the magnetic axis, which is at a radius of 2.1m. A cross section of CIT is shown in Fig. 3–7. The CIT machine features 7 sets of external PF coil pairs, PF1 to PF7, and 3 pairs of internal coils, IC1 to IC3. The external PF coils below and above the midplane will be connected in series, while the IC coils will probably be operated independently. All coils are resistive and made of copper or copper–St 718 laminate. They are cooled by LN$_2$ between pulses. All external coils contribute to the induction of the plasma current, whose maximum is 11MA, by providing the required flux swing, which is approximately 54Vs from the beginning until the end of pulse [Pillsbury 1988].

A single complete current pulse of CIT takes 28s, where the first 6.2s are used to premagnetize the external coils. Then the voltage blip for plasma buildup occurs, the plasma current is ramped up linearly to 11MA within 7.5s and held at its maximum for 5s. At the end of plasma current flattop (EOFT), the plasma current is ramped down linearly within 7.5s, and during the final 2s of the pulse, the PF coil currents are brought to zero. This scenario can be
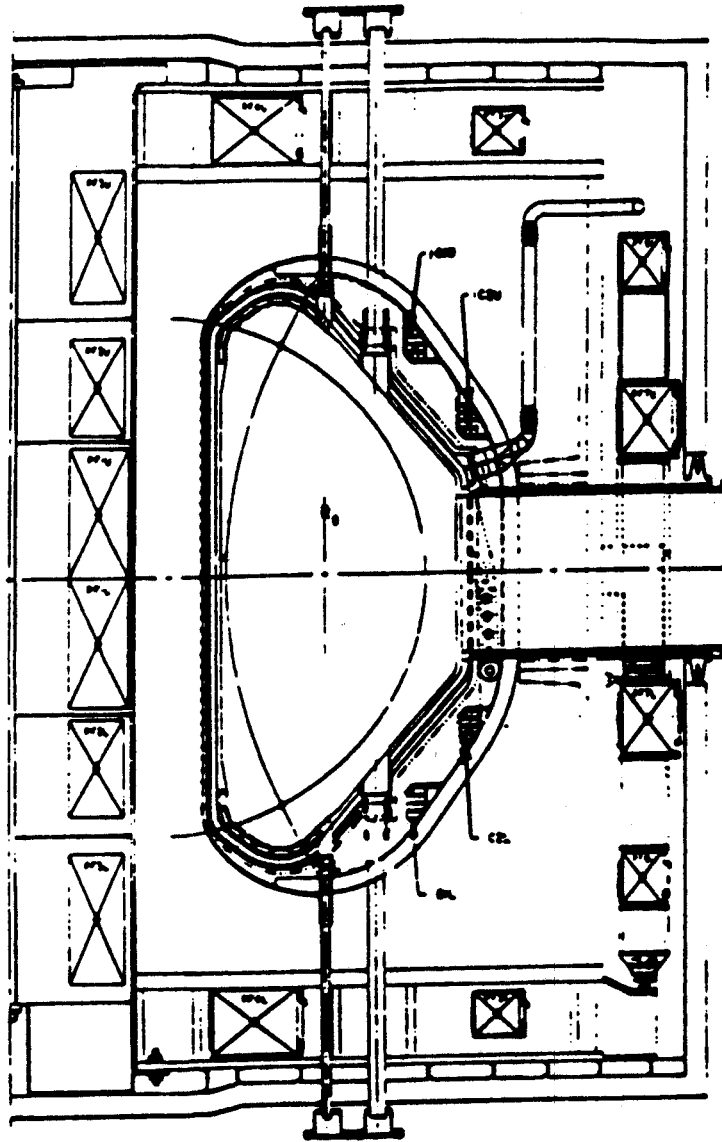
Fig. 3-7. Elevation View of One Section of the CIT 2.1m Machine [Thome 1988]
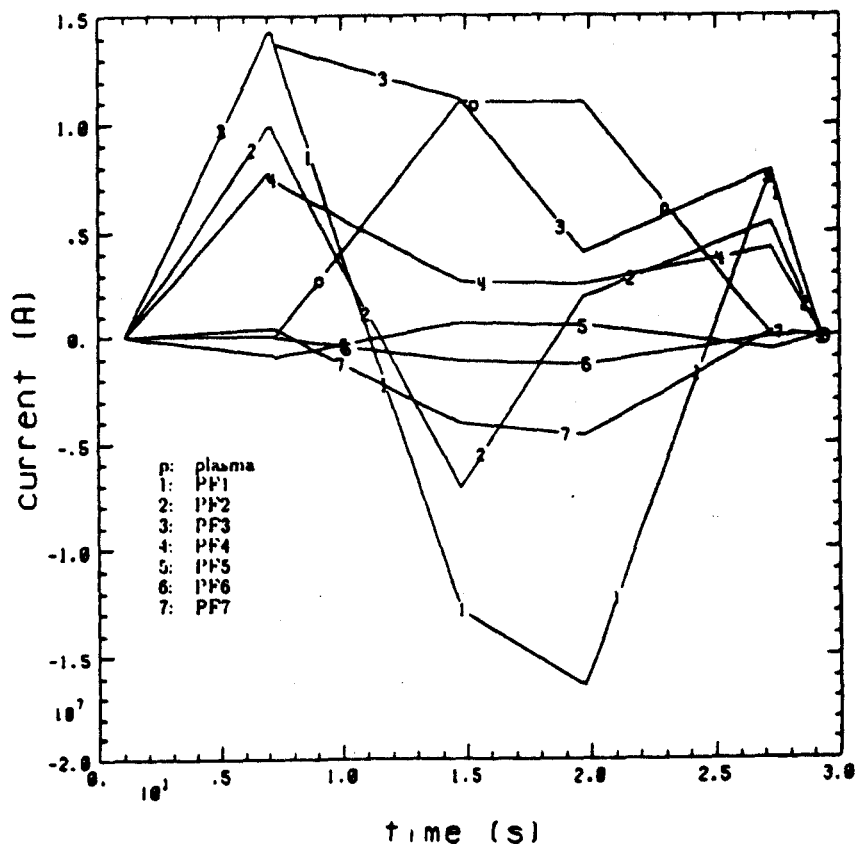
Fig. 3–8. Current Scenario for the Plasma and the External PF Coil (Data from [Pillsbury 1988])

achieved by the current scenario in Fig. 3–8 for the external PF coils, where corresponding coils above and below the midplane carry the same currents. The highest ampere turns† are in the range of $15MA$ for coils PF1 and PF3 at plasma initiation at $6.2s$ and at EOFT at about $19s$.

These current and voltage scenarios have been chosen to keep the voltage requirements at plasma initiation small, and to provide approximately the same stress level in the central solenoid coils PF1 to Pf3 at plasma initiation and at EOFT when the highest loads occur. The temperature in the external PF coils

---

† Ampere turns is the expression used for the total coil current, which is the sum of the currents in all turns of a single coil.

rises steadily during a pulse, since the resistive coils heat up almost adiabatically [Thome 1988]. For CIT, it is desired to keep the temperature of all PF coils below $330K$ during a pulse, since higher temperatures might lead to severe degradation of the insulation. The coils are then cooled down to LN_2 temperature between pulses. A more detailed description of the current, voltage, stress and temperature scenario for CIT can be found in [Pillsbury 1988], and a summary is given in Appendix B.

The TF coil current that is needed in CIT to obtain a magnetic field of $11T$ at the magnetic axis can be approximated by Eq. 1.2, by setting $B_0 = 11T$ at $R_0 = 2.1m$. Then, the total ampere turns–coils are

$$NI_{TF} = \frac{2\pi}{\mu_0} B_0 R_0$$
$$= 115MA - turn - coils \qquad (3.1)$$

where N is the total number of TF coils and I_{TF} the ampere turns in a single TF coil. CIT will have 16 TF coils, so that a single coil would carry an ampere turn product I_{TF} of

$$I_{TF} = 5.775MA \qquad (3.2)$$

The voltage requirements for the PF coil power supplies can be estimated by using the voltage per turn data given in Appendix B. Assuming that the coil voltages are entirely provided by the power supply, the maximum voltage per coil U_{PF} is given by

$$U_{PF} = N_{PF}U_i , \qquad i = 1,...,7 \qquad (3.3)$$

where U_i is the maximum voltage per turn of a PF coil, and N_{PF} is the number of turns. Performing this calculation for each external PF coil, the results of Table 3–2 are obtained. Since each power supply unit consists of several unidirectional power supply modules and the coil voltage and current requirements are fulfilled by connecting several of these units in series or in parallel, the total available power supply voltage may be different from the maximum required power supply voltage. Assuming that power supply modules

are used which are capable of providing $1kV$ and $20kA$, which is under discussion for CIT†, the coil power supply units could provide the total voltages shown in the last column of Table 3–2. Since all external PF coils require positive and negative voltages during a pulse, all power supplies need to provide these voltages bidirectionally.

The internal coils IC1 to IC3 do not contribute significantly to the breakdown voltage at plasma initiation and are only used for corrections in the plasma parameters when the plasma current is on. The maximum currents in these coils are expected to be on the order of $400kA$.

3.3.2 The Fault Scenarios

This section describes the final selection process for the fault scenarios for CIT and gives a list of the investigated fault scenarios. At the present time little is known about the power supplies and the operation scenarios for the IC coils. Hence, this study focuses on failures initiated in the electrical system of the external PF coils. However, several fault scenarios are examined for the following two limit cases for the terminal constraints at the IC coils:

1. The IC coils are completely passive, i.e., they carry no driven currents but eddy currents and are treated like shorted coils; and

2. The IC coils carry no current, as would be the case when the IC coil currents were forced to be zero by the control system.

For all fault scenarios, it is assumed that the currents rather than the voltages of the external PF coils are controlled. This means that the currents in the controlled or driven coils are undisturbed by any eddy currents which may result from changes of the magnetic fields. However, this approach is different from that in earlier fault analysis studies, like for TFTR [Pelovitz 1986] or INTOR [INTOR 1982a], where coil current enhancement factors were analyzed and voltage control was assumed. But it reflects one of the proposed control

---

† Personal communication with R.D. Pillsbury, Jr., MIT Plasma Fusion Center, May 1988.

Coil	Voltage Per Turn (V) *		Turns per Coil**	Required Voltage (kV)	Parallel Supply Units	Available Voltage (kV)
	pos.	neg.				
PF1	4.7	-11.2	280	3.1	4	4.0
PF2	4.5	-10.4	234	2.4	3	3.0
PF3	4.7	-9.5	280	2.7	3	3.0
PF4	8.4	-37.5	160	6.0	6	6.0
PF5	1.8	-49.5	52	2.6	3	3.0
PF6	9.0	-43.2	28	1.2	2	2.0
PF7	15.6	-11.2	100	3.4	4	4.0

*: data from [Pillsbury 1988]

**: data from personal communication with R.D. Pillsbury, May 1988

Table 3-2. Estimated PF Coil Power Supply Voltages for CIT
(Assuming that Power Supply Units are Independent and Made up of $1kV$, $20kA$ Supply Modules)

strategies for CIT. Therefore, in this analysis, the loads on the PF and the TF coils are examined, along with the temperatures of the external PF coils. Since the temperature in a PF coil depends basically on the integral of I^2t during a pulse, where $I(t)$ is the coil current and t the time, and the currents in the unfaulted coils are controlled, only the temperatures in faulted coils will differ from the temperatures under normal operating conditions.

From the two basic categories of faults derived in Chapter 3.2, only one type of fault per category that is a candidate case for particularly high loads on the PF and TF coils, is examined. These failures are

1. Shorts between the terminals of external PF coils, since they may involve larger changes in coil voltage and coil currents than turn-to-turn shorts or shorts to ground; and

2. The application of a constant voltage at the terminals of external PF coils, where either the applied voltage at the time of fault initiation is held constant, or the full available voltage is applied.

Here, effects like sudden temporary voltage drops due to the introduction of an additional resistance in the circuit or a mismatch during switching scenarios are not considered. Such effects may lead to nonlinear voltage distributions along the coil due to capacitive effects and require detailed knowledge of the design which is beyond the scope of this study.

The stresses and temperatures in the external PF coils (as discussed in Chapter 3.2 and Appendix B) and the effect of plasma reactions are used to decide upon the time of fault initiation and which coils are faulted. The coil stresses are particularly large during plasma initiation and at EOFT. The coil temperatures are rising steadily during a pulse, so that a fault initiated during the last phase of a pulse is more likely to lead to temperature problems than when it is initiated earlier. Furthermore, any major disturbance of the PF coil currents is likely to be followed by a plasma disruption. Thus, it can be expected that the higher the plasma current at fault initiation, the more severe will be the loads on the PF and TF coils caused by the plasma disruption.

Therefore, faults starting at EOFT and at the end of plasma current (EOPC) are investigated.

Three types of plasma disruptions are examined, which are fairly typical for tokamak reactors, but the dynamics for cases 2 and 3 have been obtained specifically for CIT using a very detailed model, the Tokamak simulation code (TSC), which is used particularly for disruption and control scenarios analysis.† The disruption scenarios are:

1. A stationary disruption, where the plasma current decays from initially $11MA$ to zero within $11ms$ at a linear rate of $-1MA/ms$, while the plasma remains at the magnetic axis. This type of disruption is used as a standard type throughout this analysis and the current decay rate is relatively high but may be typical for tokamaks of this size;

2. A horizontal disruption, where the plasma moves radially inward by about $40cm$ starting at the magnetic axis and the initial plasma current is $11MA$ and reduced to zero within about $5ms$; and

3. A vertical disruption, where the plasma current is reduced from $11MA$ to zero within $210ms$ while the plasma moves radially outwards first and then downwards and inwards.

The dynamics of these disruption scenarios are described in more detail in Appendix C.

For most of the examined fault scenarios, it is assumed that the fault remains undetected and no mitigating actions are taken. However, a fault may be detected after a certain detection time and mitigating actions may be initiated. Those reaction scenarios could be imagined to be very complicated, in that one tries to minimize the loads on the PF and TF coils by controlling the currents in the unfaulted PF coils in a coordinated fashion. But such sophisticated scenarios might not be robust enough, and may cause additional

---

† The data has been obtained from cases 0406b and 0516d from R.O. Sayer at the Fusion Engineering Design Center (internal reference FEDC–L–88–PE–0351, 1988).

reliability concerns. However, although such scenarios are not examined in this study, they might be appropriate under special circumstances when simpler scenarios cannot avoid high loads on the coils, and should be investigated in future studies.

Two simple potential mitigating actions are examined in this study:

1. To drive the coil currents in the unfaulted external PF coils to zero on detection of a coil failure; and

2. To decouple all coils from their power supplies and switch a dump resistor in each circuit, i.e., the currents in all external PF coils decay, and the energy of the unfaulted coils is deposited in their respective dump resistors.

It is assumed that an appropriate detection system yields a detection time of $2s$ or less. The dump resistor needs to be chosen to keep the discharge coil voltages below the insulation rating, which can be assumed to be about $20kV$ as suggested for NET [Salpietro 1988]. Furthermore, assuming that the current decay time of a coil is on the order of $10s$, (from the simulation results decay times of $3s$ to $15s$ could be estimated for CIT) and may be reduced to about $1s$ by introduction of a dump resistor, the coil currents are reduced to zero within approximately $3s$ after the initiation of the discharge. Also, a current rampdown within $1s$ can be imagined for mitigating actions of the first type. Then, the detection of a fault can be modeled by a single conservative scenario, where the fault is detected $2s$ after fault initiation, and the currents in the unfaulted coils are removed within the following $1s$. This scenario is used two times in this study to evaluate the potential effect of mitigating actions.

As an example of how the final scenario selection process was performed, some examples will be discussed in the following. In general, all fault scenarios involving short circuits are started at the EOFT since then coil currents are high and the plasma still carries its full current of $11MA$ so that a disruption will be most severe. It can be expected that the consequences of shorts in multiple coils will be worse than single coil shorts, in particular when those coils are located closely together. Therefore, in order to get an estimate for the

differences in the consequences of coil shorts of central solenoid coils and outer PF coils, shorts of the entire stack of central solenoid coils, PF1 to PF3, and of all outer coils, PF4 to PF7, are examined. In another case, a short in PF1 is chosen because the current in PF1 is highest for all coils at EOFT, and the coil temperature has reached $250K$ and is still rising. Also, the average axial and hoop stresses are very high for coil PF1 at EOFT (see Appendix B). The question is whether the driving currents in the neighboring coils of PF1 allow for a quick reduction of the coil current to avoid any temperature problems or whether the coupling and high inductance of PF1 causes a slow current decay in PF1. Such a slow current decay would also lead to a slow decay of the forces on PF1, and in turn possibly lead to higher forces on PF2 and PF3. It may also yield a change in the magnetic field along the inner leg of the TF coils and cause higher than normal out–of–plane forces. This fault scenario is examined with and without mitigating action.

Similar to the last case, a short in PF2 is chosen to investigate the effect on PF1 and PF2 when PF2 is completely passive and mainly driven by PF1 and PF3, which have large inductances and carry high currents at EOFT. In this case, the coil temperatures in PF2 are of no concern, but the forces on the remaining central solenoid coils and the TF coils may become a concern and are therefore evaluated.

Scenarios with asymmetric coil shorts are also examined. Then, only one of the corresponding external PF coils below and above the midplane is faulted. Central solenoid coils are major candidates for such failures since their leads are located in the compact central support structure and are designed coaxially to reduce the error from the magnetic stray field. Therefore, and for reasons mentioned in the last paragraph, asymmetric faults are investigated for the lower coil PF2. These cases are furthermore combined with horizontal and vertical disruption scenarios where the plasma moves inward and downward, towards the central PF coil stack and the lower PF2 coil in particular.

For the scenarios with voltage driven coils, faults of PF1 and PF3 are generally important because of their high temperatures (above $250K$) during the last phase of the pulse. Scenarios starting at EOFT and EOPC are considered.

In addition, coils PF4 and PF7 may have high voltage power supplies, as shown in Table 3–2, and applying the full available voltage at these coils can be expected to yield fast coil current increases. This can also have a large impact on the out–of–plane force along the top region and outer leg of the TF coils, because PF4 and PF7 contribute strongly to the magnetic field in these regions. One of the questions for these voltage driven cases is whether the coil currents, temperatures, or loads will first yield problems.

In order to have reference modes that can be compared with the fault scenarios, and to evaluate the uncertainties embedded in the selection process and the assumptions about the electrical system of the PF magnets, several reference cases without coil failures are also examined. The total number of selected scenarios is 24, and a list of the investigated scenarios is given in Table 3–3. Although these fault scenarios are selected based on the design of CIT, most of the results of the consequence analysis can be expected to be applicable to other machines with similar PF coil arrangement as well, since similar coil current profiles will be required. In the following section, the model and the simulation method that is used to simulate the selected fault scenarios is described.

3.3.3   The Model

An axisymmetric model of CIT is used to simulate the selected fault scenarios listed in Table 3–3. The model contains a representation of the external and internal PF coils, the support structure for the PF and TF coils, the vacuum vessel and the plasma. Each element in this two dimensional model is assumed to be toroidally continuous.

Two versions of this model are used and are illustrated in Fig. 3–9a and b. In the first model (M1), Fig. 3–9a, only the part of the cross section above the midplane is represented and the plasma is modeled as a single coil element at the magnetic axis. This model corresponds to an arrangement where the respective elements above and below the midplane are in series, i.e., carry the same current. Therefore, only symmetric faults can be simulated with this model, and the plasma is stationary. This model consists of 10 PF coil elements, 1 plasma element, and 128 passive structure elements, for a total of

type of fault	case	time	description
Fault Scenarios			
no fault	0	EOFT	all PF coils driven, plasma rampdown
mirror coil pair shorted stationary disruption	1	EOFT	PF1, PF2, PF3 shorted
	2	EOFT	PF4, PF5, PF6, PF7 shorted
	3	EOFT	PF1 shorted
	3a	EOFT	PF1 shorted, fault detected after 2s
	4	EOFT	PF2 shorted
	5	EOFT	PF4 shorted
	5a	EOFT	PF4 shorted, fault detected after 2s
	6	EOFT	PF7 shorted
mirror coil pair shorted horizontal disruption	7	EOFT	PF2 shorted
single coil shorted horizontal disruption	8	EOFT	PF2 (lower coil) shorted
single coil shorted vertical disruption	9	EOFT	PF2 (lower coil) shorted
constant voltage	10	EOFT	PF1, -1.6kV (voltage at EOFT)
	11	EOFT	PF1, -4kV (full voltage)
	12	EOFT	PF3, 3kV (full voltage)
	13	EOFT	PF4, -6kV (full voltage)
	14	EOFT	PF7, -1.2kV (voltage at EOFT)
	15	EOFT	PF7, -4kV (full voltage)
constant voltage	16	EOPC	PF1, 1.9kV (voltage at EOPC)
	17	EOPC	PF7, 1.3kV (voltage at EOPC)
Reference Scenarios			
no coil fault stationary disruption	R1	EOFT	all PF coils driven, IC coils shorted
no coil fault	R2	EOFT	all PF coils driven, IC coils at zero current
no coil fault	R3	BOP	all PF coils driven, IC coils shorted
no coil fault vertical disruption	R4	EOFT	all PF coils driven, IC coils shorted
constant voltage	R5	EOPC	PF1, 1.9kV (voltage at EOPC) IC coil currents zero at EOPC

BOP: beginning of pulse, at t=0s

EOFT: end of plasma current flattop, at t=18.76s for CIT

EOPC: end of plasma current, at t=26.26s for CIT

Table 3-3. List of Investigated Scenarios

139 elements. The second version of the model (M2) allows modeling of asymmetric currents in elements above and below the midplane since these elements are electrically independent. Only the top half of the model is shown in Fig. 3–9b.

Model M2 additionally features a multiple element representation of the plasma, so that plasma movements can be modeled by switching the currents in certain plasma elements on or off. This model has the same coil and structural elements as model M1, but the plasma is now modeled by 14 plasma elements below and 14 above the midplane, leading to a total number of circuit elements of 304.

In both versions of the model, a representation of the TF coil is implemented. As illustrated in Fig. 3–9, the TF coil is approximated by a set of straight line connections between 14 points for each TF coil half. These points have been digitized from a drawing of the CIT machine and have been chosen so that the straight line connections approximately follow the center of the TF coil of CIT.

3.3.4 Scenario Evaluation Indices

The model described in the previous section can be used to simulate the selected scenarios. It is desired to evaluate the magnitudes and dynamics of the loads on the PF and TF coils and the temperatures in the external PF coils. Therefore, the following indices need to be considered, all in comparison to their respective values under normal operating conditions:

- The magnitude and distribution of the forces and moments on the PF and TF coils and their support structure;

- Force reversals which do not occur under normal operating conditions or are of significantly larger magnitude under fault conditions;

- Time shifts in the occurrence of maximum loads or force reversals; and

- Temperature scenarios of the external PF coils.

The stresses in the PF and TF coils resulting from the force scenarios are not computed since the conversion from forces to stresses is highly design dependent.
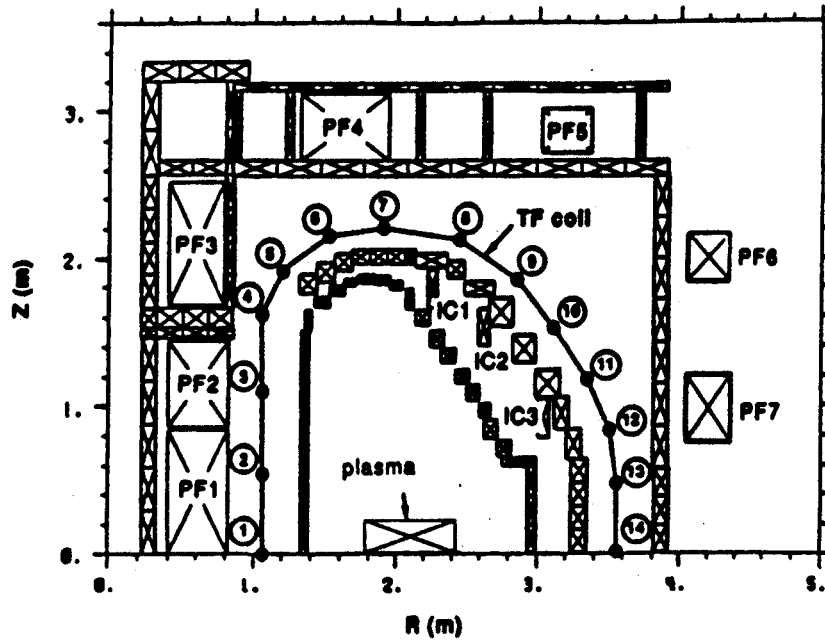
(a) Model Version M1 with a Total of 139 Elements
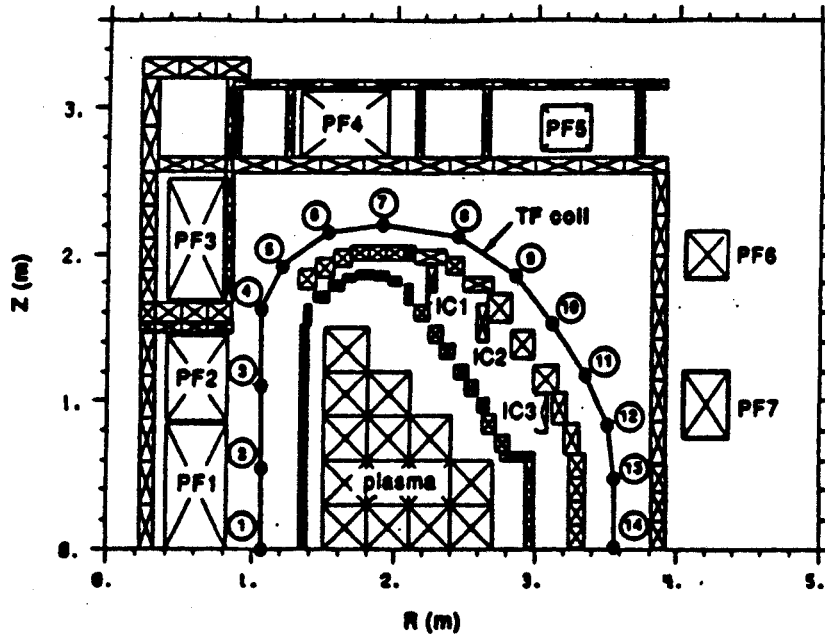
(b) Model Version M2 with a Total of 304 Elements

Fig. 3-9. Electromagnetic Model of CIT

3.3.5   The Simulation Method

The current scenario for each element in the model will be needed to evaluate the indices discussed in the previous section. Since the system is inductively coupled, the currents in each element are obtained by solving the lumped circuit loop voltage equations,

$$\mathbf{L}\dot{\underline{I}} + \mathbf{R}\underline{I} = \underline{U} \tag{3.4}$$

where $\underline{I}(t)$ is the vector of currents in all elements, $\mathbf{L}$ is the inductance and $\mathbf{R}$ the resistance matrix, and $\underline{U}(t)$ is the vector of the driving voltages. This vector $\underline{U}(t)$ is obtained from the desired current and voltage profiles of the unfaulted coils. Either piecewise linear current ramps or constant voltages per coil are used as driving functions for the external PF coils[†].

The inductance and resistance matrices are time–invariant and are computed once for the geometries shown in Fig. 3–9 and a set of element materials and temperatures. For the PF coils, these temperatures are the maximum temperatures occurring under normal operating conditions for each coil and are listed in Appendix D. The structural elements are assumed to be made of stainless steel and operated at LN_2 temperature, except the vacuum vessel, which is operated at room temperature.

The initial currents at EOFT in all passive elements and the internal PF coils are taken as zero for all investigated fault scenarios, and this assumption is discussed in more detail in Chapter 3.4.2.6. The plasma and the external PF coils carry initial currents corresponding to the plasma and PF coil current scenario from Fig. 3–8.

Once the current scenario for each element in the model is obtained, the force influence coefficients for all elements and the field influence coefficients for the points representing the TF coil are used to compute the forces in radial and

---

† The computations of the currents in each model element are performed under use of the program packages SOLDESIGN and NEWEIGEN which have been developed by R.D. Pillsbury, Jr., and are currently available on the MIT Plasma Fusion Center VAX and on the MFE computer network.

vertical direction on the external PF coils and the magnetic field at each point of the TF coil. Assuming that the TF coil current is constant and held at its maximum of $5.775MA$ per coil, as computed in eq. 3.2, the out–of–plane load at a single point of the TF coil representation is obtained as the Lorentz force resulting from the interaction of the magnetic field of the toroidally continuous elements in the model and the TF coil current. In this study, the direction of the TF coil current at a single point of the TF coil representation is approximated by the slope of the straight line connecting the two neighboring points. From the distribution of the out–of–plane forces along the TF coil, the net out–of–plane force, overturning moment about the radial axis, and torque about the vertical torus axis can then be obtained.

The temperature profiles in the external PF coils are computed with the procedure described in Appendix D, which takes the temperature dependence of the resistivity and heat capacity of the coils into account.

A more detailed description of the entire simulation method is provided in Appendix D.

3.4 Simulation Results and Evaluation

This section summarizes and evaluates the results that have been obtained from the simulations of the 24 selected scenarios in Table 3–3.

3.4.1 Temperature Results

For CIT, severe degradation of the coil insulation can occur for temperatures higher than $330K$, which is therefore adopted as the limit temperature for the external PF coils. In the simulations, this temperature is not reached in any external PF coil for faults involving shorted coils. In most of these cases, the current decay in the faulted coil is even faster than under normal operating conditions, and the temperature stays well under the maximum temperature that would be reached at the end pulse under the preprogrammed current scenario.

In cases where coils are driven with constant voltages, the adopted limit temperature will be exceeded in the faulted coil in any case after a certain

period of time since adiabatic heating of the coil is assumed, and energy is provided for the coil continuously. However, it takes a minimum of 4s (in case 11) after fault initiation to reach 330K for the considered range of scenarios, and for most cases the period of time between fault initiation and when 330K is exceeded is between 6s to 15s. This implies, that temperature problems could be avoided in the external PF coils when protective actions are taken within 4s or less from the time of fault initiation.

3.4.2   Analysis of Mechanical Loads on the PF and TF Coils

3.4.2.1   Impact of Load Magnitude and Time

Since the simulations provide the loads on the PF and TF coils as a function of time, they contain information about the dynamics and the magnitude of the examined loads. For designing protection schemes and mitigating actions, the time frame for the occurrence of the maximum loads for each external PF coil or along the TF coil are most important. For the structural design of the coils and supports, the magnitude of the loads rather than their dynamics will be the decisive factor. Therefore, the dynamics of the mechanical loads on the PF and TF coils is particularly dealt with in Sections 3.4.2.2, 3.4.2.4 and 3.4.2.5, while in the remaining sections in this Chapter the analysis of the magnitudes of the loads is particularly emphasized.

Since the maximum loads under normal operating conditions will be different for the different external PF coils or along the TF coil, the loads occurring under fault conditions can be compared and evaluated best when they are normalized to the maximum loads under normal operating conditions. This leads to the concept of a multiplication factor, which is the ratio of the maximum absolute load under fault conditions to the maximum absolute load under normal operating conditions for each external PF coil or the TF coil. Assuming that a safety factor of at least 2 will be implemented in the design for each load, multiplication factors between zero and two would define an envelope of allowable forces and moments. Multiplication factors outside this allowable envelope imply a potential for further fault consequences and point to design areas which may require additional efforts.

In this study, all fault scenarios are initiated at EOFT or EOPC, during the last phase of the pulse. While the load scenarios under normal operating conditions may be quite different for external PF coils during the pulse, as the stress scenarios in Appendix B show, the load conditions at EOFT may still be considered as the most severe during the pulse. Therefore, the normalizing loads for the computation of the multiplication factors are all taken as the maximum absolute loads occurring under normal operating conditions after EOFT during a pulse. These loads are given in Table 3–4a and 3–4b.

3.4.2.2   Time Frame of the Load Scenarios

Under normal operating conditions, the maximum loads on the PF and TF coils occur either at EOFT or EOPC. For the examined range of fault scenarios, maximum loads occur within the first 0.5 to 1 second after fault initiation at EOFT, or at EOPC. The load dynamics are dominated by the occurrence of a disruption shortly after fault initiation, and later during the pulse by the driving currents in the unfaulted external PF coils. The distribution of the coils and TF coil points which experience their maximum load shortly after EOFT or at EOPC changes only very little for the different fault scenarios. The type of plasma disruption is also of minor impact in this regard. Table 3–5 gives an overview of the times of occurrence of maximum loads for the different external PF coils, for the points on the TF coil, and for the total forces and moments on one half of the TF coil. The table contains data for case R1 where no coil is faulted and a stationary disruption occurs at EOFT.

There are only few exceptions when the maximum loads are observed at shorter times after fault initiation than in the example shown in Table 3–5. For scenarios where PF1 is involved (cases 1, 3, 3a, 10 and 16) the maximum of the total loads on a TF coil half may occur already within the first 1 to 3 seconds from fault initiation. Also, when a fault is detected and the simulated mitigating actions are taken (cases 3a, 5a), the maximum loads at the TF coil points 5 to 7 are reached within 2 to 3 seconds after fault initiation.

The loads on coils PF2 and PF4 may also be reached earlier, i.e., about $0.5s$ to $1s$ after fault initiation when the respective coils are shorted (cases 4 and 5). Furthermore, there are small differences between stationary and horizontal

Maximum Forces on PF Coils		
coil	radial force (MN/m)	vertical force (MN/m)
PF1	71.1	42.0
PF2	21.0	6.6
PF3	30.4	3.3
PF4	1.4	0.7
PF5	0.4	0.2
PF6	0.9	1.3
PF7	4.4	0.4

(a) PF Coil Loads

Maximum Out-of-plane Loads on TF Coils			
point/total	load	point/total	load
2	6.6 MN/m	10	6.7 MN/m
3	7.8 MN/m	11	6.9 MN/m
4	3.8 MN/m	12	2.7 MN/m
5	0.95 MN/m	13	2.0 MN/m
6	0.93 MN/m	F_{tot}	6.3 MN
7	4.6 MN/m	M_r	15.7 MNm
8	6.0 MN/m	M_z	28.1 MNm
9	6.6 MN/m		

(b) TF Coil Loads (Totals on Half TF Coil)

Table 3-4. Maximum Absolute Loads on the PF and TF Coils under Normal Operating Conditions (Case 0)

Type of Coil	Coil or Point/Net Load	Time of Maximum Load After Fault Initiation
PF Coil	PF1, PF2v, PF5, PF6, PF7	0.5s
	PF2r, PF3, PF4	7.5s
TF Coil	1 to 4	0.5s
	5 to 7	7.5s
	8 to 13	0.5s
	F_{tot}, M_r, M_s	7.5s

v: vertical force only

r: radial force only

F_{tot}: net out-of-plane force on a TF coil half

M_r: overturning moment on half TF coil

M_s: torque on half TF coil

Table 3-5. Time Frame for the Maximum Loads on the PF and TF Coils when no Coil is Faulted under a Stationary Plasma Disruption (Case R1)

disruptions on one side, and vertical disruptions on the other side when the lower PF2 coil is shorted, in that the vertical disruption may lead to the maximum load on coil PF7 within the first second from fault initiation. More detail on the effect of different disruption scenarios is provided in section 3.4.2.4.

In summary, the loads on the PF coils and at points of the TF coil which are located closely to the inner or outer leg of the TF coil, tend to reach their maximum shortly after fault initiation, since these areas are closest to the disrupting plasma, and the disruption will be the dominant factor during this period of time. At coils or points located around the top region of the TF coil, the maximum loads may be obtained significantly later, namely at EOPC, and the load dynamics are dominated by the driving currents in the unfaulted coils.

3.4.2.3 Evaluation of Multiplication Factors

The multiplication factors for all fault scenarios with undetected coil faults and except for cases 13 and 15, where coil PF4 or PF7 is driven with its full available voltage, are shown in Figs. 3–10 to 3–12.

In general, the multiplication factors are obtained from load scenarios between the time of fault initiation and when the first external PF coil exceeds the adopted limit temperature of $330K$.

For all these scenarios, the multiplication factors for the force on the external PF coils in the radial direction are well within the allowable envelope, as Fig. 3–10 illustrates. Fig. 3–11 shows that most of the multiplication factors for the vertical forces lie within a range of 1 to 1.8. Only the vertical forces on PF2 and PF7 reach factors larger than 2. For PF2, this occurs only when PF1 is driven with its full voltage at EOFT (case 11), since PF1 maintains a high current of about $14MA$ in this case, leading to high forces on PF2 whose current is ramped up at the same time. The vertical force on PF2 is still rising when PF1 reaches $330K$ about $4s$ after fault initiation, and would reach a maximum twice as high at EOPC if the current in PF1 could still be maintained and no insulation failure occurred and assuming that no protective action is taken.

The multiplication factor of 4 on PF7 is only obtained when PF7 itself is driven with its voltage at EOFT (case 14). In all other cases, the factors are below 2.5. In case 14, the current in PF7 stays at a value of about $4.4MA$ which is reached at EOFT. The current ramps in the unfaulted coils lead to a steady rise of the vertical force multiplication factor on PF7 from 2.4 shortly after fault initiation to 4 at EOPC. However, it is likely that this multiplication factor of 4 causes only little or no further consequences since the maximum vertical force on PF7 in case 14 is compressive, and its absolute value is of the same order as the vertical force on the neighboring coil PF6 at the same time.

The multiplication factor in the range of 2 to 2.5 that is found in all other cases started at EOFT is due to the disruption and is reached within $0.5s$ after

**Maximum Multiplication Factors
of Radial Forces on PF Coils**
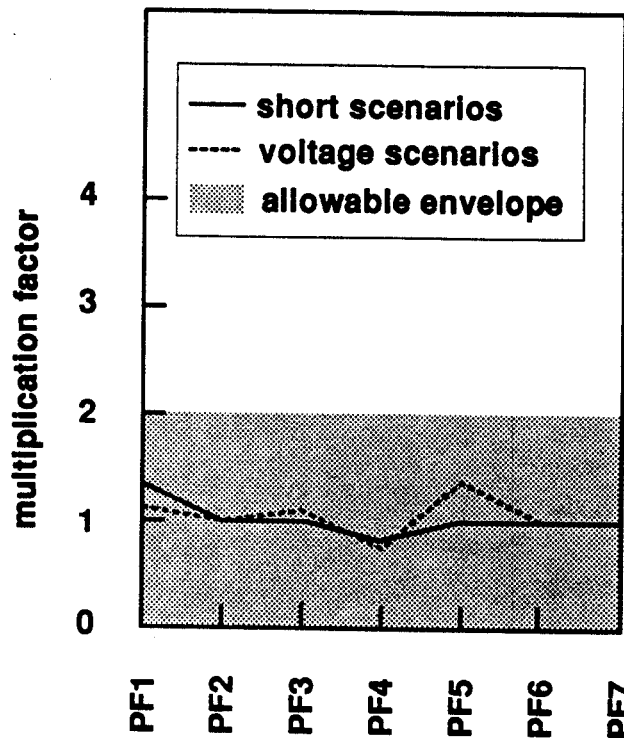
Fig. 3-10. Maximum Multiplication Factors for the Radial Forces on the External PF Coils for Scenarios 1 to 17 (Except Cases 13 and 15)

fault initiation, where the stationary disruption tends to cause higher vertical loads on PF7 than the horizontal or vertical disruptions. This can be attributed to the fact that the plasma does not move away from coil PF7 during a stationary disruption and, therefore, maintains a strong impact on the loads on PF7.

In summary, shorts in general and most of the scenarios with constant coil voltages, may pose little threat to the PF magnets for the examined range of scenarios provided that the structure is designed to accommodate load multiplication factors on the order of two under fault conditions.

**Maximum Multiplication Factors
of Vertical Forces on PF Coils**
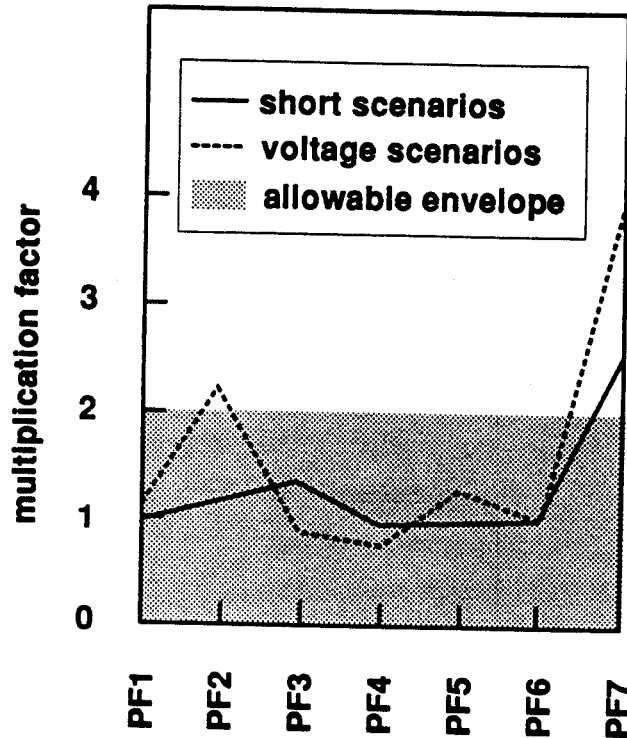
Fig. 3-11. Maximum Multiplication Factors for the Vertical Forces on the External PF Coils for Scenarios 1 to 17 (Except Cases 13 and 15)

A similar result is obtained for the out-of-plane loads along the inner and outer leg of the TF coil (points 2 to 4 and 7 to 13), which can be seen from Fig. 3-12. The multiplication factors for these points lie in the range of 1 to 1.8 and are very similar for scenarios involving shorted coils or the application of a constant coil voltage. Only at the inner corner of the TF coil (points 5 and 6), high multiplication factors of up to 4.4 are obtained. This tendency of high multiplication factors at the inner corner of the TF coil is found for almost all examined scenarios, and is particularly strong when PF4 or PF7 are faulted. This may be attributed to the strong contribution of these coils to the plasma

**Maximum Multiplication Factors
of Out-of-plane Forces on TF Coils**
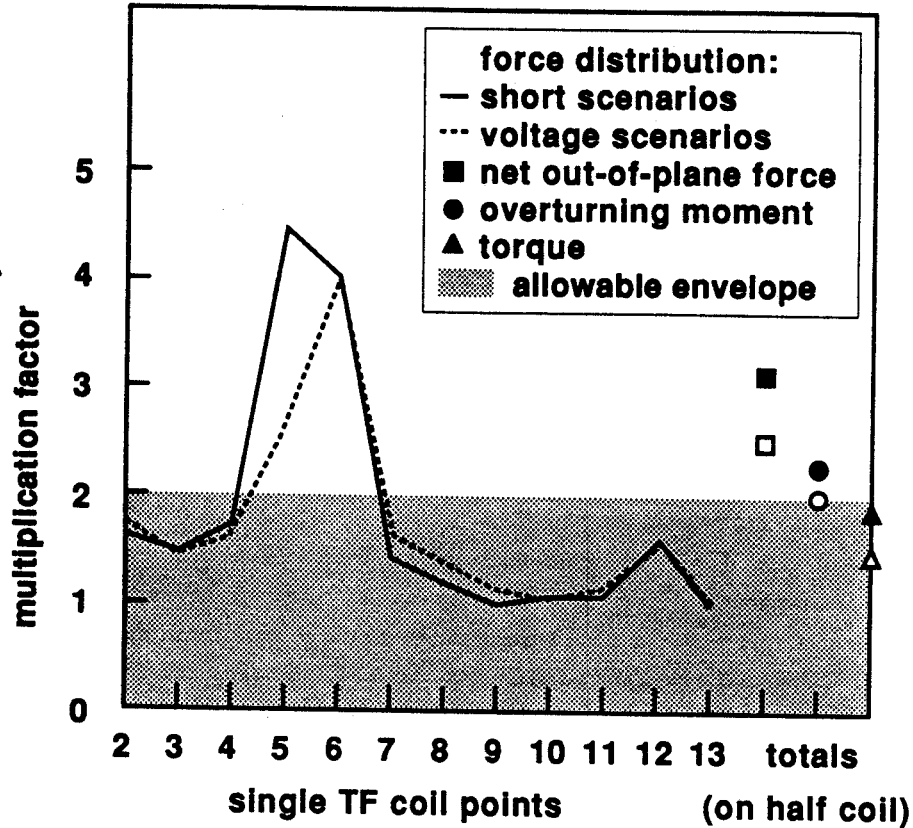
Fig. 3-12. Maximum Multiplication Factors for the Out-of-Plane Loads on the TF Coils for Scenarios 1 to 17 (Except Cases 13 and 15); Filled Symbols: Sort Scenarios; Unfilled Symbols: Voltage Scenarios

loop voltage and flux swing and their high impact on the shaping and positioning of the plasma. Combined with their large time constants, this yields the potential for strong impact on the force distribution along the TF coil.

Faults involving PF1 yield multiplication factors very close to unity at points 5 and 6, and are thus likely to be of little concern. The same can be assumed to be valid for coils PF5 and PF6, since the operating currents and voltages are smaller than for coils PF4 and PF7, as can be seen from Table 3-2.

Furthermore, coils PF5 and PF6 are relatively far away from the TF coils and the plasma. This assumes that design margins are multiplicative rather than additive. In the case of additive design margins, multiplication factors smaller than two could also lead to further consequences under high absolute loads.

The net out–of–plane loads on a half TF coil resulting from the distribution of the out–of–plane forces along the TF coil, may reach multiplication factors of up to 3.2, which is also illustrated in Fig. 3–12. Shorts generally yield smaller multiplication factors than voltage faults. However, these net forces and moments should not be of major concern provided that the support structure for the out–of–plane loads on the TF coils (i.e., the intercoil and central support structure) is be designed to accommodate significantly higher forces during faults than under normal operating conditions. For the design of the TF coil itself, the local effects at the inner corner of the TF coil are seen to be of higher importance. When one the coils PF4 or PF7 is driven with its full available voltage the load conditions for the PF and TF coils become most severe. A summary of multiplication factors for these cases (cases 13 and 15) is given in Table 3–6. High multiplication factors of forces on the driven coil may be obtained, and the force increases particularly rapidly. The limit temperature of $330K$ is reached $6s$ after fault initiation at EOFT in both cases.

In case 13 the forces at the inner corner of the TF coil may rise rapidly and lead to more than a tenfold increase over the maximum force under normal operating conditions, as Table 3–6 shows. This effect also causes multiplication factors of the net out–of–plane force and overturning moment of 5 and 3.6, while the maximum torque value changes only little. When PF7 is driven with its full available voltage, the effect on the forces at the inner corner of the TF coil is much smaller than when PF4 is driven. However, the forces along the outer leg of the TF coil are increased in case 15, leading to a torque multiplication factor of 2.8, which is the highest obtained for all investigated scenarios. The change in the force distribution along the outer leg of the TF coil also leads to the high multiplication factors of the net force and overturning moment.

In general, in both cases 13 and 15, fast fault detection and protective action taken within 1 or 2s after fault initiation will be required to prevent coil damage.

An asymmetric short of coil PF2 is examined in case 8, where only the lower coil PF2 is shortcircuited while the upper coil PF2 is driven with its preprogrammed current as a horizontal disruption takes place. It is found that the half of the system with the faulted coil experiences very similar loads on the PF and TF coils as when a symmetric fault occurs (here case 7). Otherwise, the unfaulted half of the system yields the same load scenario as if no coil at all would be faulted. This suggests that an asymmetric coil fault may not lead to significantly different load multiples on the faulted half of the system than would occur under symmetric fault conditions. More analysis of asymmetric faults in other coils will be necessary to confirm this result.

3.4.2.4 The Impact of the Type of Disruption

Several fault scenarios with different types of disruptions are compared, together with two reference cases, R1 and R4, where no coil is faulted but a stationary and a vertical disruption occurs, respectively.

It is found that the type of disruption has negligible impact on the loads on the external PF coils. However, the fact that a disruption occurs is important during the first 0.5s after fault initiation. This is illustrated by Table 3–7, where multiplication factors for the loads on the PF and TF coils are given for a scenario with a stationary disruption.

Furthermore, the load distribution and load magnitudes along the TF coil are slightly affected by the type of disruption. Mainly the loads at the inner corner of the TF coil can change, but the magnitude of the changes is found to be in a range of only 10% to 20% for the examined types of disruptions, with the higher loads appearing for horizontal or vertical disruptions rather than for stationary disruptions.

coil	radial direction		vertical direction	
	case 13	case 15	case 13	case 15
PF1	1	1.1	1	1
PF2	0.2	0.5	1.2	1.2
PF3	0.9	1.6	5	0.6
PF4	79 (13)*	1.2	19 (2.8)*	0.5
PF5	1	1.4	1	1.5
PF6	1	1	1	1
PF7	1	2.8	1	13

* after 2s
limit temperature reached after 6s

(a) PF Coil Load Multiplication Factors

TF coil point/total	case 13	case 15
2	1.5	1.5
3	1.5	1.4
4	4	1.4
5	38 (14)*	1.5
6	35 (13)*	3
7	1	1.6
8	1	1.8
9	1	1.6
10	1.1	1.8
11	1.1	2
12	1.7	3
13	1	1
F_t	5	4.2
M_r	3.6	3
M_z	1.1	2.8

* after 2s
F_t total separating force on half coil
M_r overturning moment on half coil
M_z torque on half coil

(b) TF Coil Load Multiplication Factors (Totals on Half TF Coil)

Table 3-6. Multiplication Factors for the Loads on the PF and TF Coils for Cases 13 and 15

Coil	Radial Direction	Vertical Direction
PF1	1.2	1
PF2	1	1.2
PF3	1	1
PF4	0.7	0.7
PF5	1	1
PF6	1	1
PF7	1	2.5

(a) PF Coil Load Multiplication Factors

Point/Total	Factor	Point/Total	Factor
2	1.7	10	1.1
3	1.5	11	1.1
4	1.6	12	1.7
5	1.9	13	1
6	0.7	F_{tot}	1.2
7	1.1	M_r	1
8	1	M_z	1.1
9	1		

F_{tot}: net out-of-plane force on a TF coil half
M_r: overturning moment on half TF coil
M_z: torque on half TF coil

(b) TF Coil Load Multiplication Factors (Totals on Half TF Coil)

Table 3-7. Effect of a Stationary Disruption on the Multiplication Factors for the Loads on the PF and TF Coils

The differences in the load dynamics are essentially constrained to the first $0.5s$ from fault initiation, and are primarily caused by the currents induced in the IC coils by the moving plasma during the disruption. The main difference arises for a vertical disruption, where the currents in the lower IC coils peak downward and upward within a very short time frame, leading to a similarly fast reaction of the loads on points 4 to 6 of the TF coil. This is caused by the movement of the plasma outward, downward and then inward, while it carries a current close to its maximum. Such a reaction is not observed for stationary or horizontal disruptions where the loads along the TF coil increase immediately after fault initiation. However, the reaction of the IC coils is still highly important for the load dynamics in these cases. As an example, the IC coil currents for cases 0 and R1, i.e. when no coil is faulted but with and without a stationary disruption, are shown in Fig. 3–13.

Without a disruption the plasma current is reduced slowly enough to drive the IC coil current immediately to negative currents until EOPC, when they are ramped up again until they decay after the end of the pulse. When a stationary disruption occurs, the fast decay of the plasma current first leads to a strong change in the magnetic field. However, the IC coils then try to counteract this change, and high positive currents in the IC coils are induced. The effect of the driven external PF coil currents seems to be negligible during this phase. Finally, when the plasma current has decayed, the IC coils are driven to negative currents by the external PF coils, similar to the case without disruption, but now at a higher rate of change and to higher negative currents.

This behavior explains the dominance of the effect of the plasma disruption during the first $0.5s$ after fault initiation and the somewhat increased loads along the TF coil, and particularly at points 4 to 6. Otherwise, the differences in the fast changes of the IC coil currents for the different disruptions are too small to have significant impact on the load conditions for the PF coils.
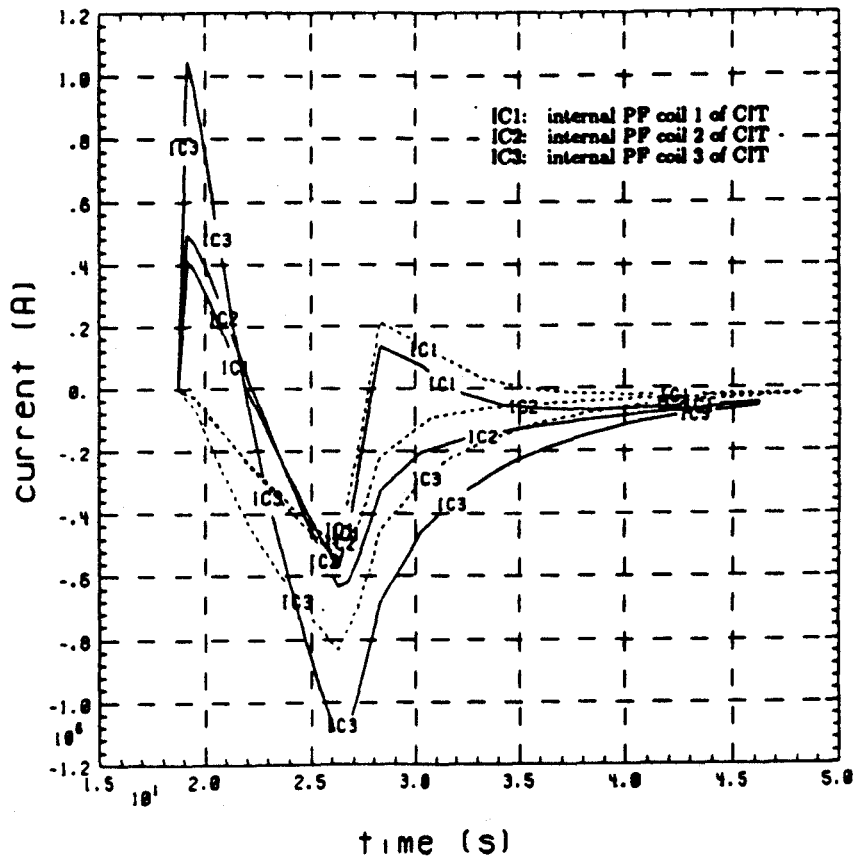
Fig. 3-13. Current Scenarios of the Internal PF Coils with and without Disruption when no Coil is Faulted; Solid Lines: No Disruption; Dashed Lines: Stationary Disruption

3.4.2.5 Effect of Potential Mitigating Actions

The effect of a fast current rampdown within $1s$ of fault detection when the fault is detected $2s$ after fault initiation is examined in cases 3a and 5a, i.e., for shorts of coils PF1 or PF4.

In both cases, the forces on the external PF coils can be reduced rapidly after initiation of the mitigating action, and the multiplication factors may be
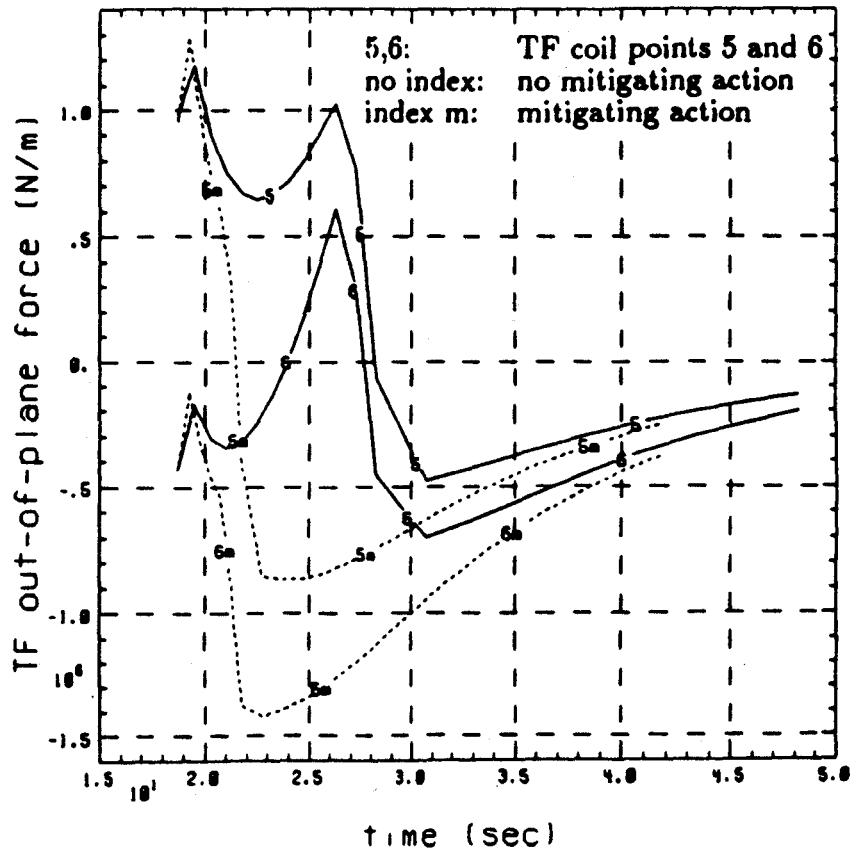
Fig. 3-14. Effect of Fast Current Rampdown after Detection of a Coil Fault
(Cases 3 and 3a)

equal or, for most loads on the external PF coils, less than without fault
detection.

The same result is obtained when PF4 is shorted and the proposed
mitigating action is taken. However, in case 3a, where a fault of PF1 is
examined, the force on the TF coils may be locally increased by an additional
factor of 2.3, and the maximum load on the TF coil is reached when the coil
currents in the unfaulted coils are ramped down. This is illustrated in Fig.
3-14.

This timing may be caused by the IC coils. The out-of-plane loads on the TF coil are determined by the magnetic field at the TF coil, and the IC coils have a strong impact on the magnetic field at the inner corner of the TF coils. Since it is assumed that the IC coils are passive, the currents in the IC coils are induced by changes in the magnetic field. The fast current rampdown after fault detection obviously leads to such a fast change in the magnetic field that the IC coil currents are ramped up, and contribute to the higher loads at the inner corner of the TF coil. It may be that the main contributor to this field change at the IC coils is coil PF4, since the load enhancement is not observed when PF4 is faulted in case 5a.

3.4.2.6   The Impact of the Terminal Constraints on the Internal PF Coils

In this section, the impact of the assumptions made for the terminal constraints and initial currents of the IC coils is evaluated. The importance of the IC coil currents on the loads for the TF coils has already been discussed in previous sections. This strong impact is a direct consequence of the design objectives for the IC coils, which require that the IC coils allow for fast changes of the magnetic field in the plasma area.

An example of how strongly the IC coils contribute to the magnetic field at the TF coils is given in Table 3–8. Without any coil being faulted (case 0), the IC coils contribute about three quarters of the vertical magnetic field at TF coil point 1 at EOPC, and almost half of the radial magnetic field at point 7 about $1s$ after EOPC. This is significantly more than the contribution from the external PF coils or from the remaining structural elements. Obviously, this explains the dominant impact of the IC coil currents on the out-of-plane loads on the TF coil.

For all the scenarios discussed so far, it has been assumed that the IC coils are shorted, i.e., completely passive. This assumption is justified as a first approximation since the IC coil current scenarios are not well defined at the present time. However, the IC coils may not be completely passive, i.e., there may be diodes, etc., in the circuit that lead to some terminal constraints. The high transient eddy currents of up to $1.2MA$ observed in the simulations must be

Time (s) (from BOP)	TF Coil Point	Magnetic Field (T)	Contribution in % to Magnetic Field from		
			IC Coils	Ext. PF Coils	Other Elements
26.26	1	$B_z = 1$	73.6	11.7	14.7
27.26	7	$B_r = 0.6$	44.8	27.9	27.3

B_z: vertical magnetic field
B_r: radial magnetic field
BOP: beginning of pulse

Table 3-8. Examples for the Contribution of the IC Coils to the Magnetic Field at the TF Coils (Case 0)

considered in the design of these coils, which are sized to sustain currents around $0.5MA$. On the other side, high voltages at the IC coil terminals may be required to control the observed current peaks which follow disruptions.

A reference scenario (case R2) is simulated where no coil is faulted, no disruption occurs, but all IC coil currents are zero at all times. This is another limit case in that it assumes total control of the IC coil current. It is found that the load scenarios for the external PF coils are essentially unchanged when compared to the case with the IC coils being passive (case 0). This is due to the distant location of the external PF coils from the IC coils. The same is true for the loads on the TF coil along its inner and outer leg. But at TF coil points 4 to 8, the load scenarios change significantly, and the maximum loads at points 5 and 6 are considerably larger than when the IC coils are shorted. This is illustrated in Fig. 3–15, and the enhancement factors for the maximum loads are 2.5 and 3.5 for points 5 and 6 when compared to case 0. Thus, the loads at the inner corner of the TF coil may even increase when the currents in the IC coils are controlled. This could be attributed to a lack of opposition to fast changes in the magnetic field which is usually provided by the IC coils.

Another issue related to the IC coils is concerned with the initial currents in the IC coils and structural elements at the beginning of fault initiation. All scenarios starting at EOFT are started with zero initial currents in the IC coils. Simulations of faults initiated at EOPC start with initial currents obtained at EOPC in case 0, i.e., under normal operating conditions when started with zero initial IC coil currents at EOFT. This arrangement is chosen since it can be expected that the eddy currents in the structural elements have died out at the EOFT, since few changes in the external PF coils are imposed during the plasma current flattop, as illustrated in Fig. 3–8. For the IC coils, similar arguments can be made, but clearly with less certainty. Reference scenario R3, which assumes passive IC coils and zero initial currents at the beginning of pulse (BOP) demonstrates that the loads at EOFT on the PF and TF coils may be quite different from the case where the initial currents in the IC coils and structural elements are zero at EOFT. For coil PF4, and at the inner corner of the TF coil, the loads at EOFT are higher by factors of up to 2 for the scenario starting at BOP compared to the scenario starting at EOFT. But the
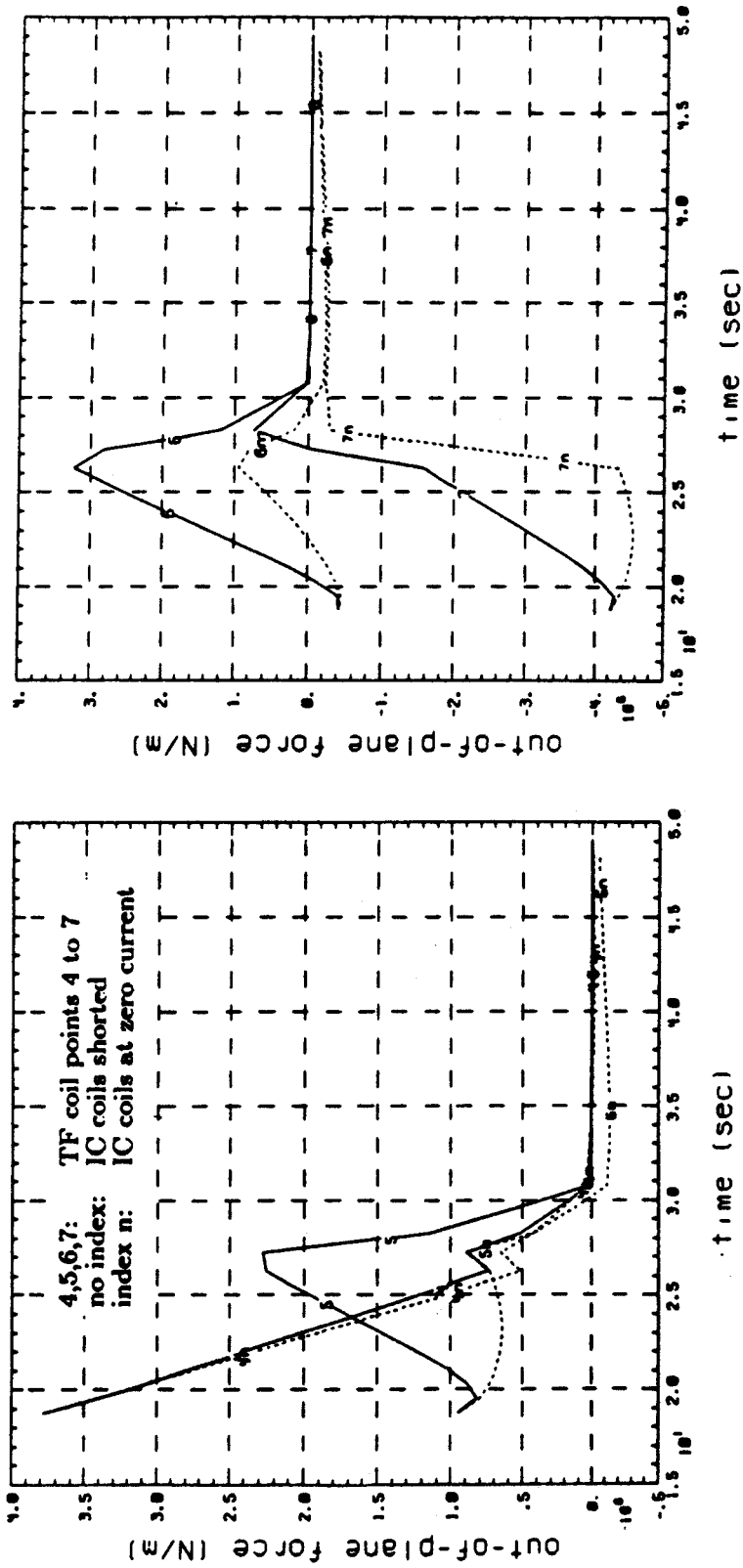
Fig. 3-15 Effect of the Terminal Constraint at the Internal PF Coils
on the Loads at Points 4 to 7 of the TF Coil

maximum absolute forces observed in case R3 are higher as well, by factors of 1.5 to 5 for coils PF2 to PF4 and at the TF coil points 5 and 6. This example illustrates that the load condition of the PF and TF coils are very sensitive to the initial conditions for the IC coil currents and thereby the terminal constraints on the IC coils.

Reference case R5 evaluates the effect of the initial currents for scenarios started at EOPC. The same fault scenario as in case 16 is adopted, but now all initial currents except for the external PF coils are set to zero. It is found, that the load conditions at the inner corner of the TF coil and for coil PF4 are again more severe, with additional enhancement factors of 3 to 5.

In summary, the terminal constraints on the IC coils are very important for the load conditions which develop under fault and under normal operating conditions. In particular the loads at the inner corner of the TF coil, points 4 and 5, and on coil PF4 may be increased when the IC coils are controlled rather than passive. These loads also depend on the initial conditions at fault initiation.

3.5   Comparison of the Loads on CIT and NET

A number of similarities between CIT and NET have already been mentioned in previous chapters. Both machines are experimental tokamak devices which are expected to achieve operation in the ignited plasma regime. However, the size of both machines and their magnet technology differs significantly. CIT is a machine with a major radius of $2.1m$ and features resistive coils, while the major radius of the NET machine may be almost $6m$ and all magnets are superconducting except the internal PF coils [Salpietro 1988]. There is no unique scaling factor for the sizes of these machines, but the dimensions of NET are radially larger by about 2.4 and axially larger by about 2.55. Table 3–9 gives an overview of the major parameters of the magnet systems of both machines.

Both devices have D–shaped TF coils and a similar arrangement of the PF coils, with internal and external PF coils. The current NET design calls for

	NET*			CIT**		
TF Coils:						
TF coil inner radius (m)	2.5			1.2†		
TF coil outer radius (m)	8.3			3.4†		
Major plasma radius (m) (magnetic axis)	5.9†			2.1		
Maximum field at winding (T) (1/R scaled)	11.4			19.3†		
Field at axis (T)	4.8 - 5			11		
Number of TF coils	16			20		
TF coil current per coil (MA)	7.35†			5.775†		
PF Coils:						
Plasma current (MA)	10.8, 11.4, 14.8			11		
Internal PF coils	1 (copper)			3 (copper)		
PF coil coordinates	coil	R (m)	Z (m)	coil	R (m)	Z (m)
Central solenoid coils	P1	1.48	±6.5	PF1,2,3	0.6	±2.75†
Upper coils	P3	4.05	±6.7	PF4,5	1.6/3.2	±2.9
Outside coils	P4	9.65	±2.5	PF6,7	4.2	±2/0.95

*: NET data from [Salpietro 1988]
**: CIT data from [CIT 1987, Pillsbury 1988]
†: estimate

Table 3-9. Comparison of the Parameters of the Magnet Systems of CIT and NET

	NET*		CIT**
plasma current (MA)	11	15	11
peak out-of-plane force (MN/m)	16	20	8
net out-of-plane force on half TF coil (MN)	75	75	8
overturning moment on half TF coil (MNm)	40	28.5	16
torque on half TF coil (MNm)	na	na	8

na: not available
*: NET data from [Salpietro 1988]
**: CIT data from case 0

Fig. 3-10. Comparison of the Out-of-Plane Loads on the TF Coils for CIT and NET under Normal Operating Conditions

only one pair of internal PF coils and possibly a second redundant internal coil pair, while CIT currently features 3 pairs of internal PF coils. These internal coils must provide the fast feedback control of the plasma in both designs. The slow preprogrammed control is performed by the external PF coils, where NET and CIT have a stack of central solenoid coils and outer PF coils. However, NET features only two outer coils, P3 and P4, compared to four outer coils, PF4 to PF7, at CIT.

When an average scaling factor of 2.5 is used, it is found that the NET coils P3 and P4 are approximately at the same relative location to the central solenoid coils and the TF coil as the coils PF4 and PF7 of CIT.

Some data on the out-of-plane loads on the TF coils exist for NET [Salpietro 1988] and are compared with the loads found in this study under normal operating conditions (case 0) in Table 3-10. This table illustrates that there exists no linear relationship between the scaling factors for the machine dimensions and the loads on the TF coil. The net out-of-plane force found in the simulations for CIT is only about one tenth of that for NET, while the peak out-of-plane forces and the overturning moment are almost half the value given for NET.

In principle, the results of the consequence analysis for CIT in this study should be transferable to other machines like NET. However, further studies are needed to establish a relation between the scaling factors for the machine size and those for the dynamics and magnitudes of the load multiplication factors.

Chapter 4

SUMMARY AND CONCLUSIONS

Highly reliable, safe and cost-efficient magnet systems will be required to achieve the desirable availability, safety and cost goals for future fusion devices. It is therefore important to ensure the reliability, reduce the risk, and enhance the design of magnet systems. A failure and fault consequence analysis of magnet systems can contribute to these goals to a high degree. So far, such failure analysis has primarily been performed for Toroidal Field (TF) magnet systems. The Poloidal Field (PF) magnet system has been considered to have similar properties as the TF system. One reason for this is that only little published data about the analysis of PF coil faults exists, and the database of fault consequences is not well developed for the PF magnets.

The first part of this study examines the failure modes of the entire magnet system and identifies the essential differences between the TF and PF magnet systems. In particular, the pulsed operation and the diverse operational tasks of the PF magnet system can lead to a number of interactions with other reactor subsystems and need particular attention. As an example, a large number of basic failure modes of the TF magnet system are connected to interactions with the PF magnets. One important group of failures which may contribute highly to those interactions, are electrical failures of the PF magnet system. The second part of this study therefore investigates the consequences for the PF and TF coils resulting from two basic categories of electrical failures of the PF magnet system.

4.1   Summary

4.1.1   Breakdown of a Magnet System

The functional breakdown of the magnet system is a first step in the analysis of failure modes and the development of fault trees. Thus, the choice of the subsystem boundaries of the magnet system is important for the clarity of the following failure analysis, since an appropriate choice may simplify the tracking of failure modes and interactions significantly. In this study, the magnet system is first broken down into the TF and PF magnet systems, since these systems have entirely different operation modes. The interactions between these systems are then considered in a separate interaction analysis. While the TF magnet system contains multiple coils of the same design, the PF magnet system comprises two different coil systems. These systems are the external and internal coil system, in which each coil is of the same type but not exactly of the same design. Furthermore, each coil contributes to the multiple functions of the coil system. Besides the coil systems, each magnet system also includes a coil cooling system, a power supply system, and a protection and control system. It is found that the boundaries of the coil cooling system and the protection and control system are most difficult to draw when it is desired to keep the number of interactions across system boundaries small. In general, systems like the plant cryogenic cooling system or the external TF coils power supply system, whose design has little implications for the design of the magnet system ought to be excluded from the analysis of the magnet system. However, the external PF power supply system may be highly important for the design of the PF magnets and need to be examined.

4.1.2   Failure Analysis of Magnet Systems

The analytical method used in this study to derive the failure modes is fault tree analysis. Fault tree analysis is now a widely accepted tool for failure mode analysis. Fault trees allow visualizing the failure logic of a system and are thereby a powerful communication tool.

The functional breakdown of the magnet system can directly guide the development of fault trees for each magnet subsystem. It is found that the fault trees contain mostly OR–gates at the higher levels of failures. At lower levels, a number of failures are caused by continuous combinations of multiple variables. Often, such failures involve cyclic mechanical loadings of equipment under severe environmental conditions, i.e., magnetic fields, thermal gradients or irradiation.

In general, the environmental conditions are also of high importance for a large number of failures of the instrumentation and signal processing. Similarly, the quality of manufacturing and assembly may have a large impact on the reliability, in particular for superconducting coils, due to the sensitivity of superconducting material to mechanical impacts. Furthermore, a number of failures may be caused by inadequate cooling of equipment, so that either passive cooling should be used wherever applicable or deformations of cooling lines and their sensitivity to foreign materials need particular attention during the design.

In general, there exist broad similarities between the fault trees for the TF and PF magnets, but some areas show significant differences. The main differences in the failure analysis between the PF and TF magnet system stem from the design of the central solenoid coil support structure, the internal PF coils, and the power supply and control system.

The central solenoid coils need to be supported in radial and axial direction by a structure which avoids contact with the central TF coil support structure and whose radial dimensions are constrained by the size of the fusion device. This also leads to constraints on the design of the current leads, which may in turn increase the danger of shorts between coil terminals. The internal PF coils

are subject to high mechanical and thermal loads and irradiation due to their proximity to the plasma. However, if space permits, redundant coils can be installed to allow for increased reliability. The PF power supply and control system is significantly different from that of the TF system since each PF coil needs to be provided with a different current scenario and the feedback control of the plasma parameters is to be performed on a faster time scale. Therefore, the potential for control and command failures, failures of protecting and switching equipment, and of the external power supply system is greatly increased for the PF power supply and control system when compared to the respective TF systems.

In general, a number of failure modes of the TF magnet system is found to be caused by interactions with the PF magnet system. Since these interactions are not included in the failure mode analysis, they need to be examined in a separate interaction analysis.

4.1.3 Interactions Analysis

The PF coil system is used for initiating and inducing the plasma current and for controlling the position and shape of the plasma. This requires the pulsed operation of the PF coils, where each coil will usually follow a different current scenario.

The operational as well as the structural characteristics of the PF magnet system can cause several types of interactions with other reactor subsystems. Table 4–1 shows an interaction matrix for the PF magnet system which describes the interactions caused by the four main PF magnet subsystems (in the top row) to several reactor subsystems (in the left column). The table includes the interactions that can occur during normal operation or under fault conditions. Since most elements of the interaction matrix are occupied, the PF magnet system is coupled with a large number of reactor subsystems. Most of the coupling is due to the pulsed operation of the PF coils, and the strong reliance on feedback information from the plasma which requires a large number of control actions. The complex task of the PF magnet system also requires a complex electrical system which can produce a large potential for fault initiation.

Thus, a large number of interactions with other PF coils or reactor systems can be triggered by failures in the electrical system of the PF magnets.

4.1.4   Electrical Failures of the PF Magnet System

The electrical and control system for the PF magnets needs to fulfill two basic tasks: (1) to provide the predesigned voltages and currents at the coil terminals; and (2) to allow for fast corrections of these voltages and currents depending on the state of the plasma.   In order to accomplish this task, designs for devices like CIT or the Next European Torus (NET), include PF coils external and internal to the TF coils.   The external PF coils will be operated in a slow control mode following preprogrammed current scenarios, while the internal (IC) coils will allow for fast reaction based on plasma feedback control.

Since, at present, little information is available about the operating scenarios for the IC coils, this work is focused on failures initiated in the electrical system of the external PF coils.   In general, each pair of external PF coils (above and below the midplane) is likely to be powered independently by unidirectional power supply modules.   A switching network between each power supply and the corresponding PF coil terminals is then required to obtain the designed output voltages [Greenough 1987, Bertolini 1987].   The potential electrical failures of such an electrical system can be grouped in two basic categories: (1) electrical shorts of a coil pair or a single PF coil; and (2) erroneous control or switching leading to undesired voltages at the coil terminals.   For the study of specific fault scenarios, the design of the CIT machine with a major radius of $2.1m$ [Pillsbury 1988] is used.   The two versions of an electromagnetic model of CIT which are used in this study, are shown in Fig. 3–9. CIT has 7 pairs of external PF coils, PF1 to PF7, and 3 pairs of IC coils, IC1 to IC3.   All coils are resistive and inertially cooled during a pulse, i.e., the Joule losses will lead to a monotonic temperature rise.   The maximum toroidal magnetic field at $2.1m$ is $11T$ and the maximum plasma current which is held for $5s$, is $11MA$.   One complete current pulse takes $28s$, and the coils are cooled down to LN_2 temperature between pulses.

Interaction Matrix for the Poloidal Field Magnet System			
	Poloidal Field Coils System	Poloidal Field Coils Cooling System	Poloidal Field Power Supply System	PF Protection and Control and System (PIC)
PF Coils System	EM,M,T	T	E,P	M,E,P,C
PF Cooling System	EM,M	-	E	P,C
PF Power Supply System	EM,M	E	E	C
PF PIC System	EM,M	E	E	E,C
TF Magnet System	EM,M	T	E,P	P,C
First Wall, Blanket, and Limiter System	EM,M,P		P	P
Vacuum Vessel and Shield	EM,M		P	P
Divertor System	EM,M		P	P,C
Cryogenics Cooling System and Cryostat	EM,M	M,T	P	P
Intermediate Cooling Cycles	EM,M		-	-
Plasma Heating System	EM,M		E,P	P,C
Plasma Fueling System	M		P	P,C
Plant Power Supply	EM	E	E	E,P
Central Plant PIC System	EM	E	P	E,P

EM: electromagnetic interaction, e.g. via eddy currents or electromagnetic force

M: mechanical interaction, e.g. via common support structure

T: thermal coupling, e.g. via common cooling media

E: electrical interaction, e.g. coupling via busbars or shorts from intermittent connections

P: plasma interaction, e.g. via plasma disruptions

C:control interactions, e.g. due to control system malfunctioning or operator errors

Table 4-1.   Interaction Matrix for the Poloidal Field Magnet System

The loads on the PF and the TF coils are examined for one type of fault out of each basic failure category. These failures are shorts between external PF coil terminals, or the application of a constant voltage at the terminals of external PF coils. They are candidate cases for high loads on the PF and the TF coils. The stresses and the temperatures in the external PF coils and the effect of plasma reactions are then used as the main factors to decide upon the time of fault initiation. The coil stresses are particularly large during the plasma initiation phase and at the end of the plasma current flattop (EOFT). The coil temperatures are rising during a pulse, so that a fault initiated during the last phase of a pulse is more likely to lead to temperature problems than when it is initiated earlier. Also, any major disturbance of the PF coil currents is likely to be followed by a plasma disruption. Thus, it can be expected that the higher the plasma current at fault initiation, the more severe will be the loads on the PF and the TF coils caused by the plasma disruption. Therefore, faults starting at EOFT and at the end of the plasma current (EOPC) are investigated, where three types of plasma disruptions are considered: (1) a stationary disruption, where the plasma current decays from $11MA$ to zero within $11ms$; (2) a horizontal disruption, occurring within $5ms$; and (3) a vertical plasma disruption, where the plasma current is reduced to zero within $210ms$. A total of 24 scenarios have been investigated, and are shown in Table 3–3.

4.1.5   Model and Simulation Method

Two versions of an axisymmetric model of CIT are used for simulating the fault scenarios and are illustrated in Fig. 3–9. Both models contain a representation of the external and internal PF coils, the support structure for the PF and the TF coils, and the vacuum vessel. Each element is assumed to be toroidally continuous. The plasma is modeled as a current filament whose position can be varied. The TF coil is approximated by a set of straight line connections between 14 points for each half of the TF coil.

The currents in each of the elements are obtained by solving the lumped parameter circuit loop voltage equations. From the resulting current scenario, the radial and vertical forces on the external PF coils, the out–of–plane loads

(i.e., normal to the cross section shown in Fig. 3–9) on the TF coil, and the temperature scenario in the external PF coils are computed. The unfaulted coils are driven with their preprogrammed currents, assuming that the currents rather than the voltages will be controlled. The initial currents at EOFT in all passive elements and the IC coils are zero for all scenarios but the plasma and the external PF coils have initial currents corresponding to the preprogrammed current scenario. The IC coils are modeled to be shortcircuited and not connected in series above and below the midplane.

4.1.6   Simulation Results

For CIT, a degradation in the shear strength of the coil insulation may occur for temperatures higher than $330K$, which is adopted as the limit temperature in the external coils. This temperature is not reached in any external coil for faults involving shorted coils. In cases where coils are driven with constant voltages, this temperature will be exceeded in any case since adiabatic heating of the coils can be assumed. However, it takes a minimum of $4s$ after fault initiation to reach $330K$ for the considered range of scenarios. This implies that temperature problems can be avoided when protective actions are taken within $4s$ or less from the time of fault initiation.

The loads on the PF and the TF coils are evaluated by considering multiplication factors which are obtained by dividing the maximum values for each force under a fault condition by the corresponding maximum values under normal operating condition when started at the EOFT. Assuming that a safety margin of 2 would be implemented in the design, multiplication factors between zero and two would define an envelope of allowable forces and moments.

Figures 4–1 and 4–2 show the multiplication factors of all scenarios except for cases 13 and 15, where either PF4 or PF7 is driven with its full available voltage. The forces were only traced until the temperature in one of the external PF coils exceeds $330K$. Fig. 4–1 shows that most multiplication factors for the PF coils lie within a range of 1 to 2.2. Only the vertical force on PF7 reaches a factor of 4, but this occurs only when PF7 itself is driven continuously with its voltage at EOFT for more than $5s$ without protective action. In all

Maximum Multiplication Factors
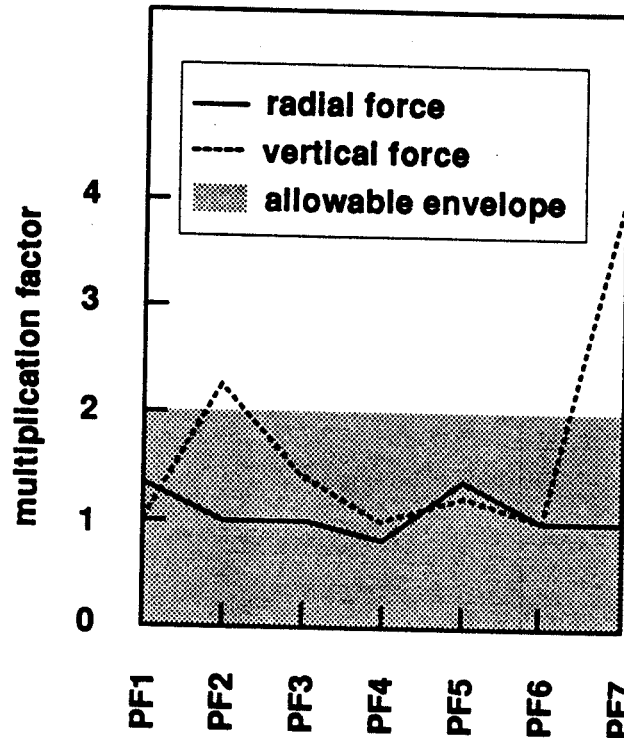## of Forces on PF Coils

Fig. 4-1. Maximum Load Multiplication Factors for the PF Coils for Cases
1 to 17 (Except Cases 13 and 15)

other cases, the factors are below 2.5. Thus, shorts in general, and most of the fault scenarios with constant coil voltages, pose little threat to the PF magnets for the examined range of scenarios.

A similar result is obtained for the out-of-plane loads along the inner and outer leg of the TF coil (points 2 to 4 and 7 to 13), as shown in Fig. 4-2. High multiplication factors of up to 4.4 are obtained only at the inner corner of the TF coil (points 5 and 6). This tendency of high multiplication factors at the inner corner of the TF coil is found for almost all the examined fault scenarios, and is particularly strong when coils PF4 or PF7 are faulted. The terminal constraints on the IC coils are also important for the loads at the inner

corner of the TF coil. Simulations with controlled IC coil current (i.e., the IC coils carry no current during the pulse) yield forces higher by a factor of 2 to 4 at the inner corner of the TF coil when compared to a circuit with passive IC coils. Clearly, the IC coils will be used to control plasma parameters and cannot be completely passive as assumed in this study, but it is also questionable whether the control voltage will be sufficient to control eddy currents of up to $1.2MA$ in the IC coils. Thus, a detailed examination of the design of the IC coils and their controls will be important for the out–of–plane loads on the TF coils. The type of plasma disruption is generally found to be of little importance for the loads on the PF coils, and has only local effects on the force distribution along the TF coil.

When one of the coils PF4 or PF7 is driven with its full available voltage, the load conditions for the PF and the TF coils become most severe. High multiplication factors on the driven coil and at the inner corner of the TF coil may be obtained within $2s$ from the time of fault initiation. Thus, in these cases, fast detection and protective action is required to prevent a severe load increase.

4.2   Conclusions and Recommendations

This study has shown that a failure mode analysis of the magnet system is a very useful tool for the designer because it helps to identify areas of uncertainty. The failure analysis of the magnet system shows that a large number of failure modes of the magnet system involve fatigue and irradiation effects. A future lifetime or reliability analysis may, therefore, need to include time dependent failure rates to describe the failure behavior appropriately. Furthermore, several failures in the magnet system can be caused by continuous combinations of multiple variables, like the combined effect of irradiation, cyclical loading and low temperatures. Work is needed to establish the boundaries between allowable and failure conditions as a function of such variables which may then be useful as input for a quantitative risk and reliability analysis of magnet systems.

Maximum Multiplication Factors
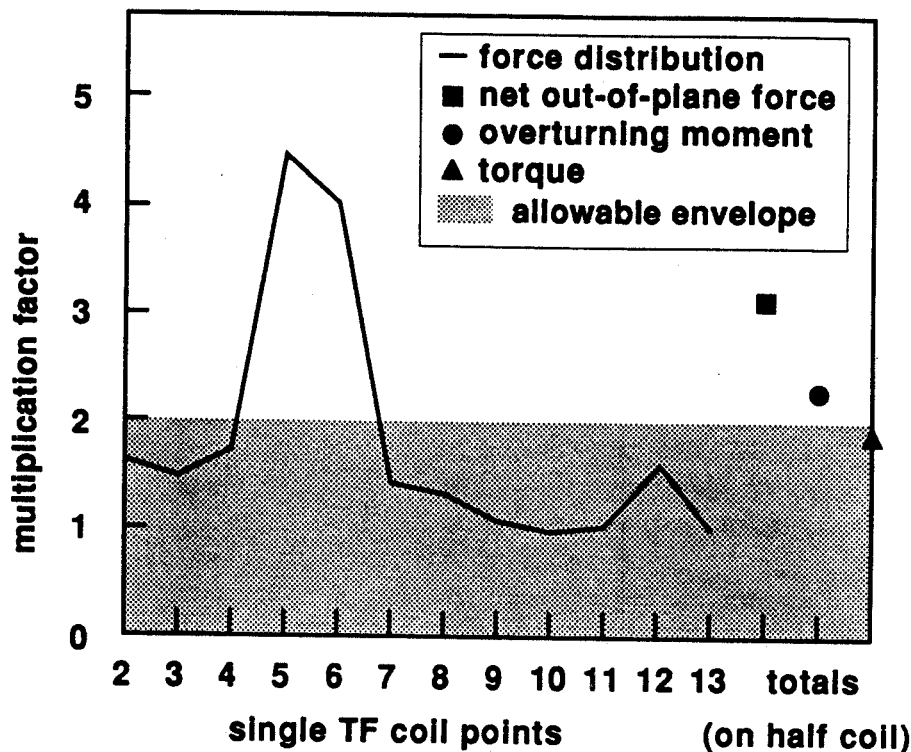## of Out-of-plane Forces on TF Coils

Fig. 4-2. Maximum Multiplication Factors for the Out-of-Plane Loads on the TF Coils for Cases 1 to 17 (Except Cases 13 and 15)

It is furthermore concluded that magnet systems may also have a significant potential for burn-in failures and for human errors stemming from manufacturing, assembly and from the initial setup of the protection and control logic. Therefore, the components of a magnet system should be tested extensively prior to their final installation in the fusion device. Furthermore, a number of failure modes may arise from failures of instrumentation or control equipment in the magnet system. Hence, the control decision logic, the repair logic and the maintenance schedule may have a strong impact on the reliability of the entire magnet system. The overall complexity of control and protection systems should therefore be examined carefully to reduce the potential for fault initiation in these systems, which could even overshadow failures of the protected or

controlled equipment. This is of particular importance for the PF magnet system since its characteristic operation requires many control and protection functions. This work has shown that such failures may lead to a variety of consequences in other reactor subsystems due to the large potential for interactions with other systems caused by the PF magnet system. Since a large number of those interactions can be triggered by electrical failures of the PF magnets, it is concluded that the electrical and control system for the PF magnets needs particular attention.

The application of model based fault tree generation techniques like the Logic Flowgraph Methodology (LFM) [Guarro 1985] should also be explored. An attempt during this study to use LFM for modeling the electrical and control system of the PF magnets has shown that two essential problems would have to be resolved in future studies in order to make use of the power of such techniques to model the complex physical processes and control structures often embedded in the design of magnet systems. The first problem involves the generic representation of complex physical processes, like the control of plasma parameters, so that the effect of deviations and the magnitude and direction of corrective actions can be traced for each path in the system. A second problem that needs to be addressed would be how to minimize the number of exogeneous inputs in the modeled system, i.e., how to incorporate basic failures as direct consequences of the operation of the system.

An analysis of the consequences of two types of electrical failures in the PF magnet system, shorts between the terminals of external PF coils, and faults where a constant voltage is applied at external PF coil terminals, reveals that shorts pose little threats to the external PF coils. Also, the type of plasma disruption following a fault is found to be of little importance in these cases. Furthermore, a modestly fast protection system, e.g., capable of reacting within $4s$ or less from fault initiation for CIT, seems to be sufficient to handle most faults. Only selected faults, involving the coils PF4 and PF7 for CIT, are found to require faster protective action, e.g., within $2s$ or less for CIT, to avoid high loads on the TF and PF coils.

Additionally, some items require attention. The loads at the inner corner of the TF coils can be substantially increased for a broad range of fault conditions. This effect can be even stronger depending on the terminal constraints on the internal PF coils. Even when mitigating actions are taken on detection of a fault, increases in the loads at the inner corner of the TF coil could be obtained under selected conditions.

As an extension to the consequence analysis in this work, future studies could explore the applicability of sensitivity analysis techniques for the selection of fault scenarios. Another aspect requiring attention in future work is the strong impact of the current scenarios of the internal PF coils on the loads on the TF coils. A future investigation of the effects of a broad range of IC coil current scenarios could yield an envelope of allowable IC coil currents. Such an analysis can then contribute to the design of the IC coils and their operating scenarios and to the search for appropriate mitigating actions. These actions are needed to allow for quickly reducing the loads on the external PF coils while controlling the load distributions along the TF coil. This might also provide robust reaction scenarios which contribute to an improved reliability of the magnet system.

Approximate scaling factors for the radial and axial dimensions are provided for CIT and NET by this study. Such scaling factors could be used as the basis for the investigation of scaling laws for the load dynamics and the magnitudes of the multiplication factors. Scaling laws would be particularly useful since several designs for major future experimental machines like CIT, NET and ITER may comprise similar coil arrangements but may have substantially different machine dimensions.

In summary, the potential for failures with high consequences for the PF and TF coils seems to be small for the examined class of failures. However, when the protection system fails, faults with voltage driven coils may cause severe consequences. Future work is needed to establish the impact of these effects on the overall reliability and availability of the magnet system and the plant. The final goal of such a failure and consequence analysis should be to develop a framework for reliability allocation which incorporates safety and cost considerations.

REFERENCES

[Bertolini 1987] E. BERTOLINI, P.L. MONDINO, and P. NOLL, "The JET Magnet Power Supplies and Plasma Control Systems," *Fsuion Technology*, 11, 71 (1987).

[Bünde 1987] BÜNDE, R., "On the Availability of the NET Toroidal Field Coils System," *Workshop on Fusion Device Reliability and Availability*, Garching, NET, F.R. Germany, February 3-4, (1987).

[Bünde 1987a] BÜNDE, R., "Reliability and Availability Assurance During the Design of the Next European Torus (NET)," *Proc. 12th Symp. on Fusion Engineering*, Monterey, CA, October 12-16, 1987, part II, p. 1258.

[Bünde 1988] BÜNDE, R., "Reliability and Availability Assessment of the Next European Torus," *Fusion Technology*, 14, 197 (1988).

[Bünde 1988a] BÜNDE, R., "Plant Component Identification Scheme (PCIS) for NET," *NET/IN/88-005*, Next European Torus (1988).

[Cadwallader 1987] CADWALLADER, L.C., D.F. HOLLAND, and R.E. LYON, "Incorporating Reliability into the Design of Experimental Fusion Facilities," *Proc. 12th Symp. on Fusion Engineering*, Monterey, CA, October 12-16, 1987, part II, p.1262.

[CIT 1988] CIT ELECTRICAL POWER SUPPLY SYSTEMS GROUP, "Power System Description Document," *WBS-N*, Princeton Plasma Physics Laboratory (1988).

[Dinsmore 1986] DINSMORE, S., J. LORENZEN, et. al., "Availability Study of the NET Protection, Instrumentation and Control System," *STUDSVIK/NP-86/ 131*, Studsvik Energiteknik AB, Nyköping, Sweden (1986).

[Garrick 1984] GARRICK, B.J., "Recent Case Studies and Advancements in Probabilistic Risk Assessment," *Risk Analysis*, 4, 4, 267 (1984).

[Greenough 1987] N.L. GREENOUGH, C.L. NEUMEYER, and D. NAYBERG, "The TFTR Energy Conversion System: Reliability in the Real World," *Proc. 12th Symp. on Fusion Engineering*, Monterey, CA, October 12-16, 1987, part I, p.432.

[Gross 1984] GROSS, R.A., *Fusion Energy*, John Wiley & Sons, New York (1984).

[Guarro 1984] GUARRO, S., and D. OKRENT, "The Logic Flowgraph: A New Approach to Process Failure Modeling and Diagnosis for Disturbance Analysis Applications," *Nuclear Technology*, **67**}, 348 (1984).

[Henley 1981] HENLEY, E.J., and H. KUMAMOTO, *Reliability Engineering and Risk Assessment*, Prentice–Hall, New York (1981).

[Hicks 1986] HICKS, J.B., N. MITCHELL, and E. SALPIETRO, "NET Plasma Engineering and Poloidal Field Coil Power Supplies," *Proc. 14th Symp. on Fusion Technology*, Avignon, September 8–12, 1986, part II, p. 707.

[How 1986] HOW, J.A., M.L. BROWNE, et. al., "The JET Pulse Termination Network," *Proc. 14th Symp. on Fusion Technology*, Avignon, September 8–12, 1986, part II, p.1421.

[Hsieh 1978] HSIEH, S.Y., M. REICH and J.R. POWELL, "Safety Issues for Superconducting Fusion Magnets," *Proc. 3rd ANS Top. Mtg. on the Technology of Controlled Fusion*, May 1978.

[Huart 1986] HUART, M., A. MOISSONNIER, et. al., "Operation of the Magnet Power Supplies. Reliability and Improvements," *Proc. 14th Symp. on Fusion Technology*, Avignon, September 8–12, 1986, part II, p. 883.

[INTOR 1982] INTOR GROUP, *Int'l Tokamak Reactor, American Contribution: Phase Two A* , *Part I,*, 1, USA FED–INTOR/82–1 (1982).

[INTOR 1982a] INTOR GROUP, *Int'l Tokamak Reactor, Japanese Contribution: Phase Two A, Part I*, 1, JAERI–M82–176 (1982).

[INTOR 1985] INTOR GROUP, *Int'l Tokamak Reactor, European Contribution: Phase Two A, Part II*, 1, EURFUBRU/XII–268/85/EDV1 (1985).

[INTOR 1985a] INTOR GROUP, *Int'l Tokamak Reactor, Japanese Contribution: Phase Two A, Part II*, 2, JAERI–M 85–081 (1985).

[INTOR 1986] INTOR GROUP, *Int'l Tokamak Reactor: Phase Two A, part II*, Rep. Int'l Tokamak Reactor Workshop 1984–85, Int'l Atomic Energy Agency, Vienna (1986).

[Jüngst 1987] JÜNGST, K.P., "Availability of the TESPE–S Superconducting Torus," *Workshop on Fusion Device Reliability and Availability*, Garching, NET, F.R. Germany, February 3–4, (1987).

[Musicki 1983] MUSICKI, Z. and C.W. MAYNARD, "The Availability Analysis of Fusion Power Plants as Applied to MARS," *Nuclear Technology/Fusion*, **4**, 284 (1983).

[NRC 1975] U.S. NUCLEAR REGULATORY COMMISSION, "An Assessment of Accident Risks in U.S. Commercial Nuclear Power Plants," *NUREG 75/014 (Wash 1400)* (1975).

[Pelovitz 1986] M. PELOVITZ, "TFTR Poloidal Coil Fault Analysis," *Fusion Technology*, **10**, 1059 (1986).

[Piet 1986] PIET, S.J., "Implications of Probabilistic Risk Assessment for Fusion Decision Making," *Fusion Technology*, **10**, 31 (1986).

[Pillsbury 1988] R.D. PILLSBURY, JR., "PF System for the CIT 2.1m Machine," *MIT-PF040888*, Plasma Fusion Center, Massachusetts Institute of Technology (1988).

[Pillsbury 1988a] R.D. PILLSBURY, JR., "The G–Function and its Use in Estimating an Adiabatic Temperature Rise," *GEM-17*, Plasma Fusion Center, Massachusetts Institute of Technology (1988).

[Raeder 1981] RAEDER, J. et. al., *Controlled Nuclear Fusion*, John Wiley & Sons, New York (1981).

[Salpietro 1988] SALPIETRO, E., F. CASCI, et. al., "Next European Torus Basic Machine", *Fusion Technology*, **14**, 58 (1987).

[Schnauder 1987] SCHNAUDER, H., and A. WICKENHÄUSER, "Potential Influence of Reliability Analysis on Component Design in Fusion Reactors," *Nuclear Engineering and Design*, **100**, 489 (1987).

[Sheffield 1986] SHEFFIELD, J., R.A. DORY, et. al., "Cost Assessment of a Generic Magnetic Fusion Reactor," *Fusion Technology*, **9**, 199 (1986).

[Siu 1988] SIU, N., and T. PAGONI, "Assessing the Reliability of Components and Complex Subsystems," *MITNE-284* Massachusetts Institute of Technology (1988).

[Thome 1986] THOME, R.J., J.B. CZIRR, and J.H. SCHULTZ, "Survey of Selected Magnet Failures and Accidents," *Fusion Technology*, **10**, (1986).

[Thome 1988] THOME, R.J., editor, "PF System Design Description Document," *WBS-G*, Rev. 3, Plasma Fusion Center, Massachusetts Institute of Technology (1988).

[Ulbricht 1987] ULBRICHT, A., "Availability of the International Fusion Superconducting Magnet Test Facility (IFSMTF)", *Workshop on Fusion Device Reliability and Availability*, Garching, NET, F.R. Germany, February 3–4, (1987).

[Watanabe 1986] WATANABE, Y., C.W. MAYNARD, and Z. MUSICKI, "Three State Model for Fusion Reactor Plant Availability Analysis," *Fusion Technology*, 10, 1590 (1986).

[Zimmermann 1988] ZIMMERMANN, M., M.S. KAZIMI, N.O. SIU, and R.J. THOME, "On the Consequences of Electrical Failures of PF Magnet Systems for Fusion Reactors," *Proc. 8th Top. Mtg. on the Technology of Fusion Engergy*, Salt Lake City, UT, October 9–13, 1988, to be published in 1989.

Appendix A
FAULT TREE SYMBOLS

Fault tree analysis is nowadays widely used for qualitative and qualitative reliability analysis and as the basis for risk assessment (see, for example [NRC 1975]). One of the main reasons for the use of fault trees is that they are a communication tool which shows how a sequence of failures can lead to a single top event. The failure logic is visualized by a tree structure whose building blocks are gate and event symbols. Each gate can have several inputs but only a single output, where each input or output is a single failure event in the system. A variety of symbols for the representation of different types of events and logical connections have been developed, and the symbols used in this study are described in Table A-1. For a more detailed discussion of fault tree symbols and fault tree analysis see for example [Henley 1981].
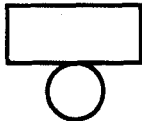
Symbol	Gate Name	Causal Relation
AND Gate	AND Gate	output event occurs if all input events occur simultaneously
OR Gate	OR Gate	output event occurs if any input event occurs
© Conditional AND Gate	Conditional AND Gate	output event occurs if any continuous combination of input variables exceeds a limit condition [Siu 1988]

Symbol	Event Description
○	circle: basic event with sufficient data, which need not be broken down further
◇	diamond: basic event which needs to be broken down further but cannot because of insufficient data (undeveloped event)
△	triangle: transfer symbol where fault tree is continued with this event as new top event

Table A-1. Explanation of Fault Tree Symbols

Appendix B
PF COIL OPERATION SCENARIOS FOR CIT

This appendix provides data for the operation scenario of the external PF coils of CIT [Pillsbury 1988] which has been used during the selection of the types of faults to be examined for each external PF coil and the time of fault initiation. Fig. B-1 provides the temperatures in the external PF coils under normal operating conditions. Table B-1 presents the voltage per turn scenario for CIT, Fig. B-2 the axial and radial (hoop) stresses in the external PF coils under normal operating conditions.
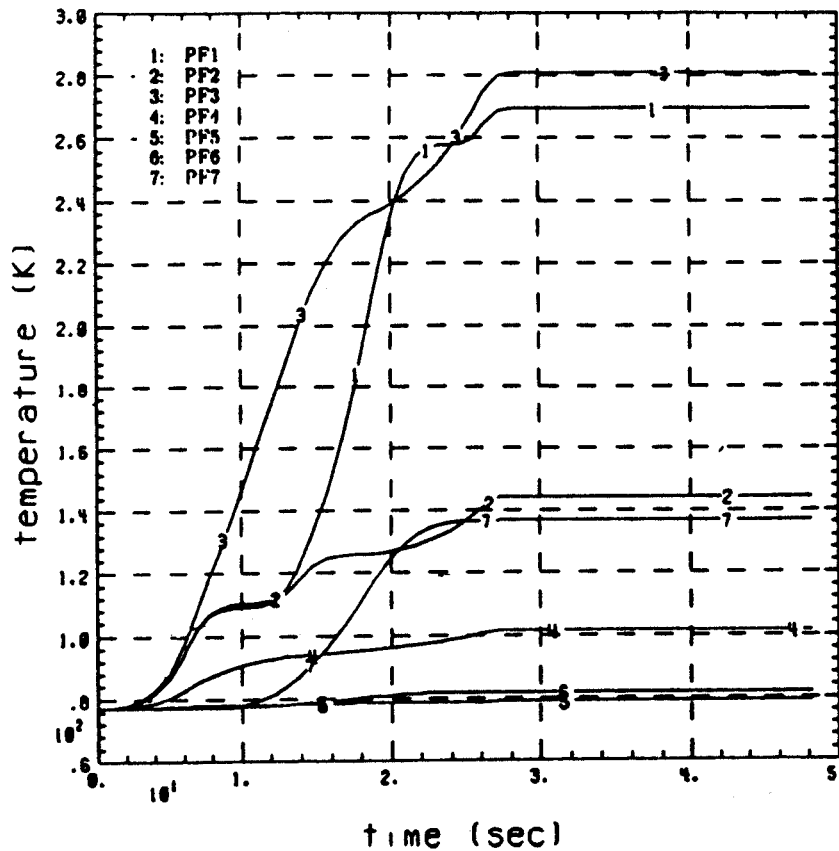

Fig. B-1. Temperatures of the External PF Coils of CIT
under Normal Operating Conditions (Case R3)

	PF Coil Voltage per Turn Scenario (V)							
Time (s)	BOP		BOB		BOFT	EOFT	EOPC	EOP
	0.0	6.0	6.2	6.26	13.76	18.76	26.26	28.26
PF1	0.0	4.7	1.5	-11.2	-6.2	-5.8	6.9	-5.5
PF2	0.0	4.4	1.5	-10.4	-4.8	1.6	3.1	-5.0
PF3	0.0	4.3	1.7	-9.5	2.7	0.8	4.7	-4.4
PF4	0.0	8.4	1.3	-37.5	-3.2	-0.03	2.9	-11.5
PF5	0.0	1.75	-0.6	-49.5	-1.6	-0.8	1.5	-2.6
PF6	0.0	3.4	0.0	-43.2	-9.9	-3.35	89.0	-4.7
PF7	0.0	4.7	0.3	-33.9	-18.9	-11.7	15.6	-6.7

BOP: beginning of pulse
BOB: beginning of burn, startup of plasma current
BOFT: beginning of plasma current flattop
EOFT: end of plasma current flattop
EOPC: end of plasma current
EOP: end of pulse

Table B-1. Voltages per Turn of the External PF Coils of CIT under Normal Operating Conditions (data from [Pillsbury 1988])
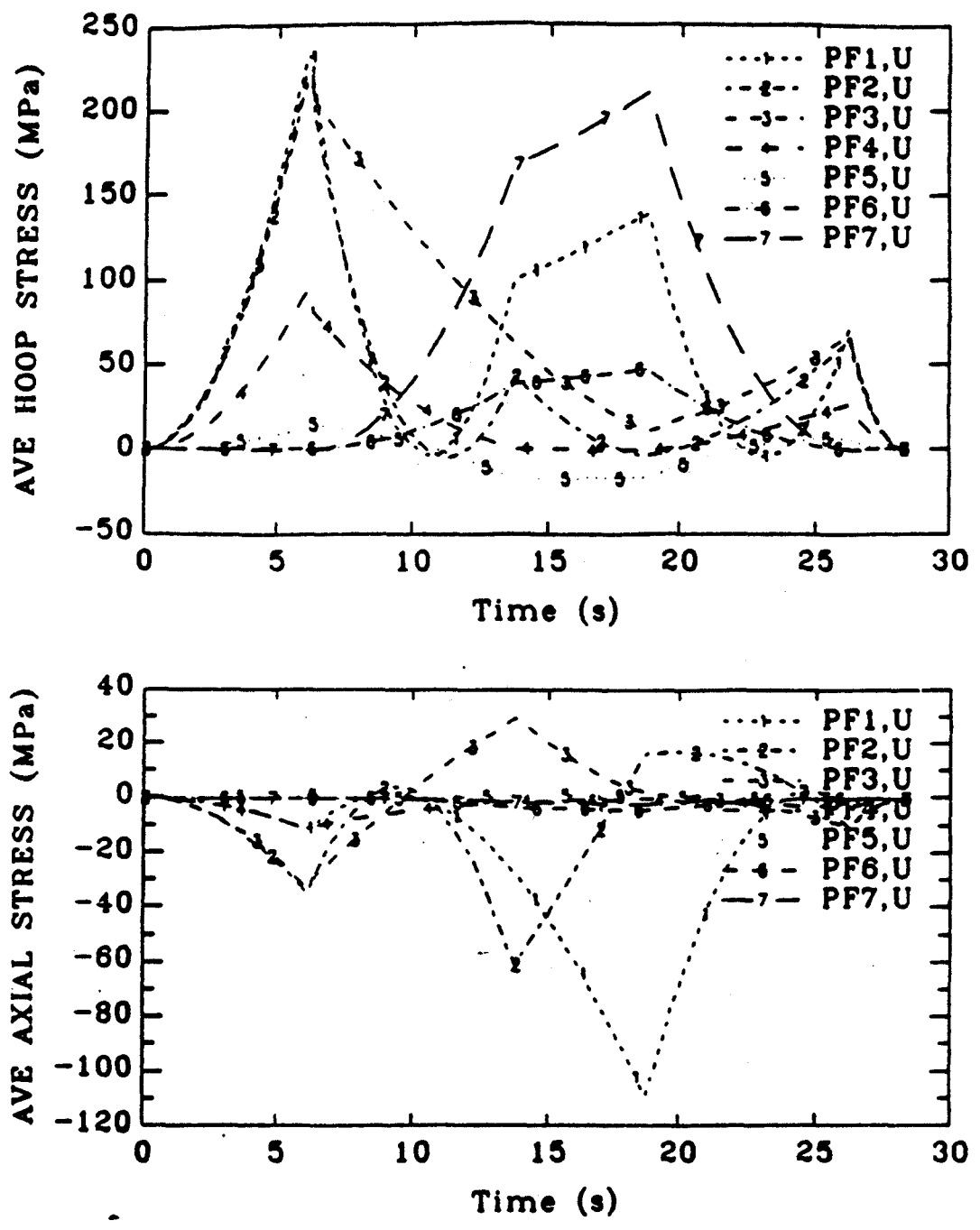
Fig. B-2. Average Hoop and Axial Stresses in the External PF Coils under Normal Operating Conditions [Pillsbury 1988]

Appendix C
DISRUPTION SCENARIOS

Three different types of disruptions have been examined in this study. For the first type of disruption, it has been assumed that the plasma is stationary at the major radius of the machine while the plasma current decays from initially $11MA$ to zero within $11s$. The data for the remaining disruption scenarios was obtained from runs of the Tokamak Simulation Code (TSC), which uses an electromagnetic model of CIT with a much finer element grid in the plasma region and for the vacuum vessel than the model used in this study. It can therefore be used for disruption analysis, and two sets of disruption data obtained from the TSC model, for a radial or horizontal and a vertical disruption[†], are used in this study. This data has been used to compute which plasma elements needed to be switched on and off to simulate the movement of a current carrying plasma during the disruption. The plasma current scenarios and the trajectories for the center of the plasma current that have finally been used in the simulations are shown in Fig. C-1 and C-2.

[†]   The data has been obtained from R.O. Sayer at the Fusion Engineering Design Center (internal reference FEDC-L-88-PE-0351, 1988).
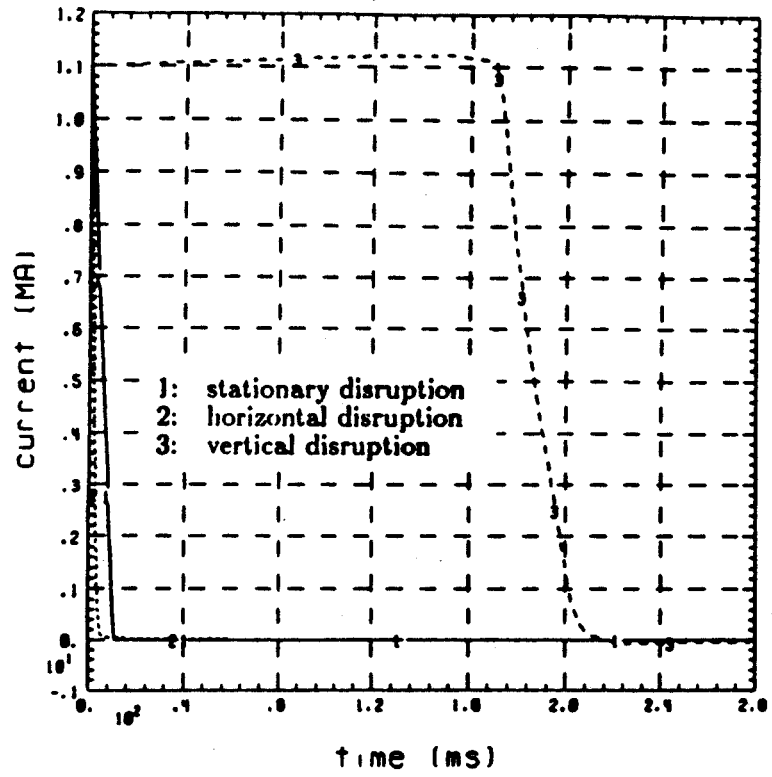
Fig. C-1. Plasma Current Scenarios
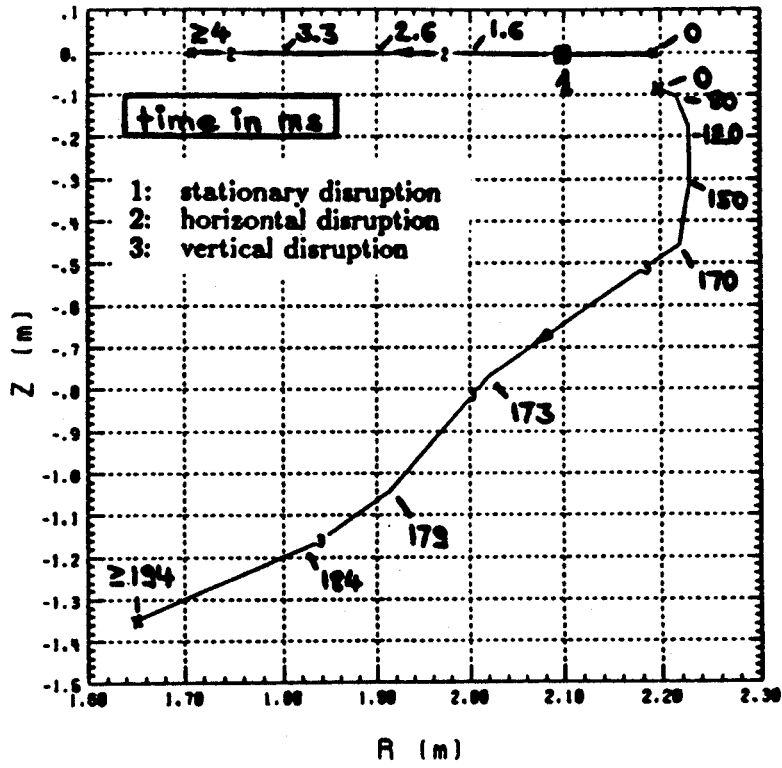
for the Simulated Disruption Schemes

Fig. C-2. Trajectories of the Plasma Filament
for the Simulated Disruption Scenarios

Appendix D

SIMULATION MODEL

D.1   Comutation of the PF and Coil Loads

This appendix provides the methods that are used to simulate the fault scenarios using of the electromagnetic model of CIT shown in Fig. 3–9. The toroidally continuous elements in this model represent a set of inductively coupled elements, where each element can carry a current in toroidal direction. Given a set of of initial element currents and a vector of forcing voltages $\underline{U}(t)$, the current scenario for all elements can be obtained by solving the linear matrix differential equation

$$\mathbf{L}\underline{\dot{I}} + \mathbf{R}\underline{I} = \underline{U} \tag{D.1}$$

where $\underline{I}(t)$ is the vector of currents and $\mathbf{L}$ and $\mathbf{R}$ are the inductance and resistance matrices of the circuit.

The inductance matrix $\mathbf{L}$ contains the self– and mutual inductances for all circuit elements and will be symmetric. The resistance matrix $\mathbf{R}$ is a diagonal matrix whose elements are the resistances of the elements in the model. Both matrices depend on the model geometry, the geometry of the elements, and the resistivity of each circuit element. The resistivity is in turn a function of the materials and the element temperature, and a higher resistivity will usually be obtained for higher temperatures. For this study, the temperature dependence of the resistivity of a single element during the pulse will be neglected, and the resistivities of coils and structural elements are computed once for the approximately highest temperature obtained under normal operating conditions and hold constant during the computation of the current scenario. Table D–1 shows the assignment of element temperatures and resistivities used in this study. Since each PF coil consists of conductor (copper), and structural and insulating materials, the effective resistivity ρ_{eff} of a PF coil is computed by

$$\rho_{\text{eff}} = \frac{\rho_{cu}(T)}{\lambda_{cu}} \tag{D.2}$$

where λ_{cu} is the fraction of copper in the coil and $\rho_{cu}(T)$ is the resistivity of the copper at the adopted maximum temperature T. The inductance and resistance matrices for both models are then obtained under use of the program package SOLDESIGN.†

Once the inductance and resistance matrices are obtained the circuit equation D.1 can be solved. Assuming that the forcing function $\underline{U}$ is constant, the current vector $\underline{I}(t)$ can be computed under use of an eigenexpansion technique‡ which yields a solution of the form

$$\underline{I}(t) = \underline{I}_{ss} + \sum_{i=1}^{n} \underline{v}_i e^{\lambda_i t} \tag{D.3}$$

where $\underline{I}_{ss}$ is the vector of steady state currents, n is the number of circuit elements in the model, $\underline{v}_i$ is the eigenvector i of the matrix $\mathbf{L^{-1}R}$, and λ_i is the eigenvalue corresponding to the eigenvector $\underline{v}_i$.

The vector of steady state currents $\underline{I}_{ss}$ is determined by the driving voltages $\underline{U}_{driv}$ and induced voltages $\underline{U}_{ind}$, to

$$I_{ss} = \mathbf{R^{-1}}(\underline{U}_{ind} + \underline{U}_{driv}) \tag{D.4}$$

The vector of driving voltages $\underline{U}_{driv}$ includes the driving voltages of all circuit elements that are voltage driven and zeros for all other elements, while the vector of induced voltages $\underline{U}_{ind}$ is obtained form the current driven circuits by

$$\underline{U}_{ind} = \mathbf{L}\dot{\underline{I}}_{driv} \tag{D.5}$$

where $\underline{I}_{driv}$ includes the driving currents for all current driven elements and zeros for all other elements. Obviously, in order to fulfill the initial assumption of a constant forcing function $\underline{U}(t)$, the driving voltages need to be constant or the driving current functions need to be linear functions so that $\dot{\underline{I}}_{driv}$ will be constant.

---

† SOLDESIGN is a program developed by R.D. Pillsbury, Jr. and is currently available on the MIT Plasma Fusion Center VAX and the MFE computer network.

‡ The program NEWEIGEN used in this study uses such an eigenexpansion technique and has been developed by R.D. Pillsbury, Jr. NEWEIGEN is currently available on the MIT Plasma Fusion Center VAX and under the name EIGENCIRC on the MFE computer network.

Coil or Structure	Maximum Temp. (K)	Temp. for Simulation (K)	Resistivity ρ (Ωm)	Fraction of Conductor λ_{cu}	Effective Resistivity ρ_{eff} (Ωm)
PF1	280	300	1.773×10^{-8}	0.39	4.547×10^{-8}
PF2	150	160	7.839×10^{-9}	0.39	2.010×10^{-8}
PF3	291	300	1.773×10^{-8}	0.39	4.547×10^{-8}
PF4	105	100	3.598×10^{-9}	0.8	4.497×10^{-9}
PF5	82	80	2.184×10^{-9}	0.8	2.730×10^{-9}
PF6	85	80	2.184×10^{-9}	0.8	2.730×10^{-9}
PF7	142	130	5.719×10^{-9}	0.8	7.148×10^{-9}
IC1	-	80	2.184×10^{-9}	0.8	2.730×10^{-9}
IC2	-	80	2.184×10^{-9}	0.8	2.730×10^{-9}
IC3	-	80	2.184×10^{-9}	0.8	2.730×10^{-9}
Vacuum Vessel (St-L304)	≈ 300	300	7.000×10^{-7}	1	7.000×10^{-7}
Remaining Structure (SS)	≈ 77	77	5.500×10^{-7}	1	5.500×10^{-7}

Table D-1. Material Data for the Simulations

Then, the differential equation system from eq. D.1 can be rewritten:

$$\mathbf{L}\,\underline{\dot{I}} + \mathbf{R}\,(\underline{I} - \underline{I}_{ss}) = \underline{0} \tag{D.6}$$

and can be solved with

$$\underline{I}(t_0) = \underline{I}_0 \tag{D.7}$$

being the vector of initial currents. This eigenexpansion technique can also be used for piecewise constant driving voltages and piecewise linear driving current ramps when the currents are tracked and the initial currents and time are reset after each time interval.

Once the current vector $\underline{I}(t)$ is computed the forces on the toroidally continuous elements and the TF coil can be obtained. Each current I_j in a single circuit element j will contribute to the magnetic field $\underline{B}_i$ at a point i in the r-z-plane (which has only components in radial and vertical direction since all elements carry toroidal currents, see Fig. 3-9), so that

$$\underline{B}_i = \sum_{j=1}^{n} \underline{b}_{ij}\, I_j \tag{D.8}$$

where n is the number of circuit elements and $\underline{b}_{ij}$ is a vector of field influence coefficients from element j to point i with components in radial and axial direction. These field influence coefficients are only a function of the model geometry and are thus constant for a given model.

The forces on a toroidally continuous element carrying a current I_i are then obtained from the crossproduct of its current with the magnetic field $\underline{B}_i$. Since the current I_i is always perpendicular to the magnetic field in the r-z-plane, the radial and axial forces per unit circumferential length are obtained from

$$\begin{aligned}
\underline{F}_i &= I_i\,\underline{B}_i \\
&= I_i \sum_{i=1}^{n} \underline{b}_{ij}\, I_j \\
&= \sum_{i=1}^{n} \underline{b}_{ij}\, I_i\, I_j
\end{aligned} \tag{D.9}$$

When the forces on an element with radial and axial extension are to be calculated, like for all the elements in the CIT model, a similar procedure can be used but the forces need to be integrated over the entire cross section of the element. Similar to eq. D.9, the total force on this element can then be obtained from

$$\underline{F}_i = \sum_{i=1}^{n} \underline{k}_{ij}\, I_i\, I_j \qquad \text{(D.10)}$$

where $\underline{k}_{ij}$ now defines force influence coefficients for this element. These coefficients depend only on the model geometry. The force influence coefficients for each toroidally continuous element and the field influence coefficients for each point of the TF coil can also be obtained under use of the program package SOLDESIGN.

The out-of-plane loads at each point of the TF coil can be computed from eq. D.9 under use of the field influence coefficients. Since the TF coil current lies in the same plane as the magnetic field, the force q_i (per unit circumferential length) on the TF coil perpendicular to the r-z-plane (or out of the plane of the TF current) is determined by

$$q_i = I_{TF}\, \underline{d}_{TF_i} \times \underline{B}_i \qquad \text{(D.11)}$$

where I_{TF} is the total TF coil current, $\underline{d}_{TF_i}$ defines the direction of the TF coil current at point i, and $\underline{B}_i$ is the magnetic field at point i from the toroidally continuous elements of the model. In this study, the direction of the TF coil current at a point i of the TF coil is approximated by the slope of the straight line connection between the two adjacent points $i-1$ and $i+1$.

The net out-of-plane force on a TF coil half is obtained by integrating the force per unit length q_i along the TF coil. Approximating the force distribution $q(r)$ along the TF coil by linear functions between two points i and $i+1$ yields for a single coil segment

$$q(r) = \frac{q_{i+1} - q_i}{\Delta r_i}\,(r - r_i) + q_i \qquad \text{(D.12)}$$

for r between r_i and r_{i+1}. The TF coil is approximated by straight line connections, so that the running length of the connection between points i and $i + 1$ is given by

$$l_i = \left((r - r_i)^2 + (z - z_i)^2 \right)^{0.5} \tag{D.13}$$

and

$$z(r) = z_i + \frac{\Delta z_i}{\Delta r_i} \, (r - r_i)$$

with $\Delta r_i = r_{i+1} - r_i$ $\tag{D.14}$

and $\Delta z_i = z_{i+1} - z_i$

Similarly, the moment M_r about the radial axis or the overturning moment on a half TF coil is obtained by

$$M_r = \sum_{i=1}^{m-1} \int_0^{\Delta l_i} q(r) \, z(r) \, dl_i \tag{D.15}$$

where m is the number of points representing the TF coil and Δl_i is the distance between points i and $i + 1$. Combining eq. D.15 with eq. D.12 and D.14 yields

$$M_r = \sum_{i=1}^{m-1} \left(\frac{2\,q_{i+1} + q_i}{6} \, \Delta z_i \, \Delta l_i + \frac{1}{2} \, (q_{i+1} + q_i) \, \Delta l_i \, z_i \right) \tag{D.16}$$

The moment M_z about the vertical axis, or the torque, on a half TF coil can be computed analogous to the overturning moment:

$$M_z = \sum_{i=1}^{m-1} \left(\frac{2\,q_{i+1} + q_i}{6} \, \Delta r_i \, \Delta l_i + \frac{1}{2} \, (q_{i+1} + q_i) \, \Delta l_i \, r_i \right) \tag{D.17}$$

D.2   Computation of the Temperature in Toroidal Elements

The temperatures in a resistive coil can be estimated by use of the G-function when the current scenario $I(t)$ for the coil is known [Pillsbury 1988a]. Assuming adiabatic heating of the coil, which is assumed for CIT [Thome 1988], the temperature rise in the coil is given by

$$\gamma\, c_p(T)\, \frac{\partial T}{\partial t} = \rho_{cu}(T)\, j_{cu}^2 \tag{D.18}$$

and $T(t_0) = T_0$, where γ is the mass density of the coil, $c_p(T)$ is the temperature dependent specific heat capacity, T is the coil temperature, $\rho_{cu}(T)$ the temperature dependent resistivity of the conductor, and j_{cu} the current density in the conductor (which is copper for CIT). Assuming furthermore that the current density in the conductor is homogeneous, j_{cu} is given by

$$j_{cu} = \frac{I}{A_{cu}} \tag{D.19}$$

where A_{cu} is the cross sectional area of the conductor.

Since the coil may consist of conductor and structure, an average heat capacity $(\gamma\, c_p(T))_{ave}$ needs to be used in eq. D.18. Since several external PF coils of CIT consist of copper and St-718, whose mass fraction are f_{cu} and f_{st}, where

$$f_{cu} + f_{st} = 1 \tag{D.20}$$

the average heat capacity of a coil is given by

$$(\gamma\, c_p(T))_{ave} = f_{cu}\, \gamma_{cu}\, c_{p_{cu}} + e_{st}\, f_{st}\, \gamma_{st}\, c_{p,t} \tag{D.21}$$

where e_{st} represents the effective fraction of steel contributing to thermal diffusion which may be less than 1 due to a thermal diffusion lag in the coil.

Combining eq. D.18, D.19, and D.21 then yields

$$\left(f_{cu}\, \gamma_{cu}\, c_{p_{cu}} + e_{st}\, f_{st}\, \gamma_{st}\, c_{p_{st}} \right) \frac{\partial T}{\partial t} = \rho_{cu}(T)\, \frac{I^2(t)}{A_{cu}^2} \qquad (D.22)$$

Integrating eq. D.22 from the initial time t_0 and temperature T_0 to the current time t and temperature T gives

$$\int_{T_0}^{T} \frac{\gamma_{cu}\, c_{p_{cu}}(T)}{\rho_{cu}(T)}\, dT + e_{st}\, \frac{f_{st}}{f_{cu}} \int_{T_0}^{T} \frac{\gamma_{st}\, c_{p_{st}}(T)}{\rho_{st}(T)}\, dT = \frac{1}{A_{cu}^2} \int_{t_0}^{t} I^2(t)\, dt \qquad (D.23)$$

The integrals on the left hand side can be computed and tabulated without prior knowledge of the current scenario. These integrals are usually called G-functions, where

$$G_{cu} = \int_{T_0}^{T} \frac{\gamma_{cu}\, c_{p_{cu}}(T)}{\rho_{cu}(T)}\, dT$$

and

$$G_{st} = \int_{T_0}^{T} \frac{\gamma_{st}\, c_{p_{st}}(T)}{\rho_{st}(T)}\, dT$$

so that

$$G_{cu}(T) + e_{st}\, \frac{f_{st}}{f_{cu}}\, G_{st}(T) = \frac{1}{A_{cu}^2} \int_{t_0}^{t} I^2(t)\, dt \qquad (D.24)$$

Then, the temperature of the coils can be estimated by first computing the G-function for the entire coil,

$$G_{tot}(T) = G_{cu}(T) + e_{st}\, \frac{f_{st}}{f_{cu}}\, G_{st}(T) \qquad (D.25)$$

at the initial temperature T_0, and then again at each time step during the scenario by

$$G_{tot}(T) = G_{tot}(T_0) + \frac{1}{A_{cu}^2} \int_{t_0}^{t} I^2(t)\, dt \qquad (D.26)$$

Once the total G-value is known, the coil temperature T can be looked up in a table for G_{tot}, obtained from eq. D.26.

In this study, it is assumed that there is no thermal diffusion lag in the coil, i.e.

$$e_{st} = 1$$

is used for all scenarios. The mass fractions for copper and St-718 used for the external PF coils are provided in Table D-2, and it is assumed that copper with a mass density of $8950 kg/m^3$ and St-718 with a mass density of $8100 kg/m^3$ are used. The specific heat capacities $c_{p_{cu}}$ and $c_{p_{st}}$ of copper and St-718 are approximated by piecewise linear functions of the temperature:

$$c_p(T) = a_{c_{p_i}} + b_{c_{p_i}} (T - T_i) \qquad (D.27)$$

for T between T_i and T_{i+1}. Similarly, the resistivities of copper and St-718 are approximated by

$$\rho(T) = \rho_0 (a + bT) \qquad (D.28)$$

These relations are then used to compute the look up tables for G_{cu} and G_{st}.

Coil	Packaging Factors	
	for copper f_{cu}	for St-718 f_{st}
PF1	0.39.	0.39
PF2	0.39	0.39
PF3	0.39	0.39
PF4	0.8	0.0
PF5	0.8	0.0
PF6	0.8	0.0
PF7	0.8	0.0

Table D-2. Packaging Factors for the External PF Coils of CIT
(Data from [Pillsbury 1988])